

Linear stability analysis of large dynamical systems on random directed graphs

Izaak Neri^{1,*} and Fernando Lucas Metz^{2,3,†}

¹*Department of Mathematics, King's College London, Strand, London, WC2R 2LS, United Kingdom*

²*Physics Institute, Federal University of Rio Grande do Sul, 91501-970 Porto Alegre, Brazil*

³*London Mathematical Laboratory, 18 Margravine Gardens, London W6 8RH, United Kingdom*



(Received 29 June 2020; accepted 21 July 2020; published 26 August 2020)

We present a linear stability analysis of stationary states (or fixed points) in large dynamical systems defined on random, directed graphs with a prescribed distribution of indegrees and outdegrees. We obtain two remarkable results for such dynamical systems. First, infinitely large systems on directed graphs can be stable even when the degree distribution has unbounded support; this result is surprising since their counterparts on nondirected graphs are unstable when system size is large enough. Second, we show that the phase transition between the stable and unstable phase is universal in the sense that it depends only on a few parameters, such as, the mean degree and a degree correlation coefficient. In addition, in the unstable regime, we characterize the nature of the destabilizing mode, which also exhibits universal features. These results follow from an exact theory for the leading eigenvalue of infinitely large graphs that are locally treelike and oriented, as well as, the right and left eigenvectors associated with the leading eigenvalue. We corroborate analytical results for infinitely large graphs with numerical experiments on random graphs of finite size. We discuss how the presented theory can be extended to graphs with diagonal disorder and to graphs that contain nondirected links. Finally, we discuss the influence of cycles and how they can destabilize large dynamical systems when they induce strong feedback loops.

DOI: [10.1103/PhysRevResearch.2.033313](https://doi.org/10.1103/PhysRevResearch.2.033313)

I. INTRODUCTION

Scientists use networks to depict the causal interactions between the constituents of large dynamical systems [1–5]. Currently, it is not well understood how the stability of a large system is affected by the topology of the underlying interaction network. Relating system stability to network topology is important to understand, among others, how systemic risk in financial markets is governed by the topology of the network of liabilities between financial institutions [6–8]; how the resilience of an ecosystem to external perturbations depends on the underlying food web of trophic interactions [9–14]; and how networks of social interactions determine the spreading of rumours [15–17]. As these examples illustrate, in order to reduce risk and instability in dynamical systems it is important to identify topological properties of networks that stabilize large systems.

In order to study the stability of large dynamical systems, we consider the linearized dynamics of a large, complex, dynamical system in the vicinity of a stationary state or fixed point. We model this dynamics with a set of randomly and

linearly coupled differential equations of the form

$$\partial_t y_j(t) = \sum_{k=1}^n y_k(t) A_{kj}, \quad (1)$$

where $t \geq 0$ is the time index, $\vec{y}^\dagger(t) = (y_1(t), y_2(t), \dots, y_n(t)) \in \mathbb{R}^n$ is a vector, and \mathbf{A} is a random matrix of size $n \times n$ that describes the underlying interaction network between the degrees of freedom. We use the notation $\vec{y}(t)$ for column vectors and $\vec{y}^\dagger(t) = (y_1(t), y_2(t), \dots, y_n(t)) \in \mathbb{R}^n$ for their transpose (or conjugate transpose). Models like Eq. (1) appear when linearizing a set of nonlinearly coupled differential equations in the vicinity of a fixed point [18–20] as occurs, for example, in the study of neural networks [21–25] and ecosystems [13,20,26,27]. The vector \vec{y} describes then the deviation of the system from its fixed point, which is located at the origin, i.e., $\vec{y} = 0$. We will use the generic model, given by Eq. (1), to study how network topology affects the stability of stationary states.

Since we aim to develop a better understanding on how network topology affects system stability, we write Eq. (1) as

$$\partial_t y_j(t) = \sum_{k=1;(k \neq j)}^n y_k(t) C_{kj} J_{kj} - d y_j(t), \quad (2)$$

where $d > 0$ represents the rate at which an isolated node relaxes to the stationary state, where $C_{kj} \in \{0, 1\}$ are the entries of the adjacency matrix of a directed graph, and where $J_{kj} \in \mathbb{R}$ are the strengths of the couplings between two nodes

*izaak.neri@kcl.ac.uk

†fmetzfmets@gmail.com

Published by the American Physical Society under the terms of the [Creative Commons Attribution 4.0 International license](https://creativecommons.org/licenses/by/4.0/). Further distribution of this work must maintain attribution to the author(s) and the published article's title, journal citation, and DOI.

k and j . Note that Eq. (2) and Eq. (1) are related by

$$\mathbf{A} = -d\mathbf{1}_n + \mathbf{J} \circ \mathbf{C}, \quad (3)$$

where

$$[\mathbf{J} \circ \mathbf{C}]_{jk} = J_{jk}C_{jk} \quad (4)$$

and $\mathbf{1}_n$ is the identity matrix. The entries of the adjacency matrix \mathbf{C} determine who interacts with whom, while the entries of the interaction matrix \mathbf{J} denote the absolute strength of the interactions and whether these are inhibitory $J_{kj} < 0$ or excitatory $J_{kj} > 0$.

In absence of interactions between system constituents ($J_{jk} = 0$), the fixed point $\bar{y} = 0$ is stable as $d > 0$. However, if the constituents of a system interact strong enough, then a small perturbation around the fixed point $\bar{y} = 0$ will propagate through the network, grow in size, and destabilize the system. It is the underlying network topology, represented by the adjacency matrix \mathbf{C} , and the strength of the interactions, given by \mathbf{J} , that determine whether an initial perturbation will grow or fade away. For example, in an online social network, the topology of the network determines whether a rumour spreads throughout the whole system or only reaches a couple of users.

The stability of the fixed point $\bar{y} = 0$ in the dynamics given by Eq. (1) is governed by the sign of the real part of the leading eigenvalue $\lambda_1(\mathbf{A})$, which is the eigenvalue with the largest real part. As discussed in Appendix A, if $\text{Re}[\lambda_1(\mathbf{A})] > 0$, then the fixed point is unstable and $\lim_{t \rightarrow \infty} |\bar{y}(t)| = \infty$. Conversely, if $\text{Re}[\lambda_1(\mathbf{A})] < 0$, then the fixed point is stable and $\lim_{t \rightarrow \infty} |\bar{y}(t)| = 0$. In addition, the left eigenvector associated with the leading eigenvalue determines the nature of the destabilizing mode.

To model dynamical systems on large networks, we consider that \mathbf{C} is the adjacency matrix of a random, directed graph with a prescribed degree distribution $p_{K^{\text{in}}, K^{\text{out}}}(k, \ell)$ of indegrees K^{in} and outdegrees K^{out} . This is a paradigmatic model for networked systems, such as, the World Wide Web [28,29], neural networks [30–32], food webs [10], and online social networks [33,34], and it is often called the configuration model [2,4,35–37] or the uniform model [38]. The percolation properties of random, directed graphs have been well understood, see Refs. [39–41], and recently also spectral properties of random, directed graphs have been studied, see Refs. [42–46], but the properties of the leading eigenvalue of the adjacency matrices of random, directed graphs have not been studied so far.

In this paper, we perform a linear stability analysis of fixed points in dynamical systems defined on random, directed graphs. To this aim, we determine the leading eigenvalue $\lambda_1(\mathbf{A})$ of the adjacency matrices \mathbf{A} of random, directed graphs with a prescribed degree distribution and with randomly weighted links. First, building on Ref. [44], we derive exact analytical expressions for the typical value of λ_1 in the limit of infinitely large n . In addition, we derive in this limit exact expressions for the statistics of the entries of right and left eigenvectors associated with λ_1 . Second, we use these results to depict a phase diagram for the linear stability of fixed points in dynamical systems defined on large, directed networks. Third, the theoretical results for infinitely large graphs are compared with numerical results for graphs of finite size,

which include random graphs with power-law degree distributions.

Two implications of these results are surprising enough that they deserve further emphasis. First, we find that dynamical systems on infinitely large, random, and directed graphs can be *stable*, even when the degree distribution has unbounded support. This result is surprising because dynamical systems on random, nondirected graphs with a degree distribution that has unbounded support are unstable if the system size is large enough. Indeed, the leading eigenvalue of nondirected, random graphs scales as $\lambda_1 \sim \sqrt{k_{\text{max}}}$ [47–49], where k_{max} is the expected largest degree of the graph, and therefore the leading eigenvalue of nondirected graphs diverges for large n . In contrast, in this paper, we obtain that the leading eigenvalue of a random, directed graph with a prescribed degree distribution is in general finite for $n \rightarrow \infty$, even when k_{max} diverges. Hence, models on random, directed graphs are significantly more stable than their counterparts on random, nondirected graphs.

Second, we obtain a *universal* phase diagram for the stability of dynamical systems on random, directed graphs with a prescribed degree distribution. Put in another way, we show that the leading eigenvalue of these random graphs only depends on a few system parameters, including the mean degree and a parameter that characterizes the correlations between indegrees and outdegrees.

Both the *stability* and *universality* of dynamical systems defined on random, directed graphs are rooted in a common fact: for large enough n , the local neighborhood of a randomly selected node is with probability one a tree graph that contains only unidirectional links. We call this the locally treelike and oriented property. Using this property, we derive a set of recursion relations for the components of right and left eigenvectors associated with the leading eigenvalue. These recursion relations have first been derived in Ref. [44] using the cavity method [42,45,50–53], a method borrowed from the statistical physics of spin glasses [54,55]. In the present paper, we present an alternative derivation for these recursion relations based on the Schur formula [56], which we believe is simpler to understand and thus more insightful.

The outline of the paper is the following. In Sec. II, we define the random matrices and spectral quantities we study in this paper. In Sec. III, we present an overview of the theoretical results derived in this paper. In Sec. IV, we apply these theoretical results to a linear stability analysis of stationary states in networked systems. In Sec. V, we compare theoretical results for infinitely large matrices with numerical data for matrices of finite size. In Sec. VI, we discuss extensions of the theory presented in Sec. III to the cases of adjacency matrices with diagonal disorder and adjacency matrices of random graphs that contain nondirected links. Lastly, in Sec. VII, we present a discussion of the main results. A detailed description of mathematical derivations are presented in the appendices. In Appendix A, we show that a linear set of randomly coupled differential equations, of the form given by Eq. (1), is stable if and only if all the eigenvalues of \mathbf{A} have negative real parts. Appendix B details the algorithm we use to generate graphs with a prescribed degree distribution, and in Appendix C, we discuss properties of oriented ring graphs. In Appendix D, we show that the algebraic multiplicity of the $-d$ -eigenvalue of a random, directed graph is related to the size of its strongly

connected component. Lastly, in Appendices E–I, we derive recursion relations for the entries of right and left eigenvectors of random, directed graphs, which are based on the Schur formula.

A. Notation

We use lower case symbols for deterministic variables, e.g., x and y . We write (column) vectors as \vec{x} and \vec{y} , while for adjoint row vectors we write \vec{x}^\dagger and \vec{y}^\dagger . The inproduct $\vec{x} \cdot \vec{y} = \vec{x}^\dagger \vec{y} = \sum_{k=1}^n x_k^* y_k$, where x_k^* is the complex conjugate of x_k . Matrices are written in boldface, e.g., \mathbf{x} and \mathbf{y} .

We write random variables in upper case, e.g., X and Y . The probability distribution of a random variable X is denoted by $p_X(x)$. There are a few exceptions to the use of upper case letters to represent random quantities. For example, we use the notation $\lambda_j(\mathbf{A})$ to denote the j th eigenvalue of a random matrix \mathbf{A} , and we write $p_X(x; \mathbf{A})$ for the probability distribution of a random variable X that depends on the matrix \mathbf{A} . We denote averages with respect to the distribution $p_{\mathbf{A}}(\mathbf{a})$ by $\langle \cdot \rangle$. We denote the identity matrix by $\mathbf{1}_n$ and we use $\{1, 2, \dots, n\} = [n]$. We write $\int_{\mathbb{R}} dx f(x)$ for an integral over the real line and $\int_{\mathbb{C}} d^2z f(z) = \int dx dy f(x + iy)$ for an integral over the complex plane. We denote the Dirac distribution over the real line by $\delta(x)$ and we denote the Dirac distribution over the complex plane by $\delta(z) = \delta(x)\delta(y)$, where $z = x + iy \in \mathbb{C}$.

II. SYSTEM SETUP AND DEFINITIONS

In this section, we define the random matrices and the spectral properties we study in this paper.

A. Adjacency matrices of random directed graphs with a prescribed degree distribution

We consider random matrices \mathbf{A} as in Eq. (3), where J is a square matrix of size n with real entries $J_{jk} \in \mathbb{R}$ that are independent and identically distributed (i.i.d.) random variables drawn from a distribution p_J , and where \mathbf{C} is the adjacency matrix of a random, directed graph \mathcal{G} of size n with a prescribed degree distribution $p_{K^{\text{in}}, K^{\text{out}}}(k, \ell)$ of indegrees K^{in} and outdegrees K^{out} [2,4,37]; note that we call the number of vertices in a graph its size.

For a simple graph \mathcal{G} the entries of the adjacency matrix satisfy $C_{jk} \in \{0, 1\}$ and $C_{jj} = 0$. We use the convention that $C_{jk} = 1$ if the graph \mathcal{G} has a directed edge from node j to node k . Therefore the indegree K_j^{in} of the j th node equals the number of nonzero elements in the j th column of \mathbf{C} ,

$$K_j^{\text{in}} := \sum_{k=1}^n C_{kj}, \tag{5}$$

and the outdegree K_j^{out} of the j th node equals the number of nonzero elements in the j th row,

$$K_j^{\text{out}} := \sum_{k=1}^n C_{jk}. \tag{6}$$

The inneighborhood ∂_j^{in} and the outneighborhood ∂_j^{out} of the j th node are defined by

$$\partial_j^{\text{in}} := \{k \in [n] : C_{kj} = 1\} \tag{7}$$

and

$$\partial_j^{\text{out}} := \{k \in [n] : C_{jk} = 1\}, \tag{8}$$

respectively, and

$$\partial_j := \partial_j^{\text{in}} \cup \partial_j^{\text{out}} \tag{9}$$

is the neighborhood of node j .

We say that \mathcal{G} is a random graph with a prescribed degree distribution $p_{K^{\text{in}}, K^{\text{out}}}(k, \ell)$ if the following properties hold: (i) the degrees $(K_j^{\text{in}}, K_j^{\text{out}})$ are i.i.d. random variables with a joint probability distribution $p_{K^{\text{in}}, K^{\text{out}}}(k, \ell)$ and with the additional constraint $\sum_{j=1}^n K_j^{\text{in}} = \sum_{j=1}^n K_j^{\text{out}}$; (ii) given a certain degree sequence $\{K_j^{\text{in}}, K_j^{\text{out}}\}_{j=1}^n$, the nodes are connected randomly and hence the edges of \mathcal{G} are generated by the configuration model [2,4,37]. In Appendix B, we describe in detail the algorithm we use to sample random graphs with a prescribed degree distribution.

In the specific case when $J_{jk} = 1$ and $d = 0$, \mathbf{A} is the adjacency matrix of a random, directed graph. The variables J_{jk} are the weights associated with the links of the graph represented by the adjacency matrix \mathbf{C} , and hence for $J_{jk} \neq 1$, the matrix \mathbf{A} is the adjacency matrix of a weighted graph. The constant parameter d affects the spectral properties of \mathbf{A} in a trivial manner, but plays an important role in a stability analysis of dynamical systems.

B. Ensemble parameters

The random matrix ensemble defined by Eq. (3) depends on the following parameters: the distribution p_J of weights J_{ij} , the joint distribution $p_{K^{\text{in}}, K^{\text{out}}}$ of indegrees and outdegrees, the real number d , and the size n .

We often use the moments of p_J and $p_{K^{\text{in}}, K^{\text{out}}}$ to specify the model of interest. The m th moment of p_J is defined by

$$\langle J^m \rangle := \int_{-\infty}^{\infty} dx x^m p_J(x), \tag{10}$$

and the (m, o) th moment of $p_{K^{\text{in}}, K^{\text{out}}}$ is given by

$$\langle (K^{\text{in}})^m (K^{\text{out}})^o \rangle := \sum_{k=0}^{\infty} \sum_{\ell=0}^{\infty} p_{K^{\text{in}}, K^{\text{out}}}(k, \ell) k^m \ell^o. \tag{11}$$

Among those, important parameters are the *mean degree*

$$c := \langle K^{\text{in}} \rangle = \langle K^{\text{out}} \rangle \tag{12}$$

and the *degree correlation coefficient*

$$\rho := \frac{\langle K^{\text{in}} K^{\text{out}} \rangle - c^2}{c^2}. \tag{13}$$

The mean degree is equal to the average number of edges that enter or leave a uniformly and randomly selected vertex in the graph. The parameter $c(J)$ is the average interaction strength felt by a degree of freedom in the dynamical system governed by Eq. (2). The degree correlation coefficient ρ characterizes the correlations between indegrees and outdegrees of vertices in the graph. If $\langle K_j^{\text{in}} K_j^{\text{out}} \rangle = \langle K_j^{\text{in}} \rangle \langle K_j^{\text{out}} \rangle$, then $\rho = 0$, which means that indegrees and outdegrees are uncorrelated. If $\rho > 0$ ($\rho < 0$), then indegrees and outdegrees are positively (negatively) correlated.

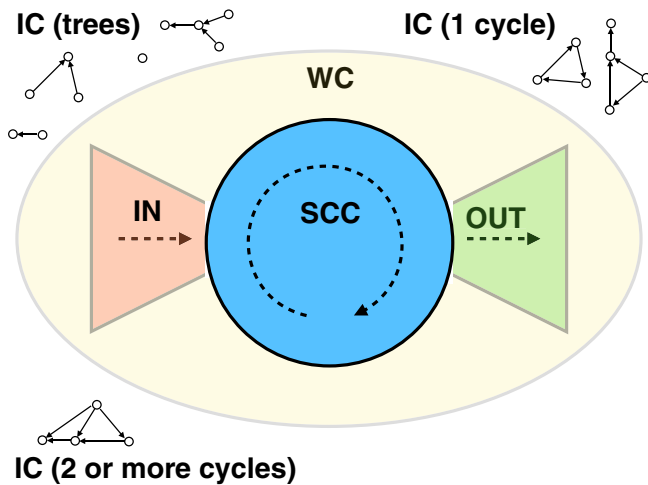


FIG. 1. Topology of directed graphs. Graphical illustration of the connected components of directed graphs (bow-tie diagram, see also Refs. [28,40,41]): largest strongly connected component (SCC), largest incomponent (IN), largest outcomponent (OUT), largest weakly connected component (WC), and isolated components (IC), which consist of isolated trees and cycles.

C. Topology of directed graphs

We discuss properties of the topology of random, directed graphs with a prescribed degree distribution that will be relevant to understand their spectra, namely, connected components, percolation transitions, the locally treelike and oriented structure, and oriented rings.

1. Connected components of directed graphs

Connected components are subgraphs that characterize the topology of a directed graph. In particular, the connected components determine which nodes in a dynamical system are affected by a local perturbation.

The topology of a directed graph can be depicted with a bow-tie diagram, see Fig. 1 and Refs. [28,40,41,57]. The bow-tie diagram depicts the following subgraphs of a directed graph: the largest strongly connected component (SCC), the incomponent (IN), and the outcomponent (OUT). Besides these three components, directed graphs also have a largest weakly connected component (WC) and isolated components (IC), also depicted in Fig. 1. Finally, directed graphs contain tendrils [40,41]. Since tendrils play a minor role in the spectral properties of directed graphs, we omit them in Fig. 1.

We present definitions of the abovementioned subgraphs. The SCC is the largest subgraph that is strongly connected. A subgraph is *strongly connected* if for each pair of vertices in the subgraph, say j and k , the following two conditions are met: (a) there exist at least one path starting in j and ending in k (b) there exist at least one path starting in k and ending in j . The IN consists of all nodes that can reach the strongly connected component and the OUT consist of all nodes that can be reached from the strongly connected component (by following the edges of the directed graph). The WC is the largest connected component obtained by ignoring the directionality of edges. The tendrils consist of all vertices that belong to the weakly connected component, but do not

belong to the incomponent and outcomponent. Finally, the IC are connected subgraphs that are disconnected from the largest weakly connected component.

2. Size of the connected components of random directed graphs with a prescribed degree distribution

For random, directed graphs with a prescribed degree distribution $p_{K^{\text{in}}, K^{\text{out}}}(k, \ell)$, the relative sizes of the connected components are deterministic in the limit of large n . We denote the limiting value of the relative size of the SCC by s_{sc} (i.e., the fraction of nodes that belong to the SCC), and analogously, we use s_{in} , s_{out} , s_{wc} , s_{t} , and s_{ic} , for the limiting values of the relative sizes of the incomponent, outcomponent, largest weakly connected component, tendrils, and isolated components, respectively.

We say that a random graph has a giant SCC when $s_{\text{sc}} > 0$ and, analogously, we say that a random graph has a giant IN, OUT, or WC when, respectively, $s_{\text{in}} > 0$, $s_{\text{out}} > 0$, or $s_{\text{wc}} > 0$.

For small enough values of $c(\rho + 1)$, it holds that $s_{\text{sc}} = 0$ and $s_{\text{wc}} = 0$, whereas for large enough values of $c(\rho + 1)$, it holds that $s_{\text{sc}} > 0$ and $s_{\text{wc}} > 0$. The percolation transitions associated with a giant SCC and a giant WC take place at the threshold values of $c(\rho + 1)$ for which the quantities s_{sc} and s_{wc} vanish, respectively. Since by definition $s_{\text{in}} \geq s_{\text{sc}}$ and $s_{\text{out}} \geq s_{\text{sc}}$, and $s_{\text{in}} = s_{\text{out}} = 0$ if $s_{\text{sc}} = 0$, the percolation transition associated with the IN and OUT is identical to the percolation transition associated with the SCC. Hence, in directed graphs, there exist two percolation transitions, namely, a transition associated with the SCC and one associated with the WC.

In Ref. [40], an exact set of equations have been derived for the relative sizes of the various connected components in directed graphs. It was found that

$$s_{\text{in}} = 1 - \sum_{k=0}^{\infty} a^k \sum_{\ell=0}^{\infty} p_{K^{\text{in}}, K^{\text{out}}}(k, \ell) \quad (14)$$

and

$$s_{\text{out}} = 1 - \sum_{\ell=0}^{\infty} b^{\ell} \sum_{k=0}^{\infty} p_{K^{\text{in}}, K^{\text{out}}}(k, \ell), \quad (15)$$

where a and b are the smallest nonnegative solutions to the equations

$$a = \sum_{k=0}^{\infty} a^k \sum_{\ell=0}^{\infty} \frac{\ell p_{K^{\text{in}}, K^{\text{out}}}(k, \ell)}{c} \quad (16)$$

and

$$b = \sum_{\ell=0}^{\infty} b^{\ell} \sum_{k=0}^{\infty} \frac{k p_{K^{\text{in}}, K^{\text{out}}}(k, \ell)}{c}. \quad (17)$$

The size of the SCC is given by

$$s_{\text{sc}} = s_{\text{in}} + s_{\text{out}} + s_{\text{t}} - s_{\text{wc}}, \quad (18)$$

where

$$s_{\text{t}} - s_{\text{wc}} = \sum_{k=0}^{\infty} \sum_{\ell=0}^{\infty} p_{K^{\text{in}}, K^{\text{out}}}(k, \ell) a^k b^{\ell} - 1. \quad (19)$$

The percolation transition of the SCC happens when s_{sc} turns positive, which happens when

$$\sum_{k=0}^{\infty} \sum_{\ell=0}^{\infty} \frac{k \ell p_{K^{in}, K^{out}}(k, \ell)}{c} = 1. \quad (20)$$

Using in Eq. (20) the definitions (12) and (13) for, respectively, the mean degree c and the degree correlation coefficient ρ , we obtain that at the critical connectivity

$$c = \frac{1}{1 + \rho} \quad (21)$$

a giant SCC emerges in a random, directed graph with a prescribed degree distribution.

Equation (21) implies that random graphs with positively correlated indegrees and outdegrees percolate at lower connectivities than random graphs with negatively correlated indegrees and outdegrees.

3. Oriented and locally treelike structure

If the mean degree c is finite, then random graphs with a prescribed degree distribution are locally treelike and oriented. This means that for large enough n , the finite neighborhood of a randomly selected node is with probability one an oriented tree [58]. We say that a graph is a tree if it is connected and does not contain a cycle and we say that a graph is oriented if all its edges are unidirectional, i.e., $C_{ij}C_{ji} = 0$ for each pair (i, j) . For a precise mathematical definition of locally treelike graphs, we refer to Sec. 2.1 of Ref. [38].

4. Oriented rings

Since random, directed graphs with a prescribed degree distribution are locally treelike, one may think that cycles of finite length are not important to describe their spectral properties in the limit of large n . However, this is only partly true since in the limit $n \rightarrow \infty$ there exist a finite number of cycles of finite length ℓ , and these cycles may affect the value of the leading eigenvalue.

We focus on subgraphs that are oriented rings since only their contribution matters to the spectrum of \mathbf{A} . An oriented ring of length ℓ is an ℓ -tuple of nodes i_1, i_2, \dots, i_ℓ for which

$$A_{i_1 i_2} A_{i_2 i_3} \dots A_{i_{\ell-1} i_\ell} A_{i_\ell i_1} \neq 0. \quad (22)$$

In the limit $n \rightarrow \infty$, the average number of oriented rings of length ℓ in a random, directed graph with a prescribed degree distribution is given by (see Appendix C)

$$\langle N(\ell) \rangle = \frac{1}{\ell} [c(\rho + 1)]^\ell, \quad (23)$$

and for $c(\rho + 1) < 1$ the total number of oriented rings of finite length reads

$$\langle N \rangle = \sum_{\ell=2}^{\infty} \langle N(\ell) \rangle = -\ln[1 - c(\rho + 1)] - c(\rho + 1).$$

Note that $\langle N \rangle$ diverges for $c(\rho + 1) \rightarrow 1$.

The distribution of $N(\ell)$ is Poissonian with mean $\langle N(\ell) \rangle$ [59], and therefore the probability p_+ that there exists at least one oriented ring of length $\ell \geq 2$ is given by

$$p_+ = 1 - e^{-\langle N \rangle} = 1 - (1 - c(\rho + 1))e^{c(\rho + 1)}. \quad (24)$$

Note that $p_+ \rightarrow 1$ when $c(\rho + 1) \rightarrow 1$ and $p_+ \rightarrow 0$ when $c(\rho + 1) \rightarrow 0$.

D. Spectral observables

1. Finite matrices

The eigenvalues $\{\lambda_\alpha(\mathbf{A})\}_{\alpha \in [n]}$ are the complex roots of the algebraic equation [60]

$$\det(\mathbf{A} - \lambda \mathbf{1}_n) = 0. \quad (25)$$

We sort the eigenvalues in decreasing order, so that

$$\text{Re}[\lambda_1(\mathbf{A})] \geq \text{Re}[\lambda_2(\mathbf{A})] \dots \geq \text{Re}[\lambda_n(\mathbf{A})]. \quad (26)$$

If an eigenvalue is degenerate, then it appears more than once in the sequence. We call λ_1 the *leading* eigenvalue of \mathbf{A} and λ_2 the *subleading* eigenvalue.

A right eigenvector $\vec{R}(\mathbf{A})$ and a left eigenvector $\vec{L}(\mathbf{A})$ associated with an eigenvalue λ_α are nonzero vectors that fulfill

$$\mathbf{A} \vec{R} = \lambda_\alpha \vec{R}, \quad \text{and} \quad \vec{L}^\dagger \mathbf{A} = \lambda_\alpha \vec{L}^\dagger. \quad (27)$$

We use the notation R_j and L_j for the components or entries of the right and left eigenvectors, respectively, where $j \in [n]$.

The number m of linearly independent right eigenvectors (or left eigenvectors) is smaller or equal than the size of the matrix and greater or equal than the number of eigenvalues of \mathbf{A} . If $m = n$, then the matrix is diagonalizable.

Right and left eigenvectors of \mathbf{A} can be chosen biorthonormal,

$$\vec{L}_\beta \cdot \vec{R}_\alpha = \delta_{\alpha\beta}, \quad (28)$$

where $\alpha, \beta \in [m]$ is a label to identify the m linearly independent right (left) eigenvectors. Biorthonormality is not sufficient to uniquely characterize right and left eigenvectors since they can be rescaled as $c_\alpha \vec{R}_\alpha$ and $c_\alpha^{-1} \vec{L}_\alpha$, with $c_\alpha \in \mathbb{C}$. In order to uniquely define the right and left eigenvectors, we take the convention that

$$\text{Im} \left[\sum_{j=1}^n R_{\alpha,j} \right] = 0, \quad \text{Re} \left[\sum_{j=1}^n R_{\alpha,j} \right] \geq 0 \quad (29)$$

and we set

$$\sum_{j=1}^n |R_{\alpha,j}|^2 = n. \quad (30)$$

The relation (29) specifies the argument of c_α and the relation (30) specifies its norm. When using the conventions (28)–(30), the norm $\sum_{j=1}^n |L_{\alpha,j}|^2$ and the argument of $\sum_{j=1}^n L_{\alpha,j}$ are functions of the entries of \mathbf{A} .

2. Infinitely large matrices

In order to characterize properties of random matrices in the limit of $n \rightarrow \infty$, we use sets and distributions. The spectrum of \mathbf{A} is the set

$$\sigma(\mathbf{A}) := \{\lambda \in \mathbb{C} : \det(\mathbf{A} - \lambda \mathbf{1}_n) = 0\} \quad (31)$$

of eigenvalues of \mathbf{A} . For finite n , $\sigma(\mathbf{A})$ is discrete. For large n , the closure $\overline{\sigma(\mathbf{A})}$ of the spectrum converges to a limit

$$\lim_{n \rightarrow \infty} \overline{\sigma(\mathbf{A})} = \sigma \cup \Gamma, \quad (32)$$

where σ is a deterministic set and Γ is a random set. The deterministic spectrum

$$\sigma = \sigma_c \cup \sigma_d \tag{33}$$

consists of a continuous part σ_c and a discrete part σ_d .

The continuous part

$$\sigma_c = \sigma_{sc} \cup \sigma_{ac} \tag{34}$$

consists of a set σ_{ac} of nonzero Lebesgue measure, which we call the absolutely continuous part, and a set σ_{sc} of zero Lebesgue measure, which we call the singular continuous part. We will be interested in the boundary $\partial\sigma_{ac}$ of the set σ_{ac} and use the notation

$$\lambda_b \in \partial\sigma_{ac} \tag{35}$$

for eigenvalues located at the boundary of σ_{ac} .

The discrete part of the spectrum consists of deterministic *outlier eigenvalues*, which we denote by λ_{isol} . We say that $\lambda_{isol} \in \sigma$ is an outlier eigenvalue—sometimes also called an isolated eigenvalue—if there exists an $\epsilon > 0$, such that

$$\sigma \cap \{\lambda \in \mathbb{C} : |\lambda_{isol} - \lambda| < \epsilon\} = \{\lambda_{isol}\}. \tag{36}$$

In the examples considered in this paper, there will be maximal one deterministic outlier eigenvalue.

Lastly, the limiting spectrum in Eq. (32) may contain a random set Γ that consists of stochastic (outlier) eigenvalues.

The spectral distribution

$$\mu(\lambda; \mathbf{A}) = \frac{1}{n} \sum_{\alpha=1}^n \delta(\lambda - \lambda_\alpha(\mathbf{A})) \tag{37}$$

denotes the relative number of eigenvalues that occupy a certain region of the complex plane, and we denote its asymptotic expression by

$$\mu(\lambda) = \lim_{n \rightarrow \infty} \mu(\lambda; \mathbf{A}). \tag{38}$$

The support of the distribution is the closure of the set $\{\lambda \in \mathbb{C} : \mu(\lambda) \neq 0\}$. Since in general $\mu(\lambda_{isol}) = 0$, the outliers do not belong to the support of μ , and therefore the support of μ is a subset of σ .

We are also interested in the statistics of the components of right and left eigenvectors. Let \vec{R} (\vec{L}) be the right (left) eigenvector associated with an eigenvalue λ . We define the random variable R (L) as a uniformly randomly sampled entry of the eigenvector. If R and L refer to an outlier, then we use the notation R_{isol} and L_{isol} ; if R and L refer to an eigenvalue located at the boundary of σ_{ac} , then we use R_b and L_b .

The distributions of the random variables R and L are defined by

$$p_R(r|\mathbf{A}) = \frac{1}{n} \sum_{i=1}^n \delta(r - R_i) \tag{39}$$

and

$$p_L(l|\mathbf{A}) = \frac{1}{n} \sum_{i=1}^n \delta(l - L_i), \tag{40}$$

respectively, where $\delta(z)$ is the Dirac-delta distribution in the complex plane. In the limit $n \rightarrow \infty$, the distributions $p_R(r|\mathbf{A})$

and $p_L(l|\mathbf{A})$ often converge to deterministic limits

$$p_R(r) = \lim_{n \rightarrow \infty} p_R(r|\mathbf{A}), \quad p_L(l) = \lim_{n \rightarrow \infty} p_L(l|\mathbf{A}). \tag{41}$$

We denote the moments of the limiting distributions $p_R(r)$ and $p_L(l)$ by

$$\langle R^m \rangle = \int d^2r p_R(r) r^m, \quad \text{and} \quad \langle L^m \rangle = \int d^2l p_L(l) l^m, \tag{42}$$

where $d^2r = d\text{Re}(r)d\text{Im}(r)$ and $d^2l = d\text{Re}(l)d\text{Im}(l)$.

We say that a spectral quantity of a random, directed graph is *universal* if it converges for $n \rightarrow \infty$ to a deterministic limit that only depends on the first few moments of the distributions p_J and $p_{K^{in}, K^{out}}$.

III. SPECTRAL PROPERTIES OF INFINITELY LARGE RANDOM AND DIRECTED GRAPHS

In this section, we present the main theoretical results in the limit of large n for the spectral properties of adjacency matrices of random, directed graphs with a prescribed degree distribution (as defined in Sec. II).

The giant SCC plays an important role in the spectrum of random, directed graphs. Let us therefore recollect that for random, directed graphs with a prescribed degree distribution

$$s_{sc} = 0 \quad \text{if} \quad c(\rho + 1) \leq 1, \tag{43}$$

and

$$s_{sc} > 0 \quad \text{if} \quad c(\rho + 1) > 1. \tag{44}$$

This section is organized as follows. First, we discuss in Sec. III A how the spectral distribution $\mu(\lambda)$ depends on the size of the SCC. Second, we discuss in Sec. III B how the deterministic part σ of the spectrum is governed by the SCC. In particular, we show that if $c(\rho + 1) > 1$, then σ contains a continuous part σ_{ac} and (possibly) a deterministic outlier λ_{isol} , both determined by the SCC. On the other hand, if $c(\rho + 1) < 1$, then the spectrum $\sigma = \{-d\}$. In Sec. III B we also discuss how the nondeterministic part Γ of the spectrum is determined by oriented ring graphs. Third, in Sec. III C, we present recursion relations in the distribution of entries of right eigenvectors associated with deterministic outliers λ_{isol} or with eigenvalues λ_b located at the boundary of σ_{ac} . Subsequently, we use in Secs. III D and III E these recursive distributional equations to derive analytical expressions for the boundary of σ_{ac} and the deterministic outliers λ_{isol} , respectively. In Sec. III F, we present results for the leading eigenvalue λ_1 . We obtain exact analytical expressions for the typical value of the leading eigenvalue λ_1 in the regime where $c(\rho + 1) > 1$, while for $c(\rho + 1) < 1$ we show that the leading eigenvalue is governed by oriented ring graphs. Lastly, in Sec. III G, we discuss the spectral gap, and in Sec. III H, we comment on the relation between the derived results and the Perron-Frobenius theorem [60].

We focus on right eigenvectors since the left eigenvectors of \mathbf{A} are simply the right eigenvectors of \mathbf{A}^T . Therefore results for left eigenvectors can be obtained from the results for right eigenvectors through the substitutions “ $R \rightarrow L$ ” and “in \leftrightarrow out.”

A. Spectral distribution

We discuss how the spectral distribution $\mu(\lambda)$ of an adjacency matrix of a random, directed graph depends on the size of its connected components. In Appendix D, we show that the spectral distribution $\mu(\lambda)$ takes the form

$$\mu(\lambda) = (1 - s_{sc})\delta(\lambda + d) + s_{sc} \tilde{\mu}(\lambda), \tag{45}$$

where $\tilde{\mu}(\lambda)$ is a normalized distribution associated with the SCC and supported on σ_{ac} ; see Fig. 9 of Ref. [45] for an example of $\tilde{\mu}(\lambda)$ in the case of directed Erdős-Rényi ensembles.

Equation (45) implies that the algebraic multiplicity of the $-d$ eigenvalue is equal to

$$n(1 - s_{sc})(1 + o_n(1)). \tag{46}$$

The high degeneracy of the $-d$ eigenvalue follows from the fact that (i) random, directed graphs with a prescribed degree distribution are locally treelike and oriented and (ii) an oriented tree graph has only zero eigenvalues, and in the present case where the diagonal elements are all set equal to $-d$, all eigenvalues of an oriented tree graph are equal to $-d$. Hence, a random, directed graph develops eigenvalues that differ from $-d$ through the presence of oriented rings, which are defined by Eq. (22) in Sec. II C 4.

B. Spectrum

The spectrum $\sigma \cup \Gamma$ of a random, directed graph in the limit of infinitely large n is determined by three topological components, namely the SCC, nodes that do not belong to the SCC, and oriented rings of finite length.

If $c(\rho + 1) > 1$, then the deterministic part σ of the spectrum consists of a continuous set σ_{ac} and (possibly) an outlier λ_{isol} , both determined by the SCC.

On the other hand, if $c(\rho + 1) < 1$, then $\sigma = \{-d\}$.

In addition, due to the presence of cycles of finite length, random, directed graphs can contain stochastic outliers. Stochastic outliers appear in the spectrum due to the presence of oriented rings in the random, directed graph. As shown in the Appendix C, the eigenvalues of an oriented ring of length ℓ are located on a circle of radius

$$\gamma = \left(\prod_{j=1}^n |J_j| \right)^{1/\ell}, \tag{47}$$

where J_j are the random weights attributed to the ring graph. If $c(\rho + 1) < 1$, then these eigenvalues appear as outliers in the spectrum. On the other hand if $c(\rho + 1) > 1$, then the eigenvalues of oriented rings form stochastic outliers only when γ is large enough, so that they do not belong to σ_{ac} . As a consequence, unweighted graphs, i.e., with $J_{ij} = 1$, do not contain stochastic outliers when $c(\rho + 1) > 1$. However, if the graph has weighted links, then stochastic outlier eigenvalues exist, even though the probability to observe them is in general small.

C. Recursive distributional equations for right eigenvectors

In Appendix E, we derive a set of recursive distributional equations for the distributions p_R as defined in Eq. (41) for right eigenvectors associated with deterministic eigenvalue

outliers λ_{isol} and with eigenvalues located at the boundary of the continuous part σ_{ac} . In particular, we show that the distribution p_R solves the recursive distributional equation

$$p_R(r) = \sum_{k=0}^{\infty} \sum_{\ell=0}^{\infty} p_{K^{in}, K^{out}}(k, \ell) \times \int \prod_{j=1}^{\ell} d^2 r_j q_R(r_j) \int \prod_{j=1}^{\ell} dx_j p_J(x_j) \times \delta \left[r - \frac{\sum_{j=1}^{\ell} x_j r_j}{\lambda + d} \right], \tag{48}$$

where q_R is a distribution that solves

$$q_R(r) = \sum_{k=0}^{\infty} \sum_{\ell=0}^{\infty} p_{K^{in}, K^{out}}(k, \ell) \frac{k}{c} \times \int \prod_{j=1}^{\ell} d^2 r_j q_R(r_j) \int \prod_{j=1}^{\ell} dx_j p_J(x_j) \times \delta \left[r - \frac{\sum_{j=1}^{\ell} x_j r_j}{\lambda + d} \right]. \tag{49}$$

When

$$p_{K^{in}, K^{out}}(k, \ell) = p_{K^{in}}(k) p_{K^{out}}(\ell), \tag{50}$$

it holds that $p_R(r) = q_R(r)$ and we recover the results from Ref. [44].

The relations (48) and (49) admit, for any value of λ , the *trivial* solution

$$p_R(r) = \delta(r), \tag{51}$$

which cannot be associated with a right eigenvector of the random matrix \mathbf{A} . However, the relations (48) and (49) also admit *normalizable* solutions for which

$$\int d^2 r p_R(r) |r|^2 \in (0, \infty). \tag{52}$$

These normalizable solutions are associated with right eigenvectors of the random matrix \mathbf{A} .

As a consequence, we can obtain explicit expressions for the outliers λ_{isol} and the eigenvalues $\lambda_b \in \partial\sigma_{ac}$ by identifying values of λ for which the relations (48) and (49) admit normalizable solutions. This is the program that we pursue in Appendix G, while we present the main results of those derivations in the next two sections.

D. Eigenvalues at the boundary of the continuous part of the spectrum

The spectrum σ contains a continuous part σ_{ac} if $c(\rho + 1) > 1$, as we have shown in Sec. III A. For values $\lambda = \lambda_b \in \partial\sigma_{ac}$ located at the boundary of σ_{ac} , the relations (48) and (49) admit a normalizable solution. Using this criterion, we obtain in Appendix G that

$$|\lambda_b + d|^2 = c(\rho + 1)\langle J^2 \rangle. \tag{53}$$

The relations (48) and (49) provide us also with the statistics of right eigenvectors \vec{R}_b associated with eigenvalues λ_b .

We distinguish between the cases where $\lambda_b \notin \mathbb{R}$ and $\lambda_b \in \mathbb{R}$. In the former case, the components R_b are complex-valued random variables with

$$\langle R_b \rangle = \langle R_b^2 \rangle = 0. \quad (54)$$

On the other hand, if $\lambda_b \in \mathbb{R}$, then the components are real-valued random variables with

$$\langle R_b \rangle = 0, \quad \langle R_b^2 \rangle = 1. \quad (55)$$

In addition to these results, we show in Appendix H that the distribution $p_{R_b}(r)$ contains a delta peak at the origin due to all nodes that do not belong to the giant outcomponent, i.e.,

$$p_{R_b}(r) = (1 - s_{\text{out}})\delta(r) + s_{\text{out}}\tilde{p}_{R_b}(r), \quad (56)$$

where s_{out} is the size of the giant outcomponent given by Eq. (15), and $\tilde{p}_{R_b}(r)$ is a normalized distribution.

E. Outlier eigenvalue

There exists a second class of normalizable solutions to Eqs. (48) and (49), which are associated with deterministic outlier eigenvalues λ_{isol} . If $c(\rho + 1) > 1$ and $\langle J^2 \rangle < c(\rho + 1)|\langle J \rangle|$, then there exists a deterministic eigenvalue outlier located at

$$\lambda_{\text{isol}} = -d + c(\rho + 1)\langle J \rangle. \quad (57)$$

Reference [61] observes that Eq. (57) describes well the largest eigenvalue of unweighted adjacency matrices of random graphs with a prescribed degree distribution. In Appendix G, we show that Eq. (57) is in fact an exact expression for the deterministic outlier.

The entries of the eigenvector \vec{R}_{isol} are real, and the first moment of R_{isol} satisfies

$$\frac{\langle R_{\text{isol}} \rangle^2}{\langle R_{\text{isol}}^2 \rangle} = \frac{c^3(\rho + 1)[c(\rho + 1)\langle J \rangle^2 - \langle J^2 \rangle]}{c^2(\rho + 1)^2\langle J \rangle^2[(\langle K^{\text{out}} \rangle^2) - c] + \langle J^2 \rangle\rho_2^{\text{out}}}, \quad (58)$$

where

$$\rho_2^{\text{out}} = \langle K^{\text{in}}(K^{\text{out}})^2 \rangle - c(1 + \rho)\langle (K^{\text{out}})^2 \rangle. \quad (59)$$

For uncorrelated indegrees and outdegrees it holds that $\rho = 0$ and $\rho_2^{\text{out}} = 0$, and we recover the results in Ref. [44].

Analogous to Eq. (56) for p_{R_b} , the distribution $p_{R_{\text{isol}}}$ takes the form

$$p_{R_{\text{isol}}}(r) = (1 - s_{\text{out}})\delta(r) + s_{\text{out}}\tilde{p}_{R_{\text{isol}}}(r), \quad (60)$$

where s_{out} is the size of the giant outcomponent (15) and $\tilde{p}_{R_{\text{isol}}}(r)$ is a normalized distribution (see Appendix H).

F. Leading eigenvalue

We discuss the implications of the results derived in Secs. III D and III E for the leading eigenvalue λ_1 of random graphs with a prescribed degree distribution $p_{K^{\text{in}}, K^{\text{out}}}$.

1. Distribution of λ_1

The theory in Secs. III E and III D provides exact expressions for the boundary $\partial\sigma_{\text{ac}}$ of the continuous part of the spectrum, which is given by the eigenvalues λ_b in Eq. (53), and the deterministic eigenvalue outlier λ_{isol} , which is given

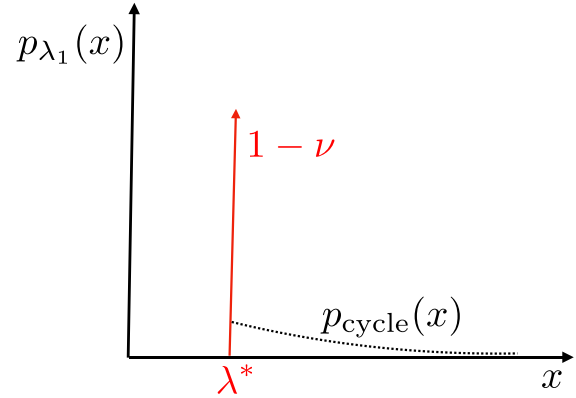


FIG. 2. Distribution of the leading eigenvalue. Sketch of the distribution p_{λ_1} of the leading eigenvalue λ_1 of random matrices \mathbf{A} , as defined in Sec. II, in the regime $c(\rho + 1) > 1$. The distribution consists of a delta distribution at the typical value λ^* given by Eq. (61) and a continuous distribution p_{cycle} with a total weight $\nu \approx 0$.

by Eq. (57), in random, directed graphs that are infinitely large. The question remains how the leading eigenvalue λ_1 is related to λ_b and λ_{isol} .

If we neglect the contributions from cycles of finite length ℓ , then the leading eigenvalue of an infinitely large random, directed graph is given by

$$\lambda^* = \begin{cases} \max\{\lambda_{\text{isol}}, |\lambda_b + d| - d\} & \text{if } c(\rho + 1) \geq 1, \\ -d & \text{if } c(\rho + 1) < 1. \end{cases} \quad (61)$$

Hence, if a random, directed graph contains no cycles of small length ℓ in the limit $n \rightarrow \infty$, then Eq. (61) is exact. However, as we have discussed in Sec. II C 4, random, directed graphs with a prescribed degree distribution $p_{K^{\text{in}}, K^{\text{out}}}$ typically contain a finite number of cycles of a given length ℓ , even in the limit $n \rightarrow \infty$, and therefore we need to discuss how these cycles will affect λ_1 .

Cycles that are oriented rings may contribute stochastic outlier eigenvalues to the spectrum, see Sec. II C 4. As a consequence, λ_1 is not a self-averaging quantity but is instead a random variable with a distribution

$$p_{\lambda_1}(x) := \lim_{n \rightarrow \infty} \langle \delta(x - \lambda_1(\mathbf{A})) \rangle \quad (62)$$

of nonzero variance.

The distribution p_{λ_1} takes the form

$$p_{\lambda_1}(x) = (1 - \nu)\delta(x - \lambda^*) + \nu p_{\text{cycle}}(x), \quad (63)$$

where ν is the probability that the leading eigenvalue is a stochastic outlier contributed by an oriented ring, and $p_{\text{cycle}}(x)$ is the distribution of those stochastic outliers that are leading eigenvalues. Note that the distribution $p_{\text{cycle}}(x)$ is supported on the half line $[\lambda^*, \infty)$, see Fig. 2 for a sketch of p_{λ_1} .

Since for $c(\rho + 1) < 1$ it holds that $\lambda^* = -d$, oriented rings will play an important role in $p_{\lambda_1}(x)$ when \mathbf{A} does not have a giant SCC. On the other hand, if \mathbf{A} has a giant SCC, i.e., $c(\rho + 1) > 1$, then it will be unlikely that the leading eigenvalue is a stochastic outlier. We show this explicitly in

the next section for unweighted graphs, and subsequently we discuss the case of weighted graphs.

2. Unweighted graphs

We consider adjacency matrices \mathbf{A} of unweighted graphs, such that $J_{ij} = 1$ for all values of i and j . In this case, we obtain an exact expression for $p_{\lambda_1}(x)$. Indeed, since the eigenvalues of oriented rings with $J_{ij} = 1$ are located on a circle of radius 1 centered around $-d$, see Eq. (47), it holds that

$$v = \begin{cases} 0 & \text{if } c(\rho + 1) \geq 1, \\ p_+ & \text{if } c(\rho + 1) < 1, \end{cases} \quad (64)$$

where p_+ is the probability that the graph contains at least one oriented ring graph, given by Eq. (24). Moreover, it holds that

$$p_{\text{cycle}}(x) = \delta(x - 1 + d), \quad (65)$$

and that

$$\lambda^* = \begin{cases} -d + c(\rho + 1) & \text{if } c(\rho + 1) \geq 1, \\ -d & \text{if } c(\rho + 1) < 1. \end{cases} \quad (66)$$

Using Eqs. (64)–(66) in Eq. (63), we obtain that

$$p_{\lambda_1}(x) = \begin{cases} \delta(x + d - c[\rho + 1]) & \text{if } c(\rho + 1) \geq 1, \\ (1 - p_+)\delta(x + d) + p_+\delta(x - 1 + d) & \text{if } c(\rho + 1) < 1. \end{cases} \quad (67)$$

Hence, the leading eigenvalue of an unweighted, random, directed graph is deterministic and given by the value λ^* if the graph contains a giant SCC. On the other hand, if there is no giant SCC, then with probability p_+ an oriented ring determines the leading eigenvalue.

From Eq. (67), we obtain the average leading eigenvalue, which is given by

$$\langle \lambda_1 \rangle = \begin{cases} -d + c(\rho + 1) & \text{if } c(\rho + 1) \geq 1, \\ -d + p_+ & \text{if } c(\rho + 1) < 1, \end{cases} \quad (68)$$

and its variance

$$\text{var}[\lambda_1] = \begin{cases} 0 & \text{if } c(\rho + 1) \geq 1, \\ p_+(1 - p_+) & \text{if } c(\rho + 1) < 1, \end{cases} \quad (69)$$

where p_+ is given by Eq. (24). Note that $\text{var}[\lambda_1] = 0$ if \mathbf{A} has a giant SCC, and the leading eigenvalue is thus self-averaging in this regime, while $\text{var}[\lambda_1] > 0$ if \mathbf{A} does not have a giant SCC, and the leading eigenvalue is thus not self-averaging in this regime.

In the next section, we discuss how these results extend to the case of weighted graphs for which the J_{ij} are drawn from a nontrivial distribution p_J .

3. Weighted graphs

In the general case of weighted graphs, it is difficult to obtain exact expressions for v and $p_{\text{cycle}}(x)$. However, we can discuss the qualitative features of $p_{\lambda_1}(x)$ in the two regimes $c(\rho + 1) < 1$ and $c(\rho + 1) > 1$.

If $c(\rho + 1) > 1$, then

$$v \approx 0, \quad (70)$$

since it is unlikely that an oriented ring contributes an eigenvalue to the spectrum that is larger than λ^* ; this would require that γ , given by Eq. (47), is larger than $\lambda^* + d$. Therefore, if the graph has a giant SCC, then the variance of λ_1 will be small and the typical value of λ_1 is given by λ^* in Eq. (61). As a consequence, if the graph has a giant SCC, then

$$\langle \lambda_1 \rangle \approx \lambda^* = \begin{cases} -d + c(\rho + 1)\langle J \rangle & \text{if } \langle J \rangle > \sqrt{\frac{\langle J^2 \rangle}{c(\rho + 1)}}, \\ -d + \sqrt{c(\rho + 1)\langle J^2 \rangle} & \text{if } \langle J \rangle \leq \sqrt{\frac{\langle J^2 \rangle}{c(\rho + 1)}}, \end{cases} \quad (71)$$

since λ^* is the typical value of λ_1 .

On the other hand, when $c(\rho + 1) < 1$, then $\lambda^* = -d$, and therefore the leading eigenvalue is with a probability

$$v = p_+ \quad (72)$$

a stochastic outlier coming from an oriented ring graph. Hence, in the absence of a SCC, the variance of $p_{\lambda_1}(x)$ is large.

4. Right eigenvector associated with λ_1

We derive exact expressions for the first moment $\langle R_1 \rangle$ of right eigenvectors associated with the leading eigenvalue λ_1 .

We first consider the case $c(\rho + 1) > 1$. Assuming that the leading eigenvalue takes its typical value λ^* , given by either the outlier λ_{isol} or the maximum value of $\text{Re}[\lambda_b]$, see Eq. (71), we obtain that

$$\frac{\langle R_1 \rangle}{\langle |R_1|^2 \rangle} = \begin{cases} \langle R_{\text{isol}} \rangle / \langle |R_{\text{isol}}|^2 \rangle & \text{if } \langle J \rangle > \sqrt{\frac{\langle J^2 \rangle}{c(\rho + 1)}}, \\ 0 & \text{if } \langle J \rangle \leq \sqrt{\frac{\langle J^2 \rangle}{c(\rho + 1)}}, \end{cases} \quad (73)$$

where $\langle R_{\text{isol}} \rangle / \langle |R_{\text{isol}}|^2 \rangle$ is given by Eq. (58).

On the other hand, if $c(\rho + 1) < 1$, then the right eigenvector of λ_1 will be localized on a finite number of nodes and

$$\frac{\langle R_1 \rangle}{\langle |R_1|^2 \rangle} = 0. \quad (74)$$

Interestingly, we observe in Eq. (73) that $\langle R_1 \rangle$ behaves as an order-parameter of a phase transition between a ferromagnetic phase ($\langle R_1 \rangle > 0$) and a spin glass phase ($\langle R_1 \rangle = 0$). A similar type of behavior has been found in sparse symmetric random matrices [49,62–64]. The analogy between $\langle R_1 \rangle$ and the order parameter of a ferromagnetic phase can be made explicit. Indeed, the leading right eigenvector \vec{R}_1 is the stationary state of a spherical model defined on the graph represented by the adjacency matrix \mathbf{A} , see equations (45) till (52) in Ref. [45]. The spherical model at zero temperature exhibits either a ferromagnetic phase or a spin-glass phase, see Ref. [65], and $\langle R_1 \rangle$ serves as the order parameter for this phase transition. Notice that the $\langle R_1 \rangle = 0$ regime does not correspond to a paramagnetic phase since the spherical model will be frozen into the configuration represented by the leading right eigenvector [65].

5. Limiting case of dense graphs

We discuss the limit of dense graphs by setting $c = n$ and $\rho = 0$. Eq. (71) then reduces to

$$\lambda_1 = \begin{cases} n\langle J \rangle & \langle J \rangle > 0, \\ \sqrt{n\langle J^2 \rangle} & \langle J \rangle \leq 0, \end{cases} \quad (75)$$

which is the well-known expression for the leading eigenvalue λ_1 of a random matrix with independent and identically distributed matrix elements drawn from a distribution p_J , see Refs. [66–71], as well as Refs. [13,20]. However, note that the formula (71) holds for graphs with $c \in O_n(1)$ and therefore the correspondence holds only formally. Analogously, we obtain in this limit that

$$\frac{\langle R_1 \rangle}{\langle |R_1|^2 \rangle} = \begin{cases} 1 & \text{if } \langle J \rangle > 0, \\ 0 & \text{if } \langle J \rangle \leq 0. \end{cases} \quad (76)$$

G. Subleading eigenvalue and spectral gap

The spectral gap is the difference $\lambda_1 - \text{Re}[\lambda_2]$ between the leading eigenvalue and the real part of the subleading eigenvalue. From the results in Secs. III E–III F, we readily obtain an expression for the typical value of the spectral gap when $c(\rho + 1) > 1$, namely,

$$\lambda_1 - \text{Re}[\lambda_2] = \begin{cases} c(\rho + 1)\langle J \rangle - \sqrt{c(\rho + 1)\langle J^2 \rangle} & \text{if } \langle J \rangle > \sqrt{\frac{\langle J^2 \rangle}{c(\rho + 1)}}, \\ 0 & \text{if } \langle J \rangle \leq \sqrt{\frac{\langle J^2 \rangle}{c(\rho + 1)}}. \end{cases} \quad (77)$$

The expected value of the entries of the right eigenvector associated with the subleading eigenvalue satisfies

$$\frac{\langle R_2 \rangle}{\langle |R_2|^2 \rangle} = 0. \quad (78)$$

H. Perron-Frobenius theorem

Here we discuss how the theoretical results are related to the celebrated Perron-Frobenius theorem [60], which states that the eigenvalue λ_1 of a nonnegative matrix, and the components of its right (left) eigenvector, are nonnegative numbers. In other words, the Perron-Frobenius theorem implies that $R_{1,j} \geq 0$ for all $j = 1, 2, \dots, n$.

Interesting conclusions about the localization of eigenvectors of \mathbf{A} are drawn if we combine the Perron-Frobenius theorem with the result (73). If $c(\rho + 1) \leq \langle J^2 \rangle / \langle J \rangle^2$ and $c(\rho + 1) > 1$, such that λ_1 is part of $\partial\sigma_{ac}$, then $\langle R_1 \rangle = 0$ and $\langle R_1^2 \rangle = 1$, see Eq. (30). Since according to the Perron-Frobenius theorem $R_1 \geq 0$, we obtain that $R_1 = 0$ holds with probability one. The two conditions $\lim_{n \rightarrow \infty} \langle R_1(\mathbf{A}_n) \rangle = 0$ and $\lim_{n \rightarrow \infty} \langle R_1^2(\mathbf{A}_n) \rangle = 1$ can be simultaneously valid provided that a few components of the eigenvector $\vec{R}_1(\mathbf{A})$ diverge, such that $\lim_{n \rightarrow \infty} \langle R_1^2(\mathbf{A}_n) \rangle \neq \langle \lim_{n \rightarrow \infty} R_1^2(\mathbf{A}_n) \rangle$.

Hence, (73) and the Perron-Frobenius theorem imply that for nonnegative matrices for which the conditions $c(\rho + 1) \leq \langle J^2 \rangle / \langle J \rangle^2$ and $c(\rho + 1) > 1$ are fulfilled, the right eigenvector \vec{R}_1 associated with the leading eigenvalue is localized on a few nodes.

IV. STABILITY OF COMPLEX SYSTEMS ON RANDOM AND DIRECTED GRAPHS

We apply the results from the previous section to a linear stability analysis of dynamical systems defined on random, directed graphs.

Let $\vec{x}^\dagger(t) = (x_1(t), \dots, x_n(t))$ be the state vector of a large dynamical system of interest, and let

$$\partial_t \vec{x}(t) = \vec{f}[\vec{x}(t)] \quad (79)$$

be a set of nonlinearly coupled differential equations that describe the dynamics of the system of interest.

We consider a fixed point or stationary state \vec{x}^* and study the dynamics described by Eq. (78) in the vicinity of \vec{x}^* . A stationary state is a vector that satisfies

$$f[\vec{x}^*] = 0. \quad (80)$$

Note that a nonlinear system may contain several stationary states [72], but here we are only interested in the dynamics of $\vec{x}(t)$ in the vicinity of one given stationary state. According to the Hartman-Grobman theorem [18,19], the dynamics described by Eq. (78) is in the vicinity of the fixed point \vec{x}^* well approximated by the set of linearly coupled equations given by Eq. (1) with \mathbf{A} the Jacobian of f and

$$\vec{y}(t) = \vec{x}(t) - \vec{x}^* \quad (81)$$

the deviation vector.

The stability of the stationary state \vec{x}^* is determined by the sign of the real part of the leading eigenvalue $\lambda_1(\mathbf{A})$. Indeed, if the matrix \mathbf{A} is diagonalizable, then the dynamics of $\vec{y}^\dagger(t)$ is governed by the eigenvalues $\lambda_j(\mathbf{A})$ and their associated right eigenvectors $\vec{R}_j(\mathbf{A})$ and left eigenvectors $\vec{L}_j(\mathbf{A})$ [60], namely,

$$\vec{y}^\dagger(t) = \sum_{j=1}^n (\vec{y}(0) \cdot \vec{R}_j) e^{\lambda_j t} \vec{L}_j^\dagger. \quad (82)$$

In the case when all eigenvalues have negative real parts, then $\lim_{t \rightarrow \infty} \vec{y}^\dagger(t) = 0$, which implies that the stationary state is stable. On the other hand, if there exists at least one eigenvalue with a positive real part, then the stationary state is unstable. With a bit more effort, one can show that the stability criterion based on the sign of the real part of the leading eigenvalue also holds for systems described by nondiagonalizable matrices, see Appendix A.

From Eq. (81), we also observe that right and left eigenvectors associated with the leading eigenvalue contain valuable information about the dynamics of a system in the vicinity of a fixed point. In particular, the nature of the mode that destabilizes the system takes the form of the left eigenvector \vec{L}_1 . For instance, if the eigenvector \vec{L}_1 has a positive mean $\langle L_1 \rangle > 0$, then the instability is reminiscent of a ferromagnetic phase, whereas if $\langle L_1 \rangle = 0$, then the instability is reminiscent of a spin-glass phase [54,55,73].

We study here the stability of large systems coupled through random matrices \mathbf{A} defined on random, directed graphs with a prescribed degree distribution $p_{K^{\text{in}}, K^{\text{out}}}$, as defined in Sec. II. To this aim, we use the theory from Sec. III F for the leading eigenvalue λ_1 and the associated values of $\langle L_1 \rangle$ and $\langle R_1 \rangle$ (which in this ensemble are equivalent).

A first interesting observation is that for random, directed graphs λ_1 is finite, even in the limit $n \rightarrow \infty$. This stands in contrast with the leading eigenvalue of random, nondirected graphs [47,48], which diverges for increasing n . As a consequence, random, directed graphs with a prescribed degree distribution are stable in the limit of large n , which provides

an interesting take on the diversity-stability debate [9]. The remarkable stability of large dynamical systems defined on directed graphs follows from their locally treelike and oriented nature. Since the local neighborhood of a randomly selected node is an oriented tree, there exist no feedback loops that can amplify the amplitude of local perturbations. On the other hand, in random, nondirected graphs local perturbations are amplified through feedback loops provided by the nondirected links. As a consequence, dynamical systems on locally treelike networks with unidirectional interactions are much more stable than dynamical systems defined on networks with bidirectional interactions.

It remains of interest to study how network architecture affects the stability of large dynamical systems defined on random, directed graphs. Since λ_1 is a random variable in the limit of infinitely large n , we focus first on its typical value λ^* , given by Eq. (71). Interestingly, for the interaction networks defined in Sec. III, the eigenvalue λ^* is solely governed by three parameters that characterize the network architecture: the *effective mean degree*

$$c(1 + \rho) \tag{83}$$

that characterizes the effective number of degrees of freedom each node in the network interacts with; the *coefficient of variation*

$$v_J := \sqrt{\langle J^2 \rangle - \langle J \rangle^2} / \langle J \rangle \tag{84}$$

that characterizes the fluctuations in the coupling strengths between the constituents of the system; and the *effective interaction strength*

$$\alpha := \langle J \rangle / d \tag{85}$$

that quantifies the relative strength of the interactions with regard to the rate d of decay. Hence, the system stability, characterized by the typical value of the leading eigenvalue λ_1 , only depends on these three parameters, and thus enjoys a high degree of universality.

In order to better understand how the three parameters $c(1 + \rho)$, v_J , and α govern the stability of dynamical systems on random, directed graphs, we present in Fig. 3 the phase diagram of the system in the $(v_J, c(1 + \rho))$ plane, for fixed values of $\alpha \in [0, 1]$ and $c(1 + \rho) > 1$. The reason we choose these parameter regimes is because for $\alpha > 1$ there exist no stable phase and for $c(1 + \rho) < 1$ the graph does not have a giant strongly connected component; in the latter regime, the system falls apart in the sense that it is a union of a large number of small isolated subsystems, and thus we are not considering anymore the linear stability of a large system of interacting degrees of freedom.

The phase diagram shows the critical connectivity c_* (black lines) that separates the stable phase ($\text{Re}[\lambda^*] < 0$), for systems at low connectivity $c(1 + \rho)$, from the unstable phase ($\text{Re}[\lambda^*] > 0$), for systems at high connectivity $c(1 + \rho)$. If $\alpha > 0$, then the critical line is determined by

$$c_* = \begin{cases} 1/\alpha, & v_J^2 < 1/\alpha - 1, \\ 1/[\alpha^2(v_J^2 + 1)], & v_J^2 \in [1/\alpha - 1, v_*^2], \\ \backslash & v_J^2 > v_*^2, \end{cases} \tag{86}$$

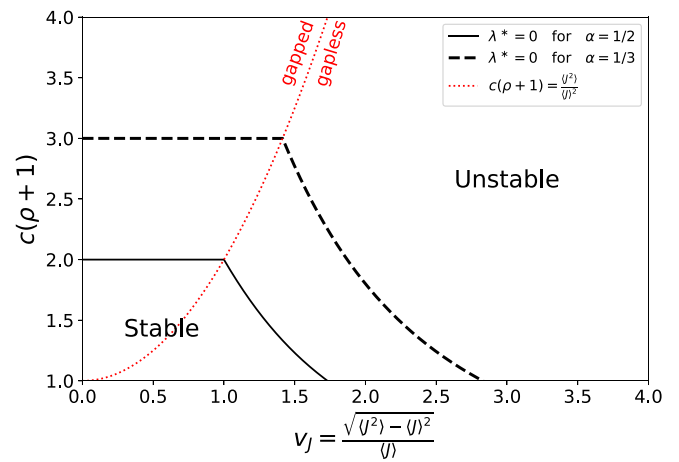


FIG. 3. Universal phase diagram for the stability of dynamical systems on random, directed graphs with positive $\langle J \rangle$. Black solid line and black dashed line separate the unstable phase at large effective connectivity $c(\rho + 1)$ from the stable phase at small connectivity $c(\rho + 1)$ for two given values of $\alpha = \langle J \rangle / d$. The red dotted line separates the gapped phase at small v_J from a gapless phase at high v_J , which can also be considered a transition line from a ferromagnetic phase (gapped) to a spin-glass phase (gapless).

which provides the effective connectivity $c_* = c(\rho + 1)$ for which $\text{Re}[\lambda^*] = 0$ as a function of α and v_J ; in formula (86) we have used the symbol $v_*^2 = \frac{1-\alpha^2}{\alpha^2}$. Since the critical connectivity is finite for all values of α and v_J , it follows that dynamical systems with large enough $c(1 + \rho)$ are unstable, which is consistent with the result in Ref. [20] that states that fully connected systems are unstable when they are large enough. Moreover, we see from Eq. (86) and Fig. 3 that the phase transition to the stable phase at low connectivities has three qualitatively different regimes, which we discuss in the following paragraphs.

The critical value v_* separates the regime $v_J > v_*$, for which the system is unstable, from the regime $v_J < v_*$, for which the system is stable when $c(\rho + 1) > 1$ is small enough. Hence, for small enough fluctuations in the interaction strengths ($v_J < v_*$) it is possible to stabilize a system by rewiring edges in its graph in such a way that the correlation ρ between indegrees and outdegrees decreases.

Stabilizing the system by rewiring edges is however not possible when $v_J > v_*$.

Moreover, the regime $v_J < v_*$ consists of two distinct regimes: a *gapped* regime, which appears when the fluctuations in the interaction strengths are small ($v_J^2 < 1/\alpha - 1$), and a *gapless* regime, which appears when the fluctuations in the interaction strengths are large ($v_J^2 > 1/\alpha - 1$). In Fig. 3, these two regimes are separated by the red dotted line. In the gapped regime the leading eigenvalue is an outlier and the critical connectivity c_* is independent of v_J^2 . This implies that fluctuations do not affect the system stability when the leading eigenvalue is an outlier. On the other hand, in the gapless regime the leading eigenvalue is part of the boundary of the continuous spectrum and the critical connectivity c_* decreases as a function of v_J . In this regime, fluctuations in the interaction strengths render the system less stable. The differences between the gapped and gapless regimes can be

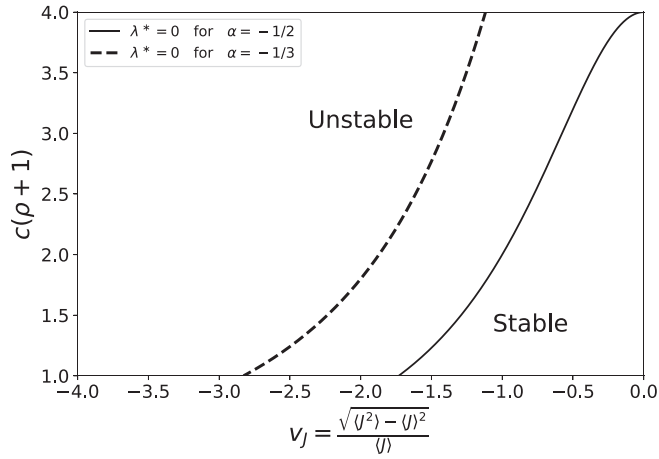


FIG. 4. Universal phase diagram for the stability of dynamical systems on random, directed graphs with negative $\langle J \rangle$. Similar as in Fig. 3, but now for negative α . In this case, there is no gapped (or ferromagnetic) phase.

understood in terms of the nature of the destabilizing mode. In the gapped regime, the mode that destabilizes the system is ferromagnetic, i.e., $\langle L_1 \rangle > 0$, whereas in the gapless regime, the mode that destabilizes the system is spin-glasslike, i.e., $\langle L_1 \rangle = 0$. Hence, increasing the fluctuations v_j for fixed values of the mean strength α does not affect the ferromagnetic mode, which gives an intuitive understanding why the location of the outlier is independent of v_j .

We can quantify the overall stability of systems coupled through random matrices (3) in terms of a single parameter a_{stab} , defined as the area in Fig. 3 where the system is stable and $c(1 + \rho) > 1$. The quantity a_{stab} is given by

$$a_{\text{stab}} = \frac{1}{\alpha} \sqrt{\frac{1-\alpha}{\alpha}} (1 - \sqrt{\alpha(1+\alpha)}) + \frac{1}{\alpha^2} \left[\tanh^{-1} \left(\sqrt{\frac{1-\alpha^2}{\alpha^2}} \right) - \tanh^{-1} \left(\frac{1-\alpha}{\alpha} \right) \right].$$

The area a_{stab} is a monotonic decreasing function of α , which approaches $a_{\text{stab}} \rightarrow 0$ as $\alpha \rightarrow 1$ and $a_{\text{stab}} \rightarrow \infty$ as $\alpha \rightarrow 0$. Thus, the increase of the average interaction strength between the elements of a network system, in the sense that $\langle J \rangle$ approaches d , makes the system less stable.

In Fig. 4, we present the phase diagram for $\alpha < 0$ or equivalently $\langle J \rangle < 0$. Since in this case the outlier is negative, the critical connectivity is

$$c_* = \begin{cases} 1/[\alpha^2(v_j^2 + 1)], & v_j^2 \in [0, v_*^2], \\ \backslash & v_j^2 > v_*^2. \end{cases} \quad (87)$$

Note that for small values of v_j^2 the system is more stable in the case of negative $\langle J \rangle$ since then there exists no outlier that renders the system less stable.

Finally, we discuss how the phase diagrams, given by Figs. 3 and 4, are modified by the presence of small cycles in the network. As illustrated in Fig. 2 and discussed in Sec. III F, there is a finite, albeit small, probability ν that the leading eigenvalue λ_1 is larger than λ^* . This happens when a random, directed graph contains a cycle that generates a

strong enough feedback loop. As a consequence, one should interpret the phase diagrams Figs. 3 and 4 as describing the typical behavior of dynamical systems defined on random, directed graphs in the limit $n \rightarrow \infty$. There is however a small nonzero probability that a random, directed graph contains a cycle that destabilizes the system through the feedback loop that it generates.

V. NUMERICAL EXAMPLES ON MATRICES OF FINITE SIZE

In this section, we compare theoretical results for infinitely large matrices with direct diagonalization results on matrices of finite size $n \sim O(10^3)$. Such numerical experiments reveal the magnitude of finite size effects, which are important for applications because real-world systems are finite. Moreover, this comparison allows us to better understand the potential limitations of the theory.

Since a nonzero d results in a constant shift of all eigenvalues by $-d$, i.e. $\lambda_j \rightarrow \lambda_j - d$, we set in all examples

$$A_{jj} = d = 0, \quad \forall j \in [n]. \quad (88)$$

The numerical experiments are designed as follows. First, we use the algorithm presented in Appendix B to sample a matrix from a random matrix ensemble with a prescribed degree distribution. Second, we use the subroutine `gsl_eigen_nonsymm` from the GNU Scientific Library to compute the n eigenvalues of the sampled matrix and the entries of their right eigenvectors. Third, in order to test the theory in Sec. III, we compute for each matrix sample \mathbf{A} the leading eigenvalue $\lambda_1(\mathbf{A})$, the real part of the subleading eigenvalue $\lambda_2(\mathbf{A})$, and the observable

$$\mathcal{R}_1(\mathbf{A}) = \frac{\sum_{j=1}^n R_{1,j}(\mathbf{A})}{\sqrt{\sum_{j=1}^n |R_{1,j}(\mathbf{A})|^2}}, \quad (89)$$

which quantifies the mean value of the components of the right eigenvector associated with $\lambda_1(\mathbf{A})$. Before we compute $\mathcal{R}_1(\mathbf{A})$ with the above equation, we rotate all the elements $R_{1,j}(\mathbf{A})$ by a constant phase $e^{i\theta}$, such that the empirical mean $\sum_{j=1}^n R_{1,j}(\mathbf{A})$ is a positive real number, in accordance with our conventions in Eq. (29). Lastly, we compute the mean values $\bar{\lambda}_1$, $\bar{\lambda}_2$, and $\bar{\mathcal{R}}_1$ of the sampled populations, together with the standard deviations for each quantity. Empirical mean values for, say $\bar{\lambda}_1$, are compared with either the theoretical ensemble averages $\langle \lambda_1 \rangle$ or with the typical value of λ_1 provided by the deterministic outlier λ_{isol} or by the boundary $|\lambda_{\text{b}}|$ of the continuous part of the spectrum. Note that we use the notation $\langle \lambda_1 \rangle$ for theoretical ensemble averages, while $\bar{\lambda}_1$ is used for empirical mean values over the sampled populations, which forms an estimate of $\langle \lambda_1 \rangle$.

The present section is organized into three sections. In Sec. V A, we consider adjacency matrices of random, directed graphs with negative degree correlations ($\rho < 0$) and unweighted links ($J_{ij} = 1$). For this ensemble, we have derived in Sec. III F 2 exact results for the statistics of the leading eigenvalue λ_1 in the limit $n \rightarrow \infty$. Hence, we expect a good correspondence between theory and experiment in all parameter regimes. Deviations between theory and experiment will be due to finite size effects and finite sampling statistics only.

In Sec. VB, we consider the adjacency matrices of random, directed graphs with positive degree correlations ($\rho > 0$) and weighted links. For this ensemble, we have derived in Sec. III F 3 exact results for the typical value of λ_1 in the regime $c(\rho + 1) > 1$. Hence, we expect in this regime a good correspondence between theory and experiment, and deviations between theory and experiment will be due to finite size effects, finite sampling statistics, and because of deviations between the mean and typical value of λ_1 .

In Sec. VC, we apply the theoretical results of Sec. III to adjacency matrices of random, directed graphs with power-law degree distributions, which have diverging moments. Since the graphs are unweighted, the theory of Sec. III F 2 applies. However, since for power-law random graphs the tails of the degree distributions decay very slowly, we expect to observe deviations between theory and experiment, and in Sec. VC we test the limitations of the theory for power-law random graphs.

Lastly, in Sec. VD, we test the predictions given by Eqs. (56) and (60) for the number of zero-valued entries in the right eigenvector \vec{R}_1 .

A. Adjacency matrices of unweighted and directed random graphs with negative degree correlations

We consider the adjacency matrices of Poissonian random graphs—also called Erdős-Rényi random graphs—and geometric random graphs with negative degree correlation coefficient $\rho \in [-1, 0]$ and with constant weights $J_{ij} = 1$.

For Poissonian random graphs, the prescribed degree distribution is given by

$$p_{K^{\text{in}}, K^{\text{out}}}(k, \ell) = (1 + \rho) p_p(k; c) p_p(\ell; c) - \frac{\rho}{2} [\delta_{k,0} p_p(\ell; 2c) + \delta_{\ell,0} p_p(k; 2c)], \quad (90)$$

where $k, \ell \in \{0, 1, \dots, n - 1\}$ and where

$$p_p(k; c) = \frac{1}{\mathcal{N}_p} \frac{c^k}{k!}, \quad (91)$$

with $\mathcal{N}_p = \sum_{k=0}^{n-1} c^k/k!$ the normalization constant. For $n \rightarrow \infty$, $p_p(k; c)$ is the Poisson distribution with mean degree c and $\mathcal{N}_p = e^c$. For geometric random graphs, the prescribed degree distribution is given by

$$p_{K^{\text{in}}, K^{\text{out}}}(k, \ell) = (1 + \rho) p_g(k; c) p_g(\ell; c) - \frac{\rho}{2} [\delta_{k,0} p_g(\ell; 2c) + \delta_{\ell,0} p_g(k; 2c)], \quad (92)$$

where $k, \ell \in \{0, 1, \dots, n - 1\}$ and where

$$p_g(k; c) = \frac{1}{\mathcal{N}_g} \left(\frac{c}{1+c} \right)^k, \quad (93)$$

with $\mathcal{N}_g = \sum_{k=0}^{n-1} \left(\frac{c}{1+c} \right)^k$ the normalization constant. For $n \rightarrow \infty$, $p_g(k; c)$ is the geometric distribution with mean degree c and $\mathcal{N}_g = c + 1$.

Throughout this section, we consider unweighted graphs for which $J_{jk} = 1$ for all $j \neq k$, and thus

$$p_J(x) = \delta(x - 1). \quad (94)$$

In Fig. 5, we show how the degree correlation coefficient ρ affects the spectral properties of adjacency matrices of random, directed graphs with mean degree $c = 2$. We compare the theoretical results given by Eqs. (57), (53), (58), (68), (73), and (77) with direct diagonalization results.

In panels (a) and (b) of Fig. 5, we provide a global picture of the spectra of adjacency matrices of Poissonian random graphs by comparing the spectra of matrices with $\rho = 0$ and -0.3 . We observe how negative degree correlations contract the spectrum: for $\rho = -0.3$ the leading eigenvalue is smaller than for $\rho = 0$, and the spectrum concentrates around the origin when ρ is more negative.

In panel (c) of Fig. 5, we present a more detailed analysis of the behavior of the leading eigenvalue λ_1 and the subleading eigenvalue λ_2 as a function of ρ . As discussed in Sec. III, for $c(\rho + 1) > 1$, the leading and subleading eigenvalues are self-averaging and given by $\lambda_1 = \lambda_{\text{isol}}$ and $\text{Re}[\lambda_2] = |\lambda_b|$, respectively. These findings are well corroborated by the numerical results in Fig. 5(c). We observe that $\lambda_1 = \lambda_2$ at the critical percolation threshold $\rho = -1 + 1/c = -0.5$, as predicted by the theory. For $c(\rho + 1) < 1$, there does not exist a giant strongly connected component, see Sec. II C 2, and therefore the leading eigenvalue is either 0 or 1, depending on whether the graph contains an oriented ring or not. In this regime, the mean value (λ_1) is given by Eq. (68) and its variance is given by Eq. (69), both findings which are well corroborated by numerical results in Fig. 5(c).

In Fig. 5(d), we present a systematic study of the first moment $\langle R_1 \rangle$ of the eigenvector \vec{R}_1 associated with the leading eigenvalue, which is an outlier for $\rho \geq -0.5$. The theoretical result Eq. (58) is well corroborated by direct diagonalization results for the empirical observable \overline{R}_1 , defined in Eq. (89). We observe a phase transition from a phase with $\langle R_1 \rangle = 0$, for $\rho < -0.5$, to a phase with $\langle R_1 \rangle > 0$, for $\rho > -0.5$. Note that $\langle R_1 \rangle = 0$ for $\rho < -0.5$ since in this regime there exists no giant SCC, and therefore the right eigenvector is localized on an isolated component with a finite number of nodes.

Taken together, the results in Fig. 5 illustrate how the leading eigenvalue of the adjacency matrix of a random, directed graph increases as a function of ρ . These results imply that one can reduce λ_1 significantly reduced a rewiring procedure that decreases correlations between indegrees and outdegrees. These results are in agreement with the phase diagram in Fig. 3, which shows that dynamical systems coupled through graphs with negative ρ are more stable than those coupled through graphs with positive $\rho > 0$.

B. Adjacency matrices of weighted and directed random graphs with positive degree correlations

We analyze the spectral properties of the adjacency matrices of Poissonian and geometric random graphs with positive ρ and random weights.

The Poissonian ensemble with positive ρ has a prescribed degree distribution

$$p_{K^{\text{in}}, K^{\text{out}}}(k, \ell) = (1 - c\rho) p_p(k) p_p(\ell) + c\rho p_p(\ell) \delta_{k,\ell}, \quad (95)$$

where $\rho \in [0, 1/c]$, and where p_p is the truncated Poisson distribution defined by Eq. (91). The geometric ensemble with

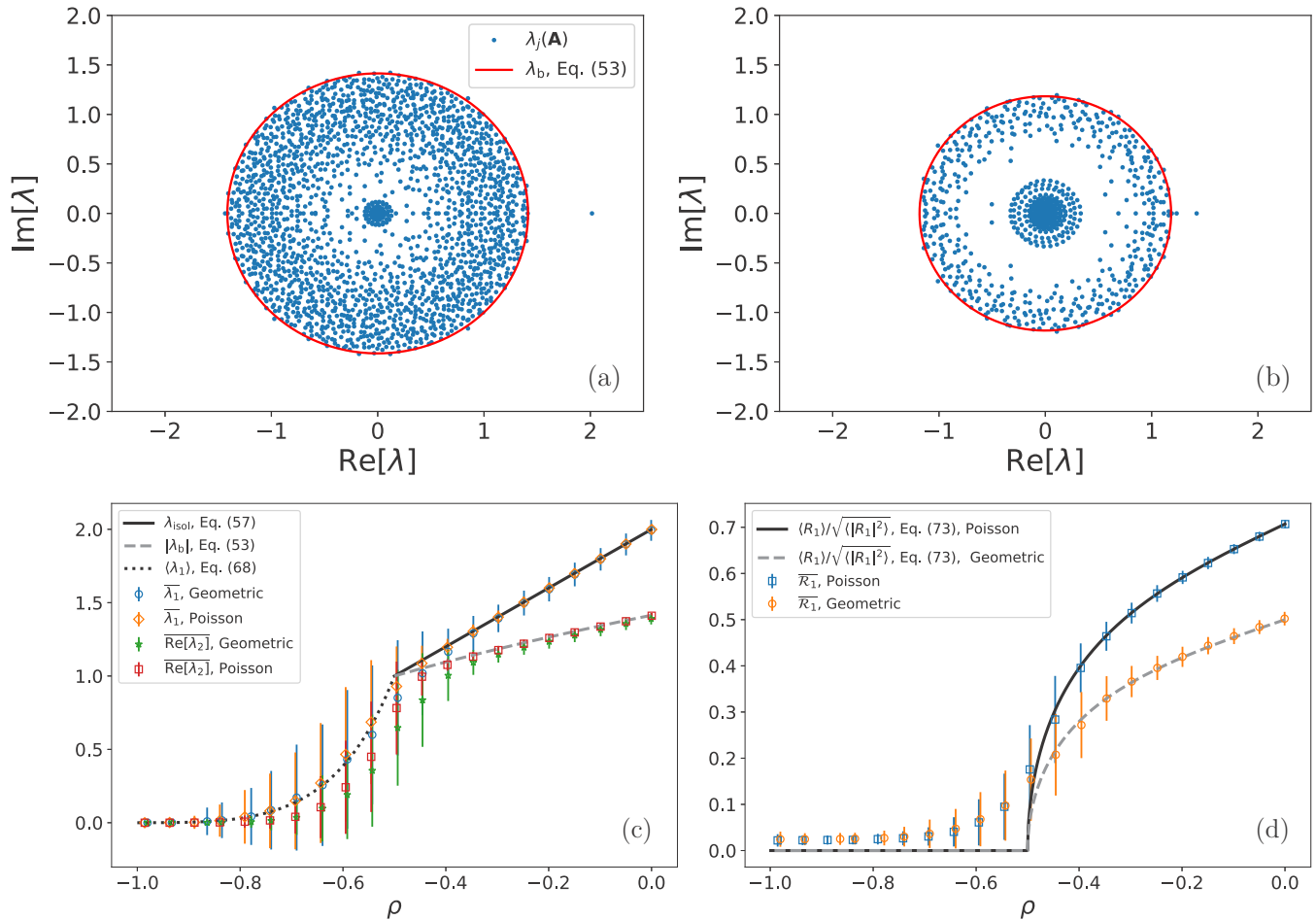


FIG. 5. Effect of negative ρ on the spectral properties of the adjacency matrices of random, directed graphs. Spectral properties for the adjacency matrices of Poissonian [see Eq. (90)] or geometric [see Eq. (92)] random, directed graphs with a mean degree $c = 2$ and negative ρ are presented. Direct diagonalization results for matrices of size $n = 4000$ (markers) are compared with the theoretical results for infinitely large matrices (lines) derived in Sec. III. [(a) and (b)] eigenvalues $\lambda_j(\mathbf{A})$ of the adjacency matrices of two Poissonian random graphs with $\rho = 0$ (a) and -0.3 (b), respectively, are plotted and compared with the theoretical boundary λ_b for the spectrum given by Eq. (53). (c) Mean values of the leading eigenvalue $\bar{\lambda}_1$ and real part of the subleading eigenvalue $\overline{\text{Re}[\lambda_2]}$ are plotted as a function of ρ and compared with theoretical results $\lambda_{\text{isol}} = 2\rho$ and $|\lambda_b| = \sqrt{2\rho}$ if $\rho > -0.5$ and $\langle \lambda_1 \rangle = 1 - (1 - c(\rho + 1))e^{c(\rho+1)}$ if $\rho < -0.5$. (d) Mean value $\overline{R_1}$ for the entries of the right eigenvector associated with the leading eigenvalue are plotted as a function of ρ and compared with the theoretical results $\frac{\langle R_1 \rangle}{\sqrt{\langle R_1^2 \rangle}} = \sqrt{\frac{1+2\rho}{2+\rho-2\rho^2}}$ and $\frac{\langle R_1 \rangle}{\sqrt{\langle R_1^2 \rangle}} = \sqrt{\frac{1+2\rho}{2(2+\rho-2\rho^2)}}$ for the Poissonian and geometric ensemble, respectively, when $\rho \geq -0.5$, and with $\frac{\langle R_1 \rangle}{\sqrt{\langle R_1^2 \rangle}} = 0$ when $\rho < -0.5$. In (c) and (d), direct diagonalization results are the sample means over 1000 matrix realizations and error bars represent the sample standard deviations.

positive ρ has the prescribed degree distribution

$$p_{K^{\text{in}}, K^{\text{out}}}(k, \ell) = \left(1 - \frac{c\rho}{c+1}\right) p_g(k) p_g(\ell) + \frac{c\rho}{c+1} p_g(\ell) \delta_{k, \ell}, \quad (96)$$

where $\rho \in [0, (c+1)/c]$, and p_g is the truncated geometric distribution defined by Eq. (93).

The off-diagonal matrix entries J_{jk} are i.i.d. random variables drawn either from a Gaussian distribution

$$p_J(x) = \frac{1}{\sqrt{2\pi}v^2} e^{-\frac{(x-\mu_0)^2}{2v^2}}, \quad (97)$$

or from a bimodal distribution

$$p_J(x) = b\delta(x - x_0) + (1 - b)\delta(x + x_0), \quad (98)$$

with the parametrization $x_0 = \sqrt{\mu_0^2 + v^2}$ and $2b = 1 + \mu_0/x_0$. In each case, the parameters μ_0 and v denote, respectively, the mean and the standard deviation of the distribution $p_J(x)$.

In Fig. 6, we analyze how positive values of ρ affect the spectral properties of adjacency matrices of randomly weighted directed graphs. We compare the spectral properties for different values of ρ and fixed parameters $c = 2$, $\mu_0 = 1$, and $v = 1.2$. We compare theoretical results from Sec. III (lines) with direct diagonalization results for matrices of size $n = 4000$ (markers).

In panels (a) and (b) of Fig. 6, we provide a global picture of the spectra of Poissonian random graphs by comparing the spectrum of a graph without degree correlations [$\rho = 0$, (a)]

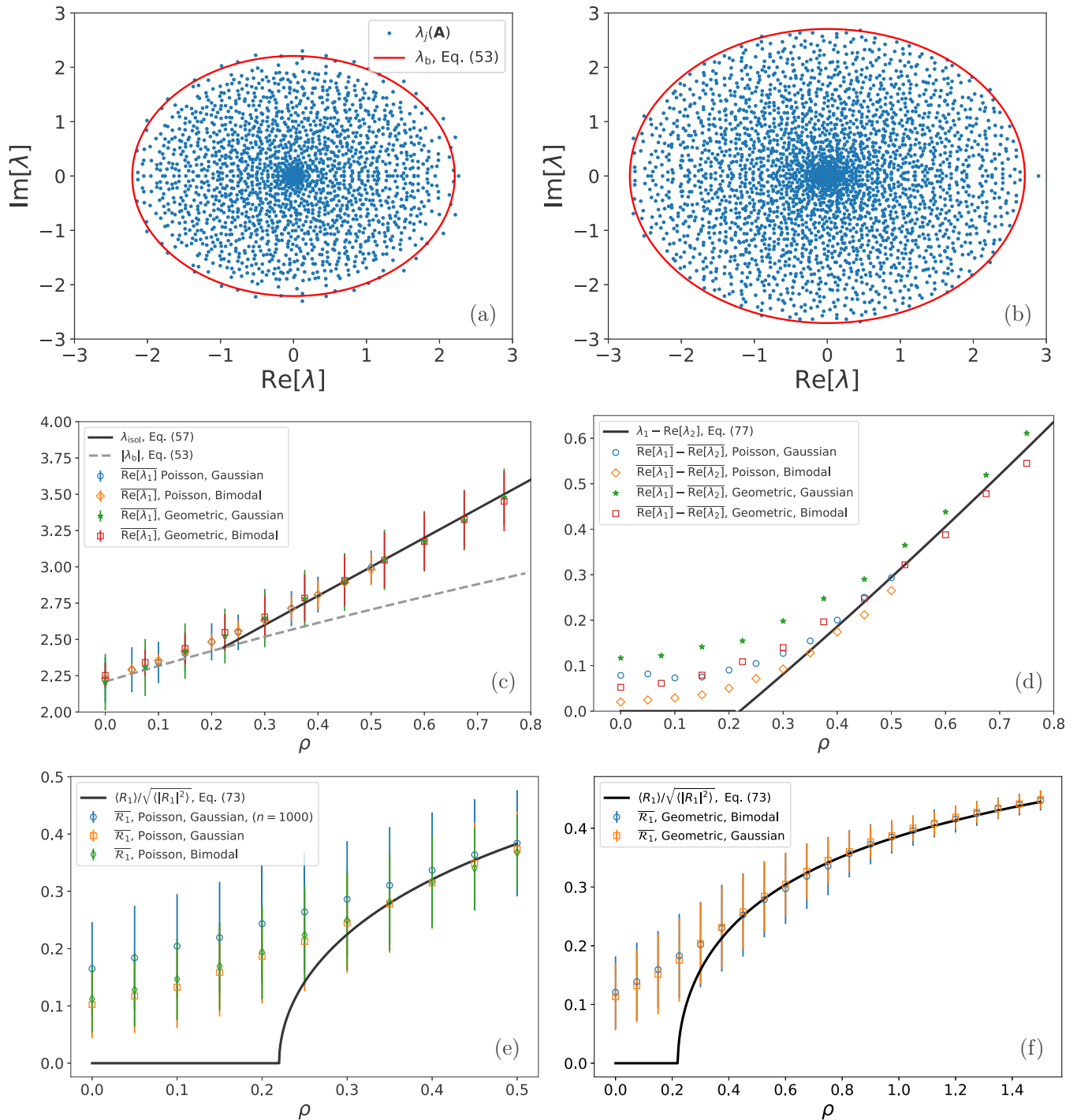


FIG. 6. Effect of positive ρ on the spectral properties of adjacency matrices of weighted, random, directed graphs. Spectral properties for the adjacency matrices of Poissonian [see Eq. (95)] or geometric [see Eq. (96)] random, directed graphs with a mean degree $c = 2$ and positive ρ are presented. The off-diagonal weights are drawn from a Gaussian or a bimodal distribution with mean $\mu_0 = 1$ and standard deviation $v = 1.2$ [see Eqs. (97) and (98)]. Direct diagonalization results of matrices of size $n = 4000$ (markers) are compared with theoretical results for $n \rightarrow \infty$ (lines), presented in Sec. III. [(a) and (b)] eigenvalues $\lambda_j(\mathbf{A})$ of the adjacency matrices of two Poissonian random graphs with $\rho = 0$ (a) and 0.5 (b), respectively, are plotted and compared with the theoretical boundary λ_b for the spectrum given by Eq. (53). [(c)–(f)] the sample means for the leading eigenvalue $\text{Re}[\lambda_1]$, the spectral gap $\text{Re}[\lambda_1] - \text{Re}[\lambda_2]$ and the first moment of the right eigenvector $\overline{\mathcal{R}}_1$ are plotted as a function of ρ and compared with the theoretical expressions λ_1 , $\lambda_1 - \text{Re}[\lambda_2]$ and $\langle R_1 \rangle$ derived in Sec. III. Sample means are over 1000 matrix realizations of size $n = 4000$ [except for the blue circles in (e), which are for $n = 1000$]. The error bars denote sample standard deviations.

with the spectrum of a graph with positive degree correlations [$\rho = 0.5$, (b)]. In the latter case, the correlations are perfect in the sense that $K_j^{\text{in}} = K_j^{\text{out}}$ for each node j . The direct diagonalization results corroborate well the formula Eq. (53) for the boundary of the continuous part of the spectrum. We also observe that the leading eigenvalue $\lambda_1(\mathbf{A})$ increases as a function of ρ , that $\lambda_1(\mathbf{A})$ is located at the boundary $\partial\sigma_{\text{ac}}$ for $\rho = 0$ (a), and that $\lambda_1(\mathbf{A})$ is an outlier for $\rho = 0.5$ (b).

In panels (c) and (d) of Fig. 6, we provide a more detailed view of the eigenvalues λ_1 and λ_2 as a function of ρ . We observe that both $\overline{\lambda_1}$ and $\overline{\lambda_2}$ are monotonically increasing functions of ρ , and that there is a continuous transition from a gapless phase for $\rho < \langle J^2 \rangle / (c \langle J \rangle^2) - 1 \approx 0.22$ to a gapped phase for $\rho > \langle J^2 \rangle / (c \langle J \rangle^2) - 1$. We observe that the values of $\overline{\lambda_1}$ and $\overline{\lambda_2}$ are universal, in the sense that they depend on the distributions p_J and $p_{K^{\text{in}}, K^{\text{out}}}$ only through the parameters c , ρ , $\langle J \rangle$, and $\langle J^2 \rangle$. Theoretical results are well corroborated with direct diagonalization results, although finite size effects are more significant for the spectral gap.

Lastly, panels (e) and (f) of Fig. 6 compare the theoretical result $\langle R_1 \rangle$ of Sec. III with the sampled average $\overline{\mathcal{R}_1}$ of the quantity \mathcal{R}_1 , as defined in Eq. (89). In the gapless phase, we have $\langle R_1 \rangle = 0$, while in the gapped phase we obtain $\langle R_1 \rangle > 0$, which is reminiscent of a continuous phase transition between a spin-glass phase and a ferromagnetic phase. We observe that in the gapped phase direct diagonalization results are in very good agreement with the theoretical expressions for infinitely large matrices, whereas in the gapless phase there are significant deviations between theory and direct diagonalization results. These deviations are due to finite size effects, which are significant because of our convention to normalize the eigenvectors with Eq. (29). In spite of that, we observe that direct diagonalization results slowly converge to the theoretical values as the matrix size n increases.

Overall, we conclude that the theoretical results for the typical values of λ_1 , λ_2 , and $\langle R_1 \rangle$, presented in Sec. III, describe well the numerically estimates for their ensemble average. This is because in the regime $c(\rho + 1) > 1$ it is unlikely that a stochastic outlier eigenvalue exists.

C. Adjacency matrices of random graphs with power-law degree distributions

In this section, we analyze the spectral properties of the adjacency matrices of random, directed graphs with power-law degree distributions. Power-law random graphs are interesting from a practical point of view, since degree distributions of real-world systems often have tails that are fitted well by power-law distributions [10, 74–76]. For example, the World Wide Web is a directed graph with a power-law degree distribution of the form $p_{K^{\text{in}}, K^{\text{out}}}(k, \ell) \sim k^{-2.1} \ell^{-2.7}$ [28]. Since power-law degree distributions have diverging moments, these ensembles exhibit strong finite size effects and large sample-to-sample fluctuations, and it is thus interesting to test the possible limitations of the theory in Sec. III for power-law random graphs.

We consider two classes of power-law random graphs, namely, an ensemble without correlations between indegrees and outdegrees ($\rho = 0$), and an ensemble with perfect degree correlations, where $K_j^{\text{in}} = K_j^{\text{out}}$ for all nodes j ($\rho > 0$). The

ensemble without degree correlations has a prescribed degree distribution

$$p_{\text{deg}}(k, \ell) = \frac{k^{-a} \ell^{-a}}{\mathcal{N}_{\text{pow}}^2}, \quad (99)$$

with $k, \ell \in [n-1]$ and with $\mathcal{N}_{\text{pow}} = \sum_{k=1}^{n-1} k^{-a}$, while the ensemble with perfect degree correlations has the prescribed degree distribution

$$p_{\text{deg}}(k, \ell) = \frac{k^{-a}}{\mathcal{M}_{\text{pow}}} \delta_{k, \ell}, \quad (100)$$

with $k, \ell \in [(n-1)/2]$ and with $\mathcal{M}_{\text{pow}} = \sum_{k=1}^{(n-1)/2} k^{-a}$ the normalization constant. The parameter a controls how fast the degree distribution decays for large degrees.

We discuss the values of the parameters c and ρ in the limit $n \rightarrow \infty$. If $a > 2$, then the mean degree is given by

$$c = \zeta(a-1)/\zeta(a), \quad (101)$$

with $\zeta(x)$ the Riemann zeta function. Also, if $a > 2$, then the ensemble of Eq. (99) has a degree-correlation coefficient

$$\rho = 0, \quad (102)$$

while if $a > 3$, then the ensemble of Eq. (100) has a degree-correlation coefficient

$$\rho = \frac{\zeta(a-2)\zeta(a)}{\zeta^2(a-1)} - 1. \quad (103)$$

Note that $c(\rho + 1) > 1$, and therefore the power-law graphs we consider have a giant SCC.

We consider unweighted power-law random graphs with $J_{jk} = 1$ for all $j, k \in [n]$.

We now resort to direct diagonalization in order to gain a better understanding of the statistics of the leading eigenvalue of power-law random graphs. In Panel (a) of Fig. 7, we plot the sample mean $\overline{\lambda_1}$ of the leading eigenvalue $\lambda_1(\mathbf{A})$ and the sample mean $\overline{\text{Re}[\lambda_2]}$ of the real part of the subleading eigenvalue $\lambda_2(\mathbf{A})$ as a function of a in the ensemble defined by Eq. (99) for which $\rho = 0$. We observe that for $a \gtrsim 3$ the theoretical expressions Eqs. (57) and (53) for λ_{isol} and $|\lambda_{\text{b}}|$, respectively, are in very good agreement with direct diagonalization results for the leading and subleading eigenvalue. In the regime $a \lesssim 3$, we observe significant deviations between theory and numerical experiments. Such deviations are expected, since $c \rightarrow \infty$ for $a \rightarrow 2^+$, and therefore the theoretical expressions for λ_{isol} and $|\lambda_{\text{b}}|$ diverge for $a \rightarrow 2^+$. Analogously, in panel (b) of Fig. 7, we present results for $\overline{\lambda_1}$ and $\overline{\text{Re}[\lambda_2]}$ as a function of a for the ensemble defined by Eq. (100) for which $\rho > 0$. In this case, the theory works well when $a \gtrsim 4$, whereas for $a \lesssim 4$, we observe significant deviations between theory and numerical experiments. This is because for $a \rightarrow 3^+$ the degree correlation coefficient ρ diverges, and therefore the theoretical expressions for λ_{isol} and $|\lambda_{\text{b}}|$ also diverge. Overall, these results show that Eqs. (57) and (53) work remarkably well for power-law random graphs.

Lastly, in panels (c) and (d) of Fig. 7, we plot the empirical mean $\overline{\mathcal{R}_1}$ as a function of a and compare results from the direct diagonalization of randomly sampled matrices with

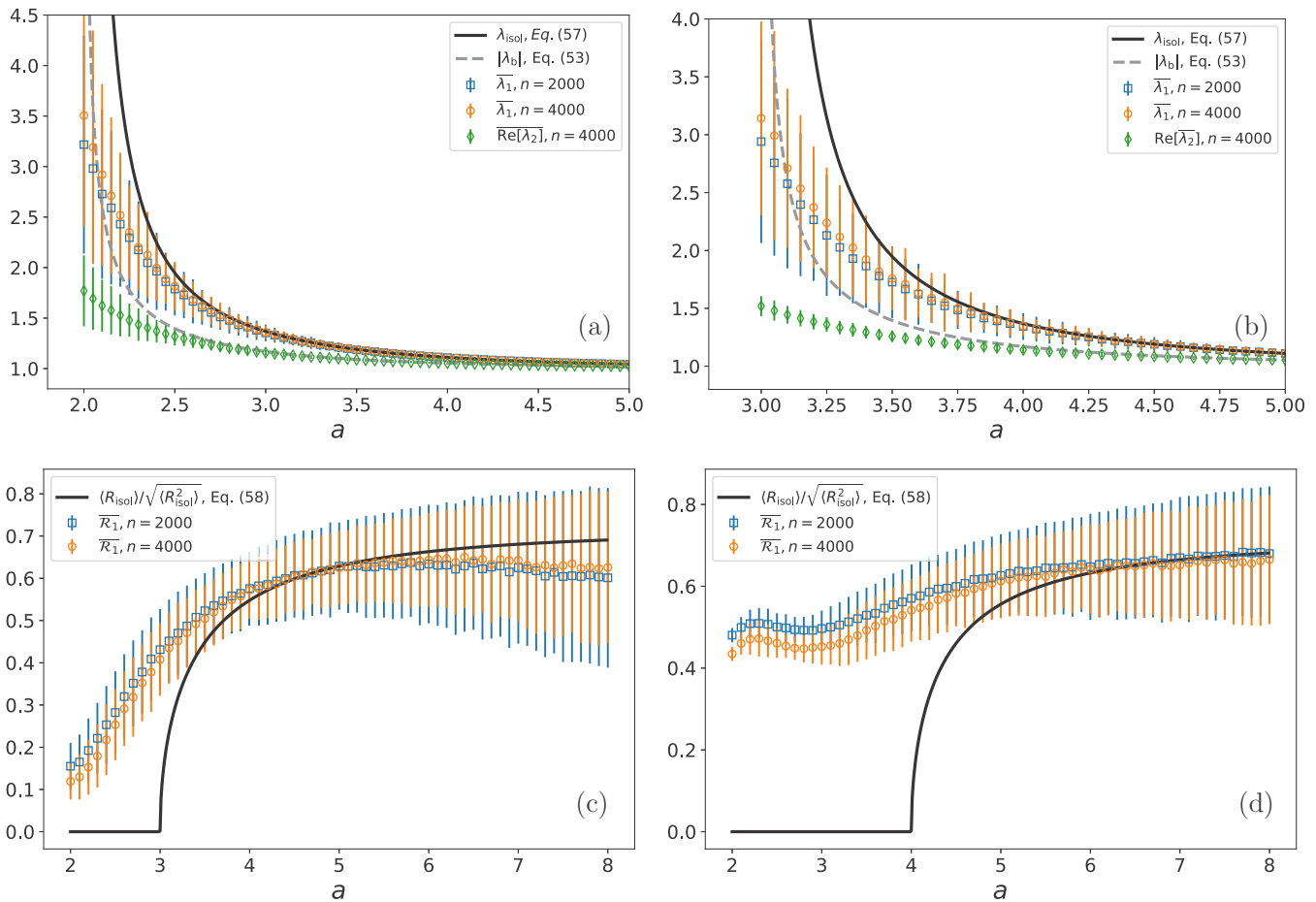


FIG. 7. Leading and subleading eigenvalues for adjacency matrices of power-law random graphs with prescribed degree distributions. [(a) and (b)] Results for the leading eigenvalue $\bar{\lambda}_1$ and the real part of the subleading eigenvalue $\text{Re}[\bar{\lambda}_2]$ are presented as a function of the exponent a of power-law random graphs with degree distributions given by either Eq. (99) (a), for which $\rho = 0$, or by Eq. (100) (b), for which $\rho > 0$. Direct diagonalization results (markers) in (a) and (b) are compared with the theoretical results (lines) given by $|\lambda_b|^2 = \lambda_{\text{isol}} = \zeta(a-1)/\zeta(a)$ and $|\lambda_b|^2 = \lambda_{\text{isol}} = \zeta(a-2)/\zeta(a-1)$, respectively. [(c) and (d)] Results for the mean values $\bar{\mathcal{R}}_1$ and $\bar{\mathcal{R}}_2$ of the entries of right eigenvectors associated with the leading and subleading eigenvalue, respectively, are presented as a function of the exponent a for power-law random graphs with degree distributions given by either Eq. (99) (c), for which $\rho = 0$, or by Eq. (100) (d), for which $\rho > 0$. In (c), direct diagonalization results are compared with $\frac{\langle R_{\text{isol}} \rangle}{\sqrt{\langle R_{\text{isol}}^2 \rangle}} = \sqrt{\frac{\zeta(a-1)[\zeta(a-1)-\zeta(a)]}{\zeta(a)[\zeta(a-2)-\zeta(a-1)]}}$ if $a > 3$, and with $\frac{\langle R_{\text{isol}} \rangle}{\sqrt{\langle R_{\text{isol}}^2 \rangle}} = 0$ if $a < 3$. In (d), direct diagonalization results are compared with $\frac{\langle R_{\text{isol}} \rangle}{\sqrt{\langle R_{\text{isol}}^2 \rangle}} = \sqrt{\frac{\zeta(a-1)\zeta(a-2)[\zeta(a-2)-\zeta(a-1)]}{\zeta(a)\zeta(a-1)\zeta(a-3)-\zeta^2(a-1)\zeta(a-2)+[\zeta(a-1)-\zeta(a)]\zeta^2(a-2)}}$, if $a > 4$, and with $\frac{\langle R_{\text{isol}} \rangle}{\sqrt{\langle R_{\text{isol}}^2 \rangle}} = 0$ if $a < 4$. In all four panels weights are set equal to $J_{jk} = 1$ and markers are sample means over either 2000 or 1000 matrices of size $n = 2000$ or 4000, respectively. Error bars denote standard deviations over the population of different matrix realizations.

the theoretical expression for $\langle R_{\text{isol}} \rangle$ given by Eq. (58). We observe a reasonable good agreement between theoretical results and numerical experiments, considering that power-law random graphs exhibit significant finite-size effects and fluctuations. Interestingly, the normalized mean $\langle R_{\text{isol}} \rangle / \sqrt{\langle R_{\text{isol}}^2 \rangle}$ vanishes at $a = 3$ and 4 for ensembles with degree distributions (99) and (100), respectively. Since the Perron-Frobenius theorem applies to this ensemble, this is a transition from a delocalized phase ($\langle R_{\text{isol}} \rangle / \sqrt{\langle R_{\text{isol}}^2 \rangle} > 0$) to a localized phase ($\langle R_{\text{isol}} \rangle / \sqrt{\langle R_{\text{isol}}^2 \rangle} = 0$), as argued in Sec. III H. In other words, the leading eigenvector is *localized* when the exponent a that characterizes the decay of the power-law degree distribution is small enough.

D. Distribution p_R for the entries of the right eigenvectors

So far, we have studied the mean value of the distribution p_R . Differently, in this section we analyze properties of the full distribution p_R .

Equations (56) and (60) state that the distribution p_R contains a delta peak at the origin with weight $1 - s_{\text{out}}$, where s_{out} is the relative size of the OUT component. In other words, the number of nonzero entries in a right eigenvector is equal to the size of the OUT component. Figure 8 tests this prediction for the adjacency matrix of a directed random graph with a Poissonian degree distribution given by Eq. (90) with $c = 3$.

In panel (a) of Fig. 8, we compare theoretical predictions for p_R , obtained by solving the recursive distributional Eqs. (48-49) at $\lambda = \lambda_{\text{isol}}$ through a population dynamics

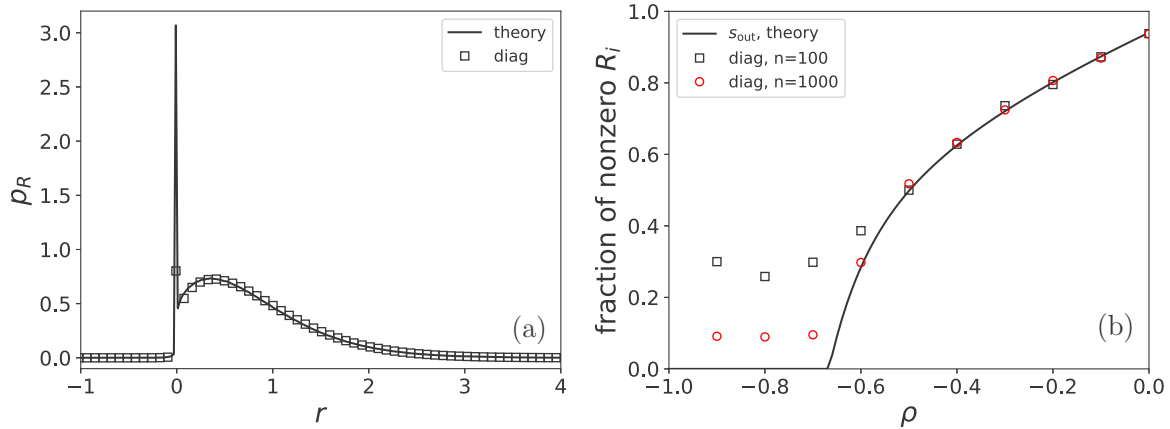


FIG. 8. Properties of the distribution p_{R_1} . Results are for the adjacency matrices of random, directed graphs with a Poisson degree distribution given by Eq. (90) and with mean $c = 3$. Edges are weighted by random couplings J_{ij} drawn from a Gaussian distribution [see Eq. (97)] with mean $\mu_0 = 1$ and variance $v^2 = 0.2$. (a) Theoretical results for p_R solving Eqs. (48) and (49) with $\lambda = \lambda_{\text{isol}}$ (solid lines) are compared with a histogram of the entries of \vec{R}_1 obtained from direct diagonalizing $2e + 4$ matrices of size $n = 1000$ (markers). The degree correlation coefficient $\rho = 0$. (b) Fraction of nonzero entries of the leading right eigenvector \vec{R}_1 as a function of the degree-correlation coefficient ρ . Direct diagonalization results for matrices of size $n = 100$ and $n = 1000$ (markers are sample averages over 100 and 20 samples, respectively) are compared with theoretical results for s_{out} (solid line) obtained from solving Eqs. (15) and (17). In the numerical experiments, we have used the criterion $|R_i|^2 < 1e - 20$ to identify a zero-valued entry.

algorithm [44,54,77,78], with a histogram of the entries of the right eigenvector associated with the leading eigenvalue λ_1 , obtained through direct diagonalization results. We have set $\rho = 0$ and the couplings J_{ij} are drawn from a Gaussian distribution. In Fig. 8, we observe an excellent agreement between theory and numerical experiments and we also observe a delta peak at the origin, which is clearly discernible in both theory and numerical experiments.

In order to quantify the weight of the delta peak at the origin, we plot in panel (b) of Fig. 8 the fraction of entries R_i that are not equal to zero. We compare direct diagonalization results for right eigenvectors associated with the leading eigenvalue λ_1 with the theoretical expression s_{out} obtained by solving Eqs. (15) and (17). We find again an excellent agreement between theory and numerical experiments, confirming that the number of nonzero elements in \vec{R} equals the size s_{out} of the OUT component

VI. EXTENSIONS OF THE THEORY

Here we extend the theory from Sec. III C to the case of random matrices with diagonal disorder and graphs that contain nondirected links.

A. Random matrices with diagonal disorder

We consider random matrices of the form

$$\mathbf{A} = -\mathbf{D} + \mathbf{J} \circ \mathbf{C}, \quad (104)$$

where \mathbf{J} and \mathbf{C} are defined in exactly the same way as in Eq. (3), but where \mathbf{D} is now a diagonal matrix with entries $[\mathbf{D}]_{jj} = D_j$ that are i.i.d. random variables drawn from a probability distribution $p_D(x)$ with $x \in \mathbb{R}^+$. Note that p_D has a support on the positive real axis since otherwise $\text{Re}[\lambda_1] > 0$ and the dynamical system described by \mathbf{A} will not be stable.

In the special case when

$$p_D(x) = \delta(x - d), \quad (105)$$

we recover the model given by Eq. (3).

The theory of Sec. III C applies to the model given by Eq. (104) after some minor modifications. As shown in Appendix I, for the present model the distribution p_R solves the recursion relation

$$p_R(r) = \sum_{k=0}^{\infty} \sum_{\ell=0}^{\infty} p_{K^{\text{in}}, K^{\text{out}}}(k, \ell) \int dy p_D(y) \int \prod_{j=1}^{\ell} d^2 r_j q_R(r_j) \times \int \prod_{j=1}^{\ell} dx_j p_J(x_j) \delta \left[r - \frac{\sum_{j=1}^{\ell} x_j r_j}{\lambda + y} \right] \quad (106)$$

and q_R solves the recursion relation

$$q_R(r) = \sum_{k=0}^{\infty} \sum_{\ell=0}^{\infty} p_{K^{\text{in}}, K^{\text{out}}}(k, \ell) \frac{k}{c} \int dy p_D(y) \int \prod_{j=1}^{\ell} d^2 r_j q_R(r_j) \times \int \prod_{j=1}^{\ell} dx_j p_J(x_j) \delta \left[r - \frac{\sum_{j=1}^{\ell} x_j r_j}{\lambda + y} \right]. \quad (107)$$

If D is deterministic, then Eq. (105) holds and we recover the recursion Eqs. (48) and (49).

In Appendix I, we derive the values of λ for which the recursion Eqs. (106) and (107) admit normalizable solutions. In this way, we obtain that the deterministic outliers of \mathbf{A} solve the equation

$$c(\rho + 1) \langle J \rangle \left\langle \frac{1}{\lambda_{\text{isol}} + D} \right\rangle = 1, \quad (108)$$

and the eigenvalues $\lambda_b \in \mathbb{C}$ at the boundary of the continuous part of the spectrum solve

$$c(\rho + 1)\langle J^2 \rangle \left\langle \frac{1}{|\lambda_b + D|^2} \right\rangle = 1. \tag{109}$$

Using Eqs. (108) and (109), it is possible to derive phase diagrams, similar to those presented in Figs. 3 and 4, for the stability of dynamical systems with disordered decay rates D_j . We leave this open for future studies.

B. Nondirected graphs with random couplings

We consider random matrices of the form

$$A_n = -d \mathbf{1}_n + \tilde{J}_n \circ \tilde{C}_n, \tag{110}$$

where \tilde{C}_n is the adjacency matrix of a nondirected, random graph with a prescribed degree distribution $p_{\text{deg}}(k)$, and where \tilde{J}_n is a random matrix with zero entries on the diagonal and with offdiagonal pairs $(\tilde{J}_{jk}, \tilde{J}_{kj})$ that are i.i.d. random variables with a distribution $p_{\tilde{J}_1, \tilde{J}_2}(x, y)$. We assume that $p_{\tilde{J}_1, \tilde{J}_2}$ satisfies the symmetry property

$$p_{\tilde{J}_1, \tilde{J}_2}(x, y) = p_{\tilde{J}_1, \tilde{J}_2}(y, x). \tag{111}$$

The random matrix model defined by Eq. (110) is locally treelike, but it is in general not locally oriented. Nevertheless,

locally oriented ensembles can be recovered in the limiting case

$$p_{\tilde{J}_1, \tilde{J}_2}(x, y) = \frac{1}{2} p_J(x) \delta(y) + \frac{1}{2} p_J(y) \delta(x). \tag{112}$$

In this case, the model given by Eq. (110) is the adjacency matrix of a directed random graph with a joint degree distribution

$$p_{K^{\text{in}}, K^{\text{out}}}(k, \ell) = \sum_{m=0}^{\infty} \frac{p_{\text{deg}}(m)}{2^m} \sum_{n=0}^m \frac{m!}{n!(m-n)!} \delta_{k,n} \delta_{\ell, m-n}, \tag{113}$$

which is a special case of the model defined by Eq. (3). On the other hand, if

$$p_{\tilde{J}_1, \tilde{J}_2}(x, y) = \delta(x - y) p_J(x), \tag{114}$$

then Eq. (110) defines symmetric random matrices.

In Appendix I, we derive a set of recursion relations for p_R . We obtain that the distribution p_R is the marginal

$$p_R(r) = \int d^2 g p_{G,R}(g, r) \tag{115}$$

of the joint distribution $p_{G,R}(g, r)$ that solves the recursion relation

$$p_{G,R}(g, r) = \sum_{k=0}^{\infty} p_{\text{deg}}(k) \int \prod_{\ell=1}^k d^2 g_{\ell} d^2 r_{\ell} q_{R,G}(r_{\ell}, g_{\ell}) \int \prod_{\ell=1}^k dx_{\ell} dy_{\ell} p_{\tilde{J}_1, \tilde{J}_2}(x_{\ell}, y_{\ell}) \times \delta \left(r + \frac{\sum_{\ell=1}^k x_{\ell} r_{\ell}}{-\lambda - d - \sum_{\ell=1}^k x_{\ell} g_{\ell} y_{\ell}} \right) \delta \left(g - \frac{1}{-\lambda - d - \sum_{\ell=1}^k x_{\ell} g_{\ell} y_{\ell}} \right), \tag{116}$$

and $q_{G,R}$ solves the equation

$$q_{G,R}(g, r) = \sum_{k=0}^{\infty} \frac{k p_{\text{deg}}(k)}{c} \int \prod_{\ell=1}^{k-1} d^2 g_{\ell} d^2 r_{\ell} q_{R,G}(r_{\ell}, g_{\ell}) \int \prod_{\ell=1}^{k-1} dx_{\ell} dy_{\ell} p_{\tilde{J}_1, \tilde{J}_2}(x_{\ell}, y_{\ell}) \times \delta \left(r + \frac{\sum_{\ell=1}^{k-1} x_{\ell} r_{\ell}}{-\lambda - d - \sum_{\ell=1}^{k-1} x_{\ell} g_{\ell} y_{\ell}} \right) \delta \left(g - \frac{1}{-\lambda - d - \sum_{\ell=1}^{k-1} x_{\ell} g_{\ell} y_{\ell}} \right). \tag{117}$$

Note that in the special case of symmetric random matrices [i.e., when Eq. (114) holds], Eqs. (116,117) are equivalent to those derived in Refs. [49,62–64].

The outliers λ_{isol} and the boundary λ_b of the continuous part of the spectrum are found as values of λ for which the relations (116) and (117) admit normalizable solutions. In the present case, we do not know how to derive compact analytical expressions for λ_{isol} and λ_b . However, Eqs. (116) and (117) can be solved numerically with a population dynamics algorithm, as described in Refs. [54,77,78], and consequently a stability phase diagram as in Figs. 3 and 4 can be derived. We leave such a study open for future work.

VII. DISCUSSION

Random matrices appear in linear stability analyses of large dynamical systems. So far, most studies have consid-

ered dynamical systems for which the system constituents interact with either a number of degrees of freedom that increases with system size, see, e.g., Refs. [13,20,22,26,27,79–84], or interact through a one-dimensional chain, see, e.g., Refs. [25,85,86]. However, real-world systems often consist of components interacting through large networks, see, e.g., Refs. [1–5]. Therefore an interesting question is how network topology affects system stability.

In this paper, we have analysed the linear stability of large dynamical systems defined on random, directed graphs with a prescribed degree distribution $p_{K^{\text{in}}, K^{\text{out}}}$, which serve as a model for, among others, the World Wide Web [28,29] and neural networks [30–32]. We have shown that dynamical systems defined on random, directed graphs are more stable than systems defined on nondirected graphs. Indeed, we have shown that for random, directed graphs the leading eigenvalue is with probability one finite in the limit of infinitely large n . This

result brings an interesting perspective in the diversity-stability debate [9]. Dynamical systems defined on dense matrices or nondirected graphs are unstable when n is large enough: in the former because λ_1 is of the order $O(\sqrt{n})$ [20], while in the latter because λ_1 is of the order $O(\sqrt{k_{\max}})$ [47–49]. Hence, a large and complex system will be in general unstable [20,87]. However, if the system is defined on a random, directed graph, then it can be infinitely large and stable since λ_1 converges to a finite limit for large n . The stabilising nature of random, directed graphs is a consequence of their locally treelike and oriented structure, which implies that there exist no feedback loops that amplify local perturbations.

A second surprising result is that the stability of dynamical systems defined on directed random graphs exhibits a universal character, in the sense that it is governed by only three network parameters: the effective mean degree $c(\rho + 1)$, the coefficient of variation $v_J = \sqrt{\langle J^2 \rangle - \langle J \rangle^2} / \langle J \rangle$, and the ratio $\alpha = \langle J \rangle / d$ between the mean interaction strength and the decay rate. This result follows from the analytical expression, given by Eq. (71), for the typical value of the leading eigenvalue of the adjacency matrix that encodes the network of interactions between the system constituents. From the analytical expression for the typical value of the leading eigenvalue, we obtain the universal phase diagrams of Figs. 3 and 4.

Analyzing these phase diagrams, we obtain the following interesting conclusions on how network topology affects system stability. First, negative correlations between indegrees and outdegrees stabilize large dynamical systems, whereas the mean coupling strength α and the coupling fluctuations v_J render dynamical systems less stable. Second, when the fluctuations v_J of the coupling strengths are small enough, then the stability is controlled by an outlier and is independent of v_J . On the other hand, when v_J is large enough, then the leading eigenvalue is determined by the boundary of the continuous part of the spectrum and the system stability decreases as a function of v_J . Moreover, in the first scenario, the unstable mode is ferromagnetic ($\langle R \rangle > 0$) whereas in the second scenario it is spin-glasslike ($\langle R \rangle = 0$). Lastly, systems with coupling fluctuations v_J larger than the critical value $v_* = \sqrt{\frac{1-\alpha^2}{\alpha^2}}$ do not contain a stable phase, no matter how large the negative correlations between indegrees and outdegrees are.

The universal phase diagrams of Figs. 3 and 4 have been derived with a mathematical method, akin to the cavity method in statistical physics, which computes the typical value of the leading eigenvalue of random, directed graphs that have a giant SCC in the limit of $n \rightarrow \infty$. The cavity method computes the typical value of λ_1 by neglecting contributions of cycles of finite length. However, if the graph contains disorder in the weights J_{ij} , then the leading eigenvalue is not a self-averaging quantity and there exists a finite (albeit) small probability that the leading eigenvalue comes from a cycle of finite length that is part of the graph, as sketched in Fig. 2. Hence, short cycles can destabilize large dynamical systems defined on random, directed graphs when they induce strong enough feedback loops.

The derived theoretical results for the spectra of large, sparse, non-Hermitian, random matrices may also be useful

for applications other than the linear stability analysis of large dynamical systems described by differential equations. For example, the theory is also useful to study the stability of dynamical systems in discrete time [88], which are relevant for the study of systemic risk in networks of banks connected through financial contracts [8,84]. For discrete-time systems, the stability is controlled by the spectral radius $r(\mathbf{A}) = \max\{|\lambda_1|, |\lambda_2|, \dots, |\lambda_n|\}$. Another example of an application is the analysis of spectral algorithms that use the right or left eigenvector associated with the (sub)leading eigenvalue to obtain information about a system, e.g., spectral clustering algorithms [89,90], centrality measures based on eigenvectors [91–93], or algorithms for the low-rank matrix estimation problem [94,95]. Detectability thresholds of spectral algorithms often depend on the location of the leading and subleading eigenvalue [90,95–98]. A fourth example of an application is the analysis of stochastic processes with spectra of Laplacian or Markov matrices [99–103]: the stationary state of a Markov process is the right (or left) eigenvector associated with the leading eigenvalue of a Markov matrix [103], the relaxation time is provided by the spectral gap [104–106], and the cumulant generating function of a time-additive observable can be expressed in terms of the leading eigenvalues of a sequence of Markov matrices [107–111]. A fifth application is the study of nonHermitian quantum mechanics on random graphs [85,112,113]. Lastly, we remark that the subleading eigenvalue, and its associated right (left) eigenvector, provide not only information about the asymptotic stability of large dynamical systems, but also about their response to random perturbations as shown in Ref. [46]. Taken together, we conclude that the spectral theory presented in this paper can be used in various contexts.

The theoretical results obtained in this paper are conjectures about the spectral properties of random, directed graphs. Reference [95] provides a mathematical proof for Eqs. (68) and (77) for the leading and subleading eigenvalues in the special case of directed Erdős-Rényi graphs with $J_{ij} = 1$. To our knowledge, there exist no proofs for Eqs. (53) and (57) for λ_{isol} and λ_{b} , respectively, for graph ensembles other than directed Erdős-Rényi graphs. Also, we are not aware of proofs for Eqs. (54), (55), and (58) for the mean value of the distribution of right eigenvector elements, the recursion relations for p_R given by Eqs. (48) and (49), the algebraic multiplicity of the trivial $-d$ eigenvalue given by Eq. (45), and Eqs. (56) and (60) for the number of zero entries of right eigenvectors. The results in the present paper are thus interesting conjectures about the spectral properties of sparse, nonHermitian, random matrices.

In the present paper, we have focused on systems that are locally treelike and oriented. For future work, it would be interesting to understand how network topology affects the linear stability of nonoriented systems [114] and systems that contain small cycles or motifs [52,53,115,116]. Based on the results in the present paper, we would expect that those systems are in general less stable than locally treelike and oriented systems.

ACKNOWLEDGMENTS

We thank C. Cammarota, Y. Fyodorov, A. Mambuca, W. M. Tarnowski, and P. Vivo for fruitful discussions. FLM thanks London Mathematical Laboratory and CNPq/Brazil for financial support.

APPENDIX A: STABILITY CRITERION FOR A LINEAR DYNAMICAL SYSTEM DESCRIBED BY EQS. (1)

We call a linear dynamical system, described by Eqs. (1), *stable* if

$$\lim_{t \rightarrow \infty} \bar{y}(t) = 0 \tag{A1}$$

for all initial states $\bar{y}(0)$.

In this Appendix, we show that a linear dynamical system is stable if and only if all the eigenvalues of \mathbf{A} have negative real parts. To this aim, we express the matrix \mathbf{A} in its canonical form, which contains as few as possible nonzero offdiagonal matrix entries. For a diagonalizable matrix, the canonical form is diagonal, whereas for a nondiagonalizable matrix, the canonical form is a Jordan matrix [60].

1. Diagonalizable matrices

If \mathbf{A} is a diagonalizable matrix of size n , then there exists a nonsingular matrix \mathbf{S} such that [60]

$$\mathbf{A} = \mathbf{S}\Delta\mathbf{S}^{-1}, \tag{A2}$$

where Δ is a diagonal matrix with diagonal elements $[\Delta]_{jj} = \lambda_j(\mathbf{A})$. As a consequence, the j th column of \mathbf{S} is a right eigenvector \vec{R}_j associated with the eigenvalue λ_j , and the j th row of \mathbf{S}^{-1} is a left eigenvector \vec{L}_j^\dagger associated with the eigenvalue λ_j . Since \mathbf{S} is a nonsingular matrix, both right eigenvectors and left eigenvectors form a set of n independent vectors that span \mathbb{C}^n , and because $\mathbf{S}^{-1}\mathbf{S} = \mathbf{1}_n$, right and left eigenvectors form a biorthonormal system,

$$\vec{L}_j \cdot \vec{R}_k = \delta_{j,k}. \tag{A3}$$

As a consequence, the matrix \mathbf{A} can be written as

$$\mathbf{A} = \sum_{j=1}^n \lambda_j \vec{R}_j \vec{L}_j^\dagger. \tag{A4}$$

We can decompose $\bar{y}^\dagger(t)$ into the basis of left eigenvectors \vec{L}_j^\dagger , such that

$$\bar{y}^\dagger(t) = \sum_{j=1}^n c_j(t) \vec{L}_j^\dagger. \tag{A5}$$

The coefficients

$$c_j(t) = \bar{y}(t) \cdot \vec{R}_j \tag{A6}$$

follow from the biorthonormality condition (A3) of left and right eigenvectors.

Substituting the canonical form of \mathbf{A} , given by Eq. (A4), into Eq. (1), and using that the decomposition (A5) is unique, we obtain the n independent and linear differential equations

$$\partial_t c_j(t) = \lambda_j c_j(t). \tag{A7}$$

Finally, solving Eqs. (A7), we obtain

$$c_j(t) = e^{\lambda_j t} c_j(0) \tag{A8}$$

and the expression Eq. (82) for $\bar{y}^\dagger(t)$ after substituting (A8) into (A5).

The expression (82) for $\bar{y}^\dagger(t)$ implies that a system described by a diagonalizable matrix is stable, if and only if, the real part of all eigenvalues is negative.

2. Nondiagonalizable matrices

A matrix \mathbf{A} is nondiagonalizable if there does not exist a nonsingular matrix \mathbf{S} for which relation (A2) holds with Δ being a diagonal matrix. Nondiagonalizable matrices contain at least one eigenvalue with a geometric multiplicity that is smaller than its algebraic multiplicity. The algebraic multiplicity of an eigenvalue λ is the multiplicity of λ as the root of the polynomial equation $\det[\mathbf{A} - \lambda\mathbf{1}_n] = 0$. The geometric multiplicity an eigenvalue is the number of linearly independent right eigenvectors associated with this eigenvalue.

If \mathbf{A} is a nondiagonalizable matrix of size n , then there exists a nonsingular matrix \mathbf{S} such that [60]

$$\mathbf{A} = \mathbf{S}\mathbf{H}\mathbf{S}^{-1}, \tag{A9}$$

where \mathbf{H} is a Jordan matrix. The Jordan matrix has the form

$$\mathbf{H} = \begin{bmatrix} J_{n_1}(\lambda_{\ell_1}) & & & 0 \\ & J_{n_2}(\lambda_{\ell_2}) & & \\ & & \ddots & \\ 0 & & & J_{n_m}(\lambda_{\ell_m}) \end{bmatrix}, \tag{A10}$$

where

$$\ell_\alpha = 1 + \sum_{\beta=1}^{\alpha-1} n_\beta, \quad \text{with } \alpha \in [m], \tag{A11}$$

and

$$J_n(\lambda) = \begin{bmatrix} \lambda & 1 & 0 & \dots & 0 \\ 0 & \lambda & 1 & & \\ \vdots & & \ddots & \ddots & \\ 0 & & & & \lambda \end{bmatrix} \tag{A12}$$

is a Jordan block of size n .

The number of Jordan blocks associated with an eigenvalue λ equals the geometric multiplicity of the eigenvalue λ . Hence, the number of independent right eigenvectors of the matrix \mathbf{A} is equal to the number m of Jordan blocks in the matrix \mathbf{H} .

The columns of \mathbf{S} are the generalized right eigenvectors \vec{R}_j of the matrix \mathbf{A} . Since the matrix \mathbf{S} is nonsingular, the generalized right eigenvectors form a set of n independent vectors that span \mathbb{C}^n . Analogously, the rows of \mathbf{S}^{-1} are the generalized left eigenvectors \vec{L}_j^\dagger of \mathbf{A} . Also, generalized left and right eigenvectors form a biorthonormal system,

$$\vec{L}_j \cdot \vec{R}_k = \delta_{j,k}, \quad \text{with } j, k \in [n], \tag{A13}$$

because $\mathbf{S}\mathbf{S}^{-1} = \mathbf{1}_n$. The m right eigenvectors of \mathbf{A} are

$$\vec{R}_\alpha = \vec{R}_{\ell_\alpha}, \quad \text{with } \alpha \in [m], \tag{A14}$$

with the ℓ_α as defined in Eq. (A11). Analogously, the m left eigenvectors are

$$\vec{L}_\alpha = \vec{L}_{\ell_\alpha+n_\alpha-1}, \quad \text{with } \alpha \in [m]. \quad (\text{A15})$$

Since the generalized right and generalized left eigenvectors form a biorthonormal system, the matrix \mathbf{A} can be expressed in the form

$$\begin{aligned} \mathbf{A} = & \sum_{\alpha=1}^m \sum_{\kappa=0}^{n_\alpha-2} \vec{\mathcal{R}}_{\ell_\alpha+\kappa} (\lambda_{\ell_\alpha} \vec{\mathcal{L}}_{\ell_\alpha+\kappa}^\dagger + \vec{\mathcal{L}}_{\ell_\alpha+\kappa+1}^\dagger) \\ & + \sum_{\alpha=1}^m \lambda_{\ell_\alpha} \vec{\mathcal{R}}_{\ell_\alpha+n_\alpha-1} \vec{\mathcal{L}}_{\ell_\alpha+n_\alpha-1}. \end{aligned} \quad (\text{A16})$$

Since \mathbf{S} is nonsingular, the $\vec{\mathcal{L}}_j^\dagger$ form a basis of \mathbb{C}^n , and therefore we can decompose $\vec{y}^\dagger(t)$ into this basis, namely,

$$\vec{y}^\dagger(t) = \sum_{j=1}^n c_j(t) \vec{\mathcal{L}}_j^\dagger. \quad (\text{A17})$$

The coefficients

$$c_j(t) = \vec{y}(t) \cdot \vec{\mathcal{R}}_j, \quad j \in [n] \quad (\text{A18})$$

follow from the biorthonormality relation (A13) of generalized left and generalized right eigenvectors.

Substituting the canonical form of \mathbf{A} , given by Eq. (A16), into Eq. (1), and using that the decomposition (A17) is unique, we obtain a set of m independent linearly coupled differential equations corresponding with each of the m Jordan blocks of the matrix \mathbf{A} . For the α th Jordan block of size n_α , we obtain the differential equation

$$\partial_t c_{\ell_\alpha+n_\alpha-1}(t) = \lambda_\alpha c_{\ell_\alpha+n_\alpha-1}(t) \quad (\text{A19})$$

together with the coupled differential equations

$$\partial_t c_{\ell_\alpha+\kappa}(t) = \lambda_{\ell_\alpha} c_{\ell_\alpha+\kappa}(t) + c_{\ell_\alpha+\kappa+1}(t) \quad (\text{A20})$$

for $\kappa = 0, 1, \dots, n_\alpha - 2$. The coupled Eqs. (A20) represent a feedforward loop [22]. Solving Eq. (A19), we obtain that

$$c_{\ell_\alpha+n_\alpha-1}(t) = e^{\lambda_\alpha t} c_{\ell_\alpha+n_\alpha-1}(0), \quad (\text{A21})$$

and solving Eqs. (A20), we obtain that

$$c_{\ell_\alpha+\kappa}(t) = e^{\lambda_\alpha t} p_\kappa^{(\alpha)}(t), \quad (\text{A22})$$

where

$$p_\kappa^{(\alpha)}(t) = \sum_{\beta=0}^{n_\alpha-1-\kappa} \frac{t^\beta}{\beta!} c_{\ell_\alpha+\kappa+\beta}(0) \quad (\text{A23})$$

is a polynomial of degree $n_\alpha - 1 - \kappa$ and where $\kappa = 0, 1, \dots, n_\alpha - 1$. Substituting the explicit solution of the coefficients $c_j(t)$ in Eq. (A17), we find that

$$\vec{y}^\dagger(t) = \sum_{\alpha=1}^m e^{\lambda_\alpha t} \sum_{\kappa=0}^{n_\alpha-1} p_\kappa^{(\alpha)}(t) \vec{\mathcal{L}}_{\ell_\alpha+\kappa}^\dagger. \quad (\text{A24})$$

For large $t \rightarrow \infty$, the dynamics of $\vec{y}^\dagger(t)$ is dominated by the eigenvalue with the largest real part, say λ_1 , such that

$$\vec{y}^\dagger(t) = O(e^{\text{Re}[\lambda_1]t} t^{n_1-1}). \quad (\text{A25})$$

Hence, the dynamical system is stable if $\text{Re}[\lambda_1] < 0$ and it is unstable if $\text{Re}[\lambda_1] > 0$.

This proves that $\vec{y}(t)$ is stable if and only if all eigenvalues of \mathbf{A} have negative real parts and it is unstable if and only if there exists at least one eigenvalue with a positive real part.

APPENDIX B: DIRECTED GRAPHS WITH A PRESCRIBED DEGREE DISTRIBUTION $p_{K^{\text{in}}, K^{\text{out}}}$

In this Appendix, we define the random, directed graphs with a prescribed degree distribution $p_{K^{\text{in}}, K^{\text{out}}}$, which we use throughout this paper. Subsequently, we detail the algorithm we use to sample graphs from this ensemble.

1. Definition

A random graph \mathcal{G} of size n is a random set $E \subset [n] \times [n]$ of directed links.

In the present paper, we consider random graphs with a given prescribed degree distribution $p_{K^{\text{in}}, K^{\text{out}}}$. In this ensemble, graphs are drawn with probability

$$\text{Prob}(E = e) = \frac{P_{\{K_j^{\text{in}}, K_j^{\text{out}}\}_{j \in [n]}}(\{k_j^{\text{in}}, k_j^{\text{out}}\}_{j \in [1, n]})}{n(\{k_j^{\text{in}}, k_j^{\text{out}}\}_{j \in [n]})}, \quad (\text{B1})$$

where $p_{\{K_j^{\text{in}}, K_j^{\text{out}}\}_{j \in [n]}}$ is the probability distribution of a degree sequence and where $n(\{k_j^{\text{in}}, k_j^{\text{out}}\}_{j \in [n]})$ is the number of graphs with a degree sequence $\{k_j^{\text{in}}, k_j^{\text{out}}\}_{j \in [n]}$. The probability distribution of a degree sequence is proportional to

$$P_{\{K_j^{\text{in}}, K_j^{\text{out}}\}_{j \in [1, n]}} \sim \delta_{\sum_{j=1}^n k_j^{\text{in}}, \sum_{j=1}^n k_j^{\text{out}}} \prod_{j=1}^n p_{K^{\text{in}}, K^{\text{out}}}(k_j^{\text{in}}, k_j^{\text{out}}). \quad (\text{B2})$$

This model is called the uniform model [38]. It is the configuration model [2,4,37] conditioned on the event that there are no self-links and multiple edges. However, since in the configuration model self-links and multiple edges are rare, the results in this paper apply both to the configurational model and the uniform model (the local neighborhood of a randomly selected node is for both models the same in the limit $n \rightarrow \infty$).

2. Algorithm

We detail the algorithm we use in this paper to sample graphs from the ensemble defined in Sec. B 1. We consider the specific case of a distribution of the form

$$p_{K^{\text{in}}, K^{\text{out}}}(k, \ell) = q p_{\text{deg}}(k) p_{\text{deg}}(\ell) + (1 - q) p_{\text{deg}}(k) \delta_{k, \ell}. \quad (\text{B3})$$

The algorithm we have used to generate random graphs from this degree distribution consists of the following steps. (1) We generate a sequence of n i.i.d. variables k_j^{in} from the distribution $p_{K^{\text{in}}}$. (2) We generate a sample of n i.i.d. Bernoulli random variables $x_j \in \{0, 1\}$, which take the value $x_j = 1$ with probability q and $x_j = 0$ with probability $1 - q$. (3) If $x_j = 0$, then we set $k_j^{\text{out}} = k_j^{\text{in}}$. (4) We generate a random permutation ζ on the set of indices $j \in [1, n]$ for which $x_j = 1$. (5) If $x_j = 1$, then we set $k_j^{\text{out}} = k_{\zeta(j)}^{\text{in}}$. (6) To each j we associate k_j^{in} insockets and k_j^{out} outsockets. (7) We randomly connect pairs of insockets with outsockets by starting with the node with the

highest total degree $k_j^{\text{in}} + k_j^{\text{out}}$ and connecting its sockets to k_j^{in} randomly selected outsockets and k_j^{out} randomly selected insockets. Two connected sockets create a directed edge. (8) We do not allow for self-links and we do not allow for multiple edges. Sometimes step seven in the algorithm fails because connecting two sockets would create either a self-link or a multiple edge. In this case, we the algorithm restarts step seven. (9) We repeat step seven until the algorithm has found a proper set of edges that defines an oriented simple random graph.

This algorithm works very well for most of the degree distributions discussed in this paper, except for power-law random graphs with a small exponent a , see Sec. VC. This is because for power-law random graphs it can be difficult to avoid multiple edges or self-links. Generating graphs with a power-law degree distribution with a small exponent a requires more sophisticated algorithms, such as, algorithms using Markov chains [117,118]. Alternatively, one could consider the configurational model instead of the uniform model and allow for self-links and multiple edges. One should however bare in mind that for power-law random graphs with small exponent a the configuration model and the uniform model may not be equivalent anymore because finite size effects will be significant.

APPENDIX C: ORIENTED RINGS IN RANDOM AND DIRECTED GRAPHS

An oriented ring graph of length ℓ is a subgraph of size ℓ that has an adjacency matrix of the form

$$A_{ij} = \begin{cases} J_i \delta_{j,i+1} & i \in [\ell - 1], \\ J_\ell \delta_{j,1} & i = \ell, \end{cases} \quad (C1)$$

where $J_i \in \mathbb{R}$.

Oriented ring graphs may contribute stochastic outliers to the spectra of random graphs with a prescribed degree distribution $p_{K^{\text{in}},K^{\text{out}}}$. Here, we first derive explicit expressions for the eigenvalues of an isolated oriented ring graph, and then we count the number of oriented ring graphs in random and directed graphs.

1. Eigenvalues of an oriented ring graph

The eigenvalues λ_j of an oriented ring graph are located on the circle centered at the origin with radius

$$\gamma = \left(\prod_{j=1}^{\ell} |J_j| \right)^{1/\ell} \quad (C2)$$

and are given by

$$\lambda_j = \gamma \operatorname{sign} \left(\prod_{j=1}^{\ell} J_j \right) e^{i\frac{2\pi}{\ell}(j-1)}, \quad j \in [\ell]. \quad (C3)$$

Notice that for simplicity we have used that $A_{ii} = 0$. If $A_{ii} = -d$, then the eigenvalues are located on the circle with radius γ centered at $-d$.

2. Number of oriented ring graphs in a random and directed graph

We count the average number $\langle N(\ell) \rangle$ of oriented ring graphs of length ℓ located in a random and directed graph with a prescribed degree distribution.

Before considering the general case, we count the number of oriented rings in the directed Erdős-Rényi ensemble. For the directed Erdős-Rényi ensemble, we obtain [119]

$$\langle N(\ell) \rangle = \frac{1}{\ell} \left(\frac{c}{n} \right)^\ell n(n-1) \dots (n-\ell+1), \quad (C4)$$

which is the probability of drawing ℓ edges multiplied by the total number of ordered sequences of ℓ indices. In the limit of large n ,

$$\langle N(\ell) \rangle = \frac{c^\ell}{\ell}. \quad (C5)$$

The expected number of cycles of finite length is for $c < 1$ given by

$$\langle N \rangle = \sum_{\ell=2}^{\infty} \langle N(\ell) \rangle = -\ln(1-c) - c. \quad (C6)$$

Consider now a random and directed graph with a prescribed degree distribution $p_{K^{\text{in}},K^{\text{out}}}$. The distribution of outdegrees obtained by following a link in a directed graph is given by

$$\frac{p_{K^{\text{in}},K^{\text{out}}}(k,\ell)k}{c}. \quad (C7)$$

Hence, the average number of oriented rings of length ℓ is given by

$$\langle N(\ell) \rangle = \frac{1}{\ell} \frac{\langle K^{\text{out}} K^{\text{in}} \rangle^\ell}{c^\ell} n(n-1) \dots (n-\ell+1) \quad (C8)$$

and in the limit of large n

$$\langle N(\ell) \rangle = \frac{1}{\ell} \frac{\langle K^{\text{out}} K^{\text{in}} \rangle^\ell}{(cn)^\ell} = \frac{1}{\ell} [c(\rho+1)]^\ell. \quad (C9)$$

If $\rho = 0$, then Eq. (C9) is equivalent to Eq. (C5).

The total expected number of cycles of finite length is for $c(\rho+1) < 1$ given by

$$\langle N \rangle = \sum_{\ell=2}^{\infty} \langle N(\ell) \rangle = -\ln[1-c(\rho+1)] - c(\rho+1).$$

The distribution of N , the number of oriented cycles of finite length, is a Poisson distribution with mean $\langle N \rangle$.

The probability p_+ to have at least one cycle of length larger than 2 is given by

$$p_+ = 1 - e^{-\langle N \rangle} = 1 - (1 - c(\rho+1))e^{c(\rho+1)}.$$

Note that $p_+ \rightarrow 0$ for $c(\rho+1) \rightarrow 0$ and $p_+ \rightarrow 1$ for $c(\rho+1) \rightarrow 1$. Hence, at the percolation transition of the SCC there exists with probability one at least one cycle of finite length.

APPENDIX D: THE ALGEBRAIC MULTIPLICITY OF THE $-d$ -EIGENVALUE IN RANDOM AND DIRECTED GRAPHS

We show that the spectral distribution $\mu(z)$ of the adjacency matrix \mathbf{A} of random and directed graphs, as defined in

Eq. (3), takes the form

$$\mu(z) = (1 - s_{sc})\delta(z + d) + s_{sc} \tilde{\mu}(z), \tag{D1}$$

where s_{sc} is the relative size of the giant strongly connected component, see Sec. II C 1, and where $\tilde{\mu}(\lambda)$ is the normalized spectral distribution associated with the giant strongly connected component. Since d only contributes a trivial shift $\lambda_j \rightarrow \lambda_j - d$ to all eigenvalues, we can set $d = 0$ without loss of generality.

In order to demonstrate Eq. (D1), we use the spectral theory for sparse, non-Hermitian, random matrices from Refs. [42,45]. As shown in those references, the spectral distribution $\mu(z)$ of matrices of the form given by Eq. (3) can be expressed as

$$\mu(z) = \frac{1}{\pi} \lim_{\eta \rightarrow 0^+} \partial_{z^*} \int d^2 \mathbf{g} p_G(\mathbf{g}) [\mathbf{g}]_{21}, \tag{D2}$$

where $\partial_{z^*} = (\partial_x + i\partial_y)/2$ and where \mathbf{g} is a 2×2 square matrix with complex-valued entries. The distribution p_G solves the recursive distributional equation

$$p_G(\mathbf{g}) = \sum_{k=0}^{\infty} \sum_{\ell=0}^{\infty} p_{K^{in}, K^{out}}(k, \ell) \int \prod_{j=1}^k d^2 \mathbf{g}_j q_{in}(\mathbf{g}_j) \int \prod_{j=1}^{\ell} d^2 \mathbf{h}_j q_{out}(\mathbf{h}_j) \delta \left[\mathbf{g} - \frac{1}{z - i\eta \mathbf{1}_2 - \sigma_- \sum_{j=1}^k \mathbf{g}_j \sigma_+ - \sigma_+ \sum_{j=1}^{\ell} \mathbf{h}_j \sigma_-} \right], \tag{D3}$$

where

$$\mathbf{z} = \begin{pmatrix} 0 & z \\ z^* & 0 \end{pmatrix}, \quad \mathbf{1}_2 = \begin{pmatrix} 1 & 0 \\ 0 & 1 \end{pmatrix}, \tag{D4}$$

and

$$\sigma_- = \begin{pmatrix} 0 & 0 \\ 1 & 0 \end{pmatrix}, \quad \sigma_+ = \begin{pmatrix} 0 & 1 \\ 0 & 0 \end{pmatrix}. \tag{D5}$$

The distributions q_{out} and q_{in} solve the recursive distributional equations

$$q_{out}(\mathbf{g}) = \sum_{k=0}^{\infty} \sum_{\ell=0}^{\infty} \frac{k p_{K^{in}, K^{out}}(k, \ell)}{c} \int \prod_{j=1}^{k-1} d^2 \mathbf{g}_j q_{in}(\mathbf{g}_j) \int \prod_{j=1}^{\ell} d^2 \mathbf{h}_j q_{out}(\mathbf{h}_j) \delta \left[\mathbf{g} - \frac{1}{z - i\eta \mathbf{1}_2 - \sigma_- \sum_{j=1}^{k-1} \mathbf{g}_j \sigma_+ - \sigma_+ \sum_{j=1}^{\ell} \mathbf{h}_j \sigma_-} \right] \tag{D6}$$

and

$$q_{in}(\mathbf{h}) = \sum_{k=0}^{\infty} \sum_{\ell=0}^{\infty} \frac{\ell p_{K^{in}, K^{out}}(k, \ell)}{c} \int \prod_{j=1}^k d^2 \mathbf{g}_j q_{in}(\mathbf{g}_j) \int \prod_{j=1}^{\ell-1} d^2 \mathbf{h}_j q_{out}(\mathbf{h}_j) \delta \left[\mathbf{h} - \frac{1}{z - i\eta \mathbf{1}_2 - \sigma_- \sum_{j=1}^k \mathbf{g}_j \sigma_+ - \sigma_+ \sum_{j=1}^{\ell-1} \mathbf{h}_j \sigma_-} \right], \tag{D7}$$

respectively.

In order to derive the result (D1), we use the ansatz

$$q_{out}(\mathbf{g}) = b \int d^2 x \hat{q}_{out}(x) \delta \left[\mathbf{g} - \begin{pmatrix} x & 1/z^* \\ 1/z & 0 \end{pmatrix} \right] + (1 - b) \tilde{q}_{out}(\mathbf{g}) \tag{D8}$$

and

$$q_{in}(\mathbf{g}) = a \int d^2 x \hat{q}_{in}(x) \delta \left[\mathbf{g} - \begin{pmatrix} 0 & 1/z^* \\ 1/z & x \end{pmatrix} \right] + (1 - a) \tilde{q}_{in}(\mathbf{g}), \tag{D9}$$

where $a, b \in [0, 1]$, and $\hat{q}_{out}(x)$, $\tilde{q}_{out}(\mathbf{g})$, $\hat{q}_{in}(x)$, and $\tilde{q}_{in}(\mathbf{g})$ are normalized distributions.

Using the ansatz (D8) and (D9) in the relations (D6) and (D7), we obtain that a and b solve the self-consistent equations (16) and (17), and the distributions $\hat{q}_{out}(x)$, $\tilde{q}_{out}(\mathbf{g})$, $\hat{q}_{in}(x)$, and $\tilde{q}_{in}(\mathbf{g})$ solve a set of recursive distributional equations, whose precise form will not matter.

Using the ansatz (D8) and (D9) in Eq. (D3), we obtain

$$p_G(\mathbf{g}) = (1 - s_{wc} + s_t) \delta(\mathbf{g} - \mathbf{z}^{-1}) + (s_{wc} - s_{in} - s_t) \int dx \hat{p}_{in}(x) \delta \left[\mathbf{g} - \begin{pmatrix} x & 1/z^* \\ 1/z & 0 \end{pmatrix} \right] \\ + (s_{wc} - s_{out} - s_t) \int dx \hat{p}_{out}(x) \delta \left[\mathbf{g} - \begin{pmatrix} 0 & 1/z^* \\ 1/z & x \end{pmatrix} \right] + (s_{in} + s_{out} + s_t - s_{wc}) \tilde{p}(\mathbf{g}), \tag{D10}$$

where s_{in} , s_{out} , s_{wc} , and s_t denote the relative sizes of the incomponent, outcomponent, weakly connected component, and tendrils, respectively (see Sec. II C or Refs. [28,40,41]). The distributions $\hat{p}_{in}(x)$, $\hat{p}_{out}(x)$, and $\tilde{p}(\mathbf{g})$ solve a set of recursive distributional equations that we have omitted because their precise form does not matter here.

Equations (D2) and (D10), together with the formulas

$$\frac{1}{\pi} \partial_{z^*} \frac{1}{z} = \delta(z) \tag{D11}$$

and

$$s_{sc} = s_{in} + s_{out} + s_t - s_{wc}, \tag{D12}$$

imply the final result (D1), which we aimed to prove in this Appendix.

APPENDIX E: DERIVATION OF THE RECURSIVE DISTRIBUTIONAL EQUATIONS FOR p_R IN RANDOM AND DIRECTED GRAPHS WITH A PRESCRIBED DEGREE DISTRIBUTION $p_{K^{in}, K^{out}}$

In this Appendix, we derive the recursive distributional equations (48) and (49) for the distribution p_R of entries of right eigenvectors in random and directed graphs with a prescribed degree distribution $p_{K^{in}, K^{out}}$. The relations (48) and (49) apply to the eigenvalues λ_b located at the boundary of the continuous part σ_{ac} of the spectrum and to deterministic eigenvalue outliers λ_{isol} .

The derivations we present are based on the theory of Ref. [44] that relies on the cavity method [45,50,54–56] (also known as the objective method in probability theory [56,58] and belief propagation in computer science [120–122]).

The theory of Ref. [44] builds on two properties of random and directed graphs with a prescribed degree distribution, namely, that these random graphs are *locally treelike* and *oriented*. In addition, it uses that eigenvalues λ_b and λ_{isol} are *stable*, i.e., insensitive to small matrix perturbations.

In a first section, we clarify what we mean by a matrix being locally treelike and oriented, and in the second and third sections, we derive the recursive distributional Eqs. (48) and (49).

1. Locally treelike and oriented random matrices

We say that a nondirected graph is a tree if it is connected and it does not contain cycles, see Ref. [123], and we say that a matrix is oriented if $A_{ij}A_{ji} = 0$ for all pairs i and j . In the following, we extend these global definitions to local definitions that apply to sequences of random matrices \mathbf{A}_n , with $n \in \mathbb{N}$.

First we define the concept of local treelikeness. Let \mathbf{A}_n , with $n \in \mathbb{N}$, be a sequence of random matrices and let \mathbf{C}_n be their associated adjacency matrices, i.e., $C_{kj} = 1$ when $A_{kj} \neq 0$ and $C_{kj} = 0$ when $A_{kj} = 0$. We also consider the associated symmetrized adjacency matrices $\tilde{\mathbf{C}}_n$ with entries $\tilde{C}_{jk} = \max\{C_{jk}, C_{kj}\}$, which are the adjacency matrices of nondirected simple graphs. We define the nondirected ℓ -neighborhood of a node i as the subgraph of $\tilde{\mathbf{C}}_n$ formed by the nodes that are separated no more than a distance ℓ from i . We say that the sequence of random matrices \mathbf{A}_n is locally treelike if, for each $\ell \in \mathbb{N}$, the nondirected ℓ neighborhood of a uniformly and randomly selected node in $\tilde{\mathbf{C}}_n$ is in the limit $n \rightarrow \infty$ with probability one a tree, see Ref. [56].

Second, we define local orientedness of a sequence of random matrices \mathbf{A}_n . We say that the sequence of random

matrices \mathbf{A}_n is locally oriented if, for each $\ell \in \mathbb{N}$, the principal submatrix of \mathbf{A}_n formed by the nodes in the nondirected ℓ neighborhood of a uniformly and randomly selected node i is in the limit $n \rightarrow \infty$ with probability one oriented.

2. Recursion relations for p_R in locally treelike and oriented matrices

Let λ be an eigenvalue of the matrix \mathbf{A} and let \vec{R} be the right eigenvector associated with λ . Equation (27) implies that

$$R_j = \frac{1}{\lambda - A_{jj}} \sum_{k=1; k \neq j}^n A_{jk} R_k, \tag{E1}$$

for all $j \in [n]$. Using Eq. (3) and the graph definitions in Sec. II A, we obtain

$$R_j = \frac{1}{\lambda + d} \sum_{k \in \partial_j^{out}} J_{jk} R_k. \tag{E2}$$

In general, the random variables R_k are correlated with the entries J_{jk} and the degree K_j^{out} , and therefore, Eq. (E2) is not useful to derive a selfconsistent distributional equation. However, if \mathbf{A} is a locally treelike and oriented matrix, then the R_k are statistically independent from the J_{jk} and K_j^{out} .

The statistical independence between R_k and A_{jk} can be understood from a recursive argument. Let $\mathbf{A}^{(j)}$ be the principal submatrix obtained from \mathbf{A} by deleting its j th column and row, and let $\vec{R}^{(j)}$ be the right eigenvector of $\mathbf{A}^{(j)}$ associated with the same eigenvalue λ ; hence, λ is an eigenvalue of both \mathbf{A} and $\mathbf{A}^{(j)}$. Then, for a locally treelike and oriented matrix it holds, in the limit $n \rightarrow \infty$, that

$$R_k = R_k^{(j)}, \tag{E3}$$

for all $k \in [n]$ and $j \in \partial_k^{in}$, where $R_k^{(j)}$ is the k th element of the right eigenvector $\vec{R}^{(j)}$. For a detailed derivation of Eq. (E3), we refer to the next Appendix F. Importantly, the derivation of Eq. (E3) in Appendix F relies on the assumption that λ is either a deterministic eigenvalue outlier λ_{isol} or an eigenvalue λ_b located at the boundary of the continuous part of the spectrum.

Equations (E2) and (E3) imply that

$$R_k^{(j)} = \frac{1}{\lambda + d} \sum_{\ell \in \partial_k^{out}} J_{k\ell} R_\ell^{(k)}, \tag{E4}$$

for all $k \in [n]$ and $j \in \partial_k^{in}$. Since we are interested in the statistics of R , we will also use the relation

$$R_j = \frac{1}{\lambda + d} \sum_{k \in \partial_j^{out}} J_{jk} R_k^{(j)}, \tag{E5}$$

which also follows from Eqs. (E2) and (E3).

In the remaining part of this Appendix, we use Eqs. (E4) and (E5) to derive the recursion relations (48) and (49). We define the distributions of right eigenvector entries R_j ,

$$p_R(r|\mathbf{A}) = \frac{1}{n} \sum_{j=1}^n \delta(r - R_j) \tag{E6}$$

and the distribution of entries $R_k^{(j)}$,

$$q_R(r|\mathbf{A}) = \frac{1}{c n} \sum_{k=1}^n \sum_{j \in \partial_k^{\text{in}}} \delta(r - R_k^{(j)}), \quad (\text{E7})$$

where c is the mean outdegree. The distribution $p_R(r|\mathbf{A})$ is obtained by selecting uniformly at random a node j and asking what is the corresponding eigenvector entry R_j , whereas the distribution $q_R(r|\mathbf{A})$ is obtained by selecting uniformly at random an edge $j \rightarrow k$ and asking what is the eigenvector entry $R_k^{(j)}$. Since the model defined in Sec. II A is locally tree-like, all random variables on the right hand side of Eqs. (E4) and (E5) are independent. In addition, using that all nodes are statistically equivalent, we obtain the recursion relations (48) and (49), which we were meant to derive.

APPENDIX F: RECURSION RELATIONS FOR THE ENTRIES R_j OF RIGHT EIGENVECTORS

We derive a set of recursion relations for the entries R_j of the right eigenvectors associated with deterministic outliers λ_{isol} or eigenvalues located at the boundary of the continuous part of the spectrum σ_{ac} in locally treelike random matrices in the limit of infinitely large n . In the special case of locally tree-like and oriented matrices, see Appendix E 1 for a definition, we show that Eq. (E3) holds.

In order to clearly show how the assumptions of locally treelikeness and locally orientedness enter in the theory, we first derive a set of recursion relations in the entries R_j of a general matrix \mathbf{A} . As we will demonstrate, the relations for general matrices are not closed and are thus not useful. In order to close these equations, we make the assumption that \mathbf{A} is locally treelike. Lastly, we show how the recursion relations simplify when \mathbf{A} is also locally treelike and oriented.

1. General matrices

The derivations we present rely on a recursive implementation of the Schur formula to the resolvent of \mathbf{A} .

The resolvent of \mathbf{A} is defined by

$$\mathbf{G}_{\mathbf{A}}(z) = \frac{1}{\mathbf{A} - z \mathbf{1}_n}, \quad z \in \mathbb{C} \setminus \{\lambda_1, \lambda_2, \dots, \lambda_n\}, \quad (\text{F1})$$

with $\mathbf{1}_n$ the identity matrix of size n . In the limit of $n \rightarrow \infty$, the resolvent $\mathbf{G}_{\mathbf{A}}(z)$ only exists for values $z \notin \sigma_{\text{ac}}$.

Let λ be a nondegenerate eigenvalue, and let \vec{R} and \vec{L} be a corresponding left and right eigenvector. We assume that there exists a path in the complex plane that reaches λ and along which $\mathbf{G}_{\mathbf{A}}(\lambda - \eta)$ exists. In addition, we assume that λ is a *stable* eigenvalue of \mathbf{A} , i.e., we assume that if λ is an eigenvalue of \mathbf{A} , then λ is also an eigenvalue of the principal submatrix $\mathbf{A}^{(j)}$, which we obtain from \mathbf{A} by deleting the j th row and column. Hence, λ is either a deterministic eigenvalue outlier or is located at the boundary of the continuous part of the spectrum σ_{ac} .

Since there exists a path that reaches λ and along which $\mathbf{G}_{\mathbf{A}}(\lambda - \eta)$ exists, we can write

$$\lim_{\eta \rightarrow 0} \eta \mathbf{G}_{\mathbf{A}}(\lambda - \eta) = \vec{R} \vec{L}^\dagger + O(|\eta|). \quad (\text{F2})$$

Note that relation (F2) also holds when the matrix \mathbf{A} is not diagonalizable since we can decompose $\mathbf{G}_{\mathbf{A}}(\lambda)$ in a biorthonormal system of generalized left and right eigenvectors, analogous to the decomposition of \mathbf{A} in Eq. (A16). Eq. (F2) implies that the components R_j of \vec{R} are given by

$$R_j = \vec{e}_j \cdot \vec{R} = \lim_{\eta \rightarrow 0} \eta \frac{\sum_{\ell=1}^n G_{j\ell}(\lambda - \eta)}{\vec{L} \cdot \vec{1}}, \quad (\text{F3})$$

where $G_{j\ell}(\lambda - \eta) = [\mathbf{G}_{\mathbf{A}}(\lambda)]_{j\ell}$, $\vec{1}$ is the column vector with all components equal to one, and \vec{e}_j is the column vector with all components equal to zero, except for the j th component, which is equal to one.

To compute the elements $G_{j\ell}(\lambda)$ of the resolvent matrix, we use the Schur formula, which is a common tool in random matrix theory (see, for instance, Sec. 2.4.3 in Ref. [124] and also Refs. [56,70,125]). Let

$$\begin{pmatrix} \mathbf{a} & \mathbf{b} \\ \mathbf{c} & \mathbf{d} \end{pmatrix} \quad (\text{F4})$$

be a block matrix, then

$$\mathbf{s}_a := \mathbf{d} - \mathbf{c} \mathbf{a}^{-1} \mathbf{b} \quad (\text{F5})$$

is the Schur complement of block \mathbf{a} , and

$$\mathbf{s}_d := \mathbf{a} - \mathbf{b} \mathbf{d}^{-1} \mathbf{c} \quad (\text{F6})$$

is the Schur complement of block \mathbf{d} . If \mathbf{a} and its Schur complement \mathbf{s}_a are invertible matrices, then the following block inversion formula holds:

$$\begin{pmatrix} \mathbf{a} & \mathbf{b} \\ \mathbf{c} & \mathbf{d} \end{pmatrix}^{-1} = \begin{pmatrix} \mathbf{s}_d^{-1} & -\mathbf{s}_d^{-1} \mathbf{b} \mathbf{d}^{-1} \\ -\mathbf{d}^{-1} \mathbf{c} \mathbf{s}_d^{-1} & \mathbf{s}_a^{-1} \end{pmatrix}, \quad (\text{F7})$$

which we call the *Schur formula*.

We use the Schur formula to derive recursion relations for the elements of the resolvent $\mathbf{G}_{\mathbf{A}}$ and eventually Eqs. (E4) and (E5). Applying the Schur formula to the off-diagonal elements $G_{j\ell}$ of the resolvent, we obtain

$$G_{j\ell} = -G_{jj} \sum_{k=1; (k \neq j)}^n A_{jk} G_{k\ell}^{(j)}, \quad (\text{F8})$$

where

$$G_{k\ell}^{(j)} = [\mathbf{G}_{\mathbf{A}^{(j)}}]_{k\ell} \quad (\text{F9})$$

$$\mathbf{G}_{\mathbf{A}^{(j)}} = (\mathbf{A}_{n-1}^{(j)} - \lambda \mathbf{1}_{n-1})^{-1}. \quad (\text{F10})$$

Summing over the index ℓ , we obtain

$$\sum_{\ell=1}^n G_{j\ell} = G_{jj} \left(1 - \sum_{k=1; (k \neq j)}^n A_{jk} \sum_{\ell=1; (\ell \neq j)}^n G_{k\ell}^{(j)} \right). \quad (\text{F11})$$

Finally, using Eq. (F3), we find

$$R_j = \lim_{\eta \rightarrow 0} \eta \frac{G_{jj}}{\vec{L} \cdot \vec{1}} - G_{jj} \sum_{k=1; (k \neq j)}^n A_{jk} \lim_{\eta \rightarrow 0} \eta \frac{\sum_{\ell=1; (\ell \neq j)}^n G_{k\ell}^{(j)}}{\vec{L} \cdot \vec{1}} + O(|\eta|). \quad (\text{F12})$$

The first term can be neglected with respect to the second term as it is a factor $O(1/n)$ smaller, and in the second term, we

identify

$$R_k^{(j)} = \lim_{\eta \rightarrow 0} \eta \frac{\sum_{\ell=1; (\ell \neq j)}^n G_{k\ell}^{(j)}}{\bar{L}^{(j)} \cdot \bar{1}}, \quad (\text{F13})$$

where we have used that $\bar{L} \cdot \bar{1} \approx \bar{L}^{(j)} \cdot \bar{1}$ for large enough n . Hence, we obtain the relation

$$R_j = -G_{jj}(\lambda - \eta) \sum_{k=1; (k \neq j)}^n A_{jk} R_k^{(j)}. \quad (\text{F14})$$

We can repeat the above line of reasoning to obtain a recursion relation for the entries $R_k^{(j)}$ of the right eigenvector $\bar{R}^{(j)}$ associated with the eigenvalue λ of $\mathbf{A}^{(j)}$. We obtain then that

$$R_k^{(j)} = -G_{kk}^{(j)}(\lambda - \eta) \sum_{\ell=1; \ell \neq j, k}^n A_{k\ell} R_\ell^{(j), (k)}, \quad (\text{F15})$$

where $R_\ell^{(j), (k)}$ is the ℓ th entry of the right eigenvector $\bar{R}^{(j), (k)}$ associated with the eigenvalue λ of the principal submatrix $\mathbf{A}^{(j), (k)}$. The principal submatrix $\mathbf{A}^{(j), (k)}$ is obtained from \mathbf{A} by removing both the j th and k th rows and columns.

In order to obtain an expression for the diagonal elements G_{kk} and $G_{kk}^{(j)}$ that appear in the recursion Eqs. (F14) and (F15), we use again the Schur formula (F7). We obtain that

$$G_{jj}(z) = \frac{1}{-z + A_{jj} - \sum_{k, k'=1; (k, k' \neq j)}^n A_{jk} G_{kk'}^{(j)}(z) A_{kj}} \quad (\text{F16})$$

and

$$G_{kk}^{(j)}(z) = \frac{1}{-z + A_{kk} - \sum_{\ell, \ell'=1; (\ell, \ell' \neq k, j)}^n A_{j\ell} G_{\ell\ell'}^{(j), (k)}(z) A_{\ell'j}}, \quad (\text{F17})$$

for all $z \notin \sigma_{ac}$.

It is insightful to rewrite these equations using the notation

$$A_{jk} = -D_j \delta_{j,k} + (1 - \delta_{j,k}) J_{jk} C_{jk} \quad (\text{F18})$$

where $C_{jk} \in \{0, 1\}$ is the adjacency matrix denoting whether $A_{kj} \neq 0$ ($C_{kj} = 1$) or $A_{kj} = 0$ ($C_{kj} = 0$).

Equations (F14) and (F15) read then

$$R_j = -G_{jj}(\lambda - \eta) \sum_{k \in \partial_j^{out}} J_{jk} R_k^{(j)} \quad (\text{F19})$$

and

$$R_k^{(j)} = -G_{kk}^{(j)}(\lambda - \eta) \sum_{\ell \in \partial_k^{out} \setminus \{j\}} J_{k\ell} R_\ell^{(j), (k)}, \quad (\text{F20})$$

where $j \in \partial_k^{in}$, and Eqs. (F16) and (F17) read

$$G_{jj} = \frac{1}{-z - D_j - \sum_{k \in \partial_j^{out}, k' \in \partial_j^{in}} J_{jk} G_{kk'}^{(j)} J_{k'j}} \quad (\text{F21})$$

and

$$G_{kk}^{(j)} = \frac{1}{-z - D_k - \sum_{\ell \in \partial_k^{out} \setminus \{j\}} \sum_{\ell' \in \partial_k^{in} \setminus \{j\}} J_{k\ell} G_{\ell\ell'}^{(j), (k)} J_{\ell'k}}. \quad (\text{F22})$$

The recursion Eqs. (F19) and (F22) hold for general matrices \mathbf{A} . However, they do not form a closed set of equations and are thus not useful. In order to close this set of recursion

relations, we make the assumption that the matrices \mathbf{A} are locally treelike.

2. Locally treelike matrices

We show how the set of recursion Eqs. (F19)–(F22) simplify for random matrices \mathbf{A} that are locally treelike.

For matrices that are locally treelike, it holds that

$$R_\ell^{(j), (k)} = R_\ell^{(k)}, \quad (\text{F23})$$

for all $\ell \in [n]$, $k \in \partial_\ell^{in}$ and $j \in \partial_k^{in}$. This is because ℓ and j belong to disjoint trees of the forest represented by the matrix $\mathbf{A}^{(k)}$. As a consequence, Eqs. (F20) simplify into

$$R_k^{(j)} = -G_{kk}^{(j)}(\lambda - \eta) \sum_{\ell \in \partial_k^{out} \setminus \{j\}} J_{k\ell} R_\ell^{(k)}, \quad (\text{F24})$$

for all $k \in [n]$ and $j \in \partial_k^{in}$.

The resolvent Eqs. (F21) and (F22) also simplify because for locally treelike graphs it holds that

$$G_{kk'}^{(j)} = 0 \quad (\text{F25})$$

for all $k \in \partial_j^{out}$ and $k \in \partial_j^{in}$, and

$$G_{\ell\ell}^{(j), (k)} = G_{\ell\ell}^{(k)} \quad (\text{F26})$$

for all $\ell \in [n]$, $k \in \partial_\ell$ and $j \in \partial_k \setminus \{\ell\}$.

The relations (F25) and (F26) follow from the fact that for values $z \notin \sigma_{ac}$, we can develop the series expansion

$$\mathbf{G}_{\mathbf{A}_n}(z) = -\frac{1}{z} \sum_{m=0}^{\infty} \frac{\mathbf{A}^m}{z^m}, \quad (\text{F27})$$

and hence

$$G_{jk}(z) := [\mathbf{G}_{\mathbf{A}_n}(z)]_{jk} = -\frac{1}{z} \sum_{m=0}^{\infty} \frac{[\mathbf{A}^m]_{jk}}{z^m}. \quad (\text{F28})$$

Equation (F25) follows now from Eq. (F28) and the fact that for locally treelike matrices it holds that

$$[(\mathbf{A}^{(j)})^m]_{kk'} = 0 \quad (\text{F29})$$

for all $k \in \partial_j^{out}$, $k' \in \partial_j^{in}$, and $m \in \mathbb{N}$, since $k \in \partial_j^{out}$ and $k' \in \partial_j^{in}$ belong to disjoint trees of the forest represented by the adjacency matrix $\mathbf{A}^{(j)}$, and hence there exists no path of finite length that connects k to k' .

Equation (F26) on the other hand, follows from Eq. (F28) and the fact that

$$[(\mathbf{A}^{(j), (k)})^m]_{\ell\ell} = [(\mathbf{A}^{(k)})^m]_{\ell\ell} \quad (\text{F30})$$

for all $\ell \in [n]$, $k \in \partial_\ell$, $j \in \partial_k \setminus \{\ell\}$ and $m \in \mathbb{N}$, since j and ℓ belong to disconnected trees of the forest represented by $\mathbf{A}^{(k)}$.

Using Eqs. (F25) and (F26) in Eqs. (F21) and (F22), we obtain [44,45]

$$G_{jj} = \frac{1}{-z - D_j - \sum_{k \in \partial_j^{out}} J_{jk} G_{kk}^{(j)} J_{kj}} \quad (\text{F31})$$

and

$$G_{kk}^{(j)} = \frac{1}{-z - D_k - \sum_{\ell \in \partial_k^{out} \setminus \{j\}} J_{k\ell} G_{\ell\ell}^{(k)} J_{\ell k}}. \quad (\text{F32})$$

Note that for symmetric random matrices, Eqs. (F31) and (F32) are equivalent to the recursion relations for the diagonal elements of the resolvent derived in Refs. [42,77,78].

Equations (F19), (F24), (F31), and (F32) form a closed set of recursion relations. They can either be solved on a given graph instance or we can solve these equations in a distributional sense for a random graph ensemble. In either case, we obtain information about the statistics of R_j .

3. Locally treelike and oriented matrices

For random matrices that are locally treelike and oriented, we can use in Eqs. (F31) and (F32) that

$$J_{jk}J_{kj} = 0. \tag{F33}$$

As a consequence, we obtain the explicit expressions

$$G_{jj} = \frac{1}{-z - D_j} \tag{F34}$$

and

$$G_{kk}^{(j)} = \frac{1}{-z - D_k}. \tag{F35}$$

Substituting Eqs. (F34) and (F35) into Eqs. (F19) and (F24), we obtain

$$R_j = \frac{1}{\lambda + D_j} \sum_{k \in \partial_j^{\text{out}}} J_{jk} R_k^{(j)} \tag{F36}$$

and

$$R_k^{(j)} = \frac{1}{\lambda + D_k} \sum_{\ell \in \partial_k^{\text{out}} \setminus \{j\}} J_{k\ell} R_\ell^{(k)}. \tag{F37}$$

From Eqs. (F36) and (F37), we observe that

$$R_k = R_k^{(j)} \tag{F38}$$

for all $k \in [n]$ and $j \in \partial_k^{\text{in}}$, since then $j \notin \partial_k^{\text{out}}$ and thus the right-hand side of Eqs. (F36) and (F37) are identical.

This concludes the derivation of Eq. (E3), which we were meant to show.

APPENDIX G: NORMALIZABLE SOLUTIONS TO THE RECURSIVE DISTRIBUTIONAL EQS. (48) AND (49) FOR p_R

In this Appendix, we derive analytical results for $\lambda_b \in \partial\sigma_{\text{ac}}$, and λ_{isol} by identifying values of λ for which Eqs. (48) and (49) admit a normalizable solution.

Since Eqs. (48) and (49) are linear distributional equations, we can derive a set of fixed-point equations for the lower-order moments of R and L . In order to distinguish averages with respect to p_R with those with respect to q_R , we introduce the notation

$$\langle f(R) \rangle = \int d^2r p_R(r) f(r) \tag{G1}$$

and

$$\langle f(R) \rangle_q = \int d^2r q_R(r) f(r), \tag{G2}$$

where f is an arbitrary function. From Eq. (49), we obtain that

$$\langle R \rangle_q = \frac{\langle K^{\text{in}} K^{\text{out}} \rangle}{c(\lambda + d)} \langle J \rangle \langle R \rangle_q, \tag{G3}$$

$$\begin{aligned} \langle R^2 \rangle_q &= \frac{\langle K^{\text{in}} K^{\text{out}} \rangle}{c(\lambda + d)^2} \langle J^2 \rangle \langle R^2 \rangle_q \\ &\quad + \frac{\langle K^{\text{in}} K^{\text{out}} (K^{\text{out}} - 1) \rangle}{c(\lambda + d)^2} \langle J \rangle^2 \langle R \rangle_q^2, \end{aligned} \tag{G4}$$

$$\begin{aligned} \langle |R|^2 \rangle_q &= \frac{\langle K^{\text{in}} K^{\text{out}} \rangle}{c|\lambda + d|^2} \langle |J|^2 \rangle \langle |R|^2 \rangle_q \\ &\quad + \frac{\langle K^{\text{in}} K^{\text{out}} (K^{\text{out}} - 1) \rangle}{c|\lambda + d|^2} |\langle J \rangle|^2 |\langle R \rangle_q|^2, \end{aligned} \tag{G5}$$

and from Eq. (48), we obtain

$$\langle R \rangle = \frac{c}{\lambda + d} \langle J \rangle \langle R \rangle_q, \tag{G6}$$

$$\begin{aligned} \langle R^2 \rangle &= \frac{c}{(\lambda + d)^2} \langle J^2 \rangle \langle R^2 \rangle_q \\ &\quad + \frac{\langle (K^{\text{out}})^2 \rangle - c}{(\lambda + d)^2} \langle J \rangle^2 \langle R \rangle_q^2, \end{aligned} \tag{G7}$$

$$\begin{aligned} \langle |R|^2 \rangle &= \frac{c}{|\lambda + d|^2} \langle |J|^2 \rangle \langle |R|^2 \rangle_q \\ &\quad + \frac{\langle (K^{\text{out}})^2 \rangle - c}{|\lambda + d|^2} |\langle J \rangle|^2 |\langle R \rangle_q|^2. \end{aligned} \tag{G8}$$

Equations (G3)–(G8) admit three kind of solutions. The first type of solution is obtained when $\langle R \rangle_q \neq 0$. We denote this solution by $\lambda = \lambda_{\text{isol}}$ and $R = R_{\text{isol}}$ since it identifies the outliers of the random matrix ensemble. In this case, Eq. (G3) implies that

$$\frac{\langle K^{\text{in}} K^{\text{out}} \rangle}{c(\lambda_{\text{isol}} + d)} \langle J \rangle = 1, \tag{G9}$$

which gives the result Eq. (57) for the outlier eigenvalue. Since $\lambda_{\text{isol}} \in \mathbb{R}$, it holds that $R_{\text{isol}} \in \mathbb{R}$. Consequently, we obtain Eq. (58) for $\langle R_{\text{isol}} \rangle$ by solving Eqs. (G3)–(G8) at $\lambda = \lambda_{\text{isol}}$.

The second type of solution is obtained when $\langle R \rangle_q = 0$ and $\lambda \notin \mathbb{R}$. We denote this solution as $\lambda = \lambda_b$ and $R = R_b$. Solving Eq. (G5), we obtain the relation

$$\frac{\langle K^{\text{in}} K^{\text{out}} \rangle}{c|\lambda_b + d|^2} \langle |J|^2 \rangle = 1, \tag{G10}$$

which leads to Eq. (53), if we use the degree correlation coefficient ρ as defined in (13). In this case, R_b is a complex random variable and its first two moments are zero.

The third type of solution is obtained when $\langle R \rangle_q = 0$ and $\lambda \in \mathbb{R}$, and we denote this solution also by $\lambda = \lambda_b$ and $R = R_b$. Solving Eq. (G3), we obtain

$$\frac{\langle K^{\text{in}} K^{\text{out}} \rangle}{c(\lambda_b + d)^2} \langle |J|^2 \rangle = 1. \tag{G11}$$

For this solution, we have that $\langle R_b \rangle = 0$, but the value of $\langle R_b^2 \rangle \neq 0$ depends on the normalization of R_b .

APPENDIX H: FRACTION OF ZERO-VALUED ENTRIES IN RIGHT EIGENVECTORS OF DIRECTED RANDOM GRAPHS

We analyze how the topology of random and directed graphs, in the sense of connected components as discussed in Sec. II C and illustrated in Fig. 1, affects the distribution $p_R(r)$. In particular, we show that for the right eigenvectors of random, directed graphs it holds that

$$p_R = (1 - s_{\text{out}})\delta(r) + s_{\text{out}}\tilde{p}_R(r), \tag{H1}$$

where s_{out} is the relative size of the OUT component.

Using the ansatz

$$q_R(r) = b\delta(r) + (1 - b)\tilde{q}_R(r). \tag{H2}$$

in Eq. (49), we obtain that b solves Eq. (17) and

$$\begin{aligned} \tilde{q}_R(r) &= \sum_{k=0}^{\infty} \sum_{\ell=0}^{\infty} p_{K^{\text{in}}, K^{\text{out}}}(k, \ell) \frac{k}{c} \\ &\times \sum_{m=1}^{\ell} b^{\ell-m} \binom{\ell}{m} \int \prod_{j=1}^m d^2 r_j \tilde{q}_R(r_j) \\ &\times \int \prod_{j=1}^m dx_j p_J(x_j) \delta \left[r - \frac{\sum_{j=1}^m x_j r_j}{\lambda + d} \right]. \end{aligned} \tag{H3}$$

Furthermore, using (H2) in (48), we obtain Eq. (H1).

Note that analogously, for the distribution p_L of entries of left eigenvectors, it holds that

$$p_L(l) = (1 - s_{\text{in}})\delta(l) + s_{\text{in}}\tilde{p}_L(l), \tag{H4}$$

with s_{in} the relative size of the IN component of the underlying graph.

APPENDIX I: MATHEMATICAL DERIVATIONS FOR RANDOM MATRICES WITH DIAGONAL DISORDER AND NONDIRECTED GRAPHS WITH RANDOM COUPLINGS

We derive recursions relations for the distribution p_R in the case of random matrices with diagonal disorder [the model defined in Eq. (104)] and for random matrices defined on random, nondirected graphs with random couplings [the model defined in Eq. (110)]. For the first model, we obtain also compact expressions for the values of λ for which the recursion relations admit a normalizable solution for p_R .

1. Random matrices with diagonal disorder

First, we derive the recursion Eqs. (106) and (107) for the random matrix model Eq. (104) with diagonal elements D_j drawn from a distribution p_D . Using Eqs. (F36) and (F37) for the eigenvector elements R_j and $R_k^{(j)}$, and the fact that for the locally treelike random matrices defined in Eq. (104) all random variables on the right-hand side of Eqs. (F36) and (F37) are independent, we readily obtain the recursion Eqs. (106) and (107), with p_R and q_R as defined in Eqs. (E6) and (E7).

Second, we determine the values of λ for which the recursion Eqs. (106) and (107) admit normalizable solutions, which provide us with the deterministic outlier eigenvalues λ_{isol} and

the eigenvalues λ_b at the boundary of the continuous part of the spectrum. To this aim, we use Eqs. (106) to derive the set of self-consistent equations

$$\langle R \rangle_q = \frac{\langle K^{\text{in}} K^{\text{out}} \rangle}{c} \left\langle \frac{1}{\lambda - D} \right\rangle \langle J \rangle \langle R \rangle_q, \tag{I1}$$

$$\begin{aligned} \langle R^2 \rangle_q &= \frac{\langle K^{\text{in}} K^{\text{out}} \rangle}{c} \left\langle \frac{1}{(\lambda - D)^2} \right\rangle \langle J^2 \rangle \langle R^2 \rangle_q \\ &+ \left\langle \frac{\langle K^{\text{in}} K^{\text{out}} (K^{\text{out}} - 1) \rangle}{c(\lambda - D)^2} \right\rangle \langle J \rangle^2 \langle R \rangle_q^2, \end{aligned}$$

$$\begin{aligned} \langle |R|^2 \rangle_q &= \frac{\langle K^{\text{in}} K^{\text{out}} \rangle}{c} \left\langle \frac{1}{|\lambda - D|^2} \right\rangle \langle |J|^2 \rangle \langle |R|^2 \rangle_q \\ &+ \left\langle \frac{\langle K^{\text{in}} K^{\text{out}} (K^{\text{out}} - 1) \rangle}{c(\lambda - D)^2} \right\rangle \langle |J|^2 \rangle \langle |R \rangle_q|^2, \end{aligned} \tag{I2}$$

in the lower order moments of q_R . Solving Eq. (I1) for $\langle R \rangle_q \neq 0$, we obtain Eq. (109) for the eigenvalue outliers $\lambda = \lambda_{\text{isol}}$ of the random matrix ensemble. On the other hand, setting $\langle R \rangle_q = 0$ in Eq. (I2), we obtain Eq. (108) for the eigenvalues $\lambda = \lambda_b$ located at the boundary $\partial\sigma_{\text{ac}}$ of the continuous part σ_{ac} of the spectrum.

The moments of the distribution p_R of right eigenvector entries associated with either $\lambda = \lambda_{\text{isol}}$ or $\lambda = \lambda_b$ solve the self-consistent equations

$$\langle R \rangle = \left\langle \frac{c}{\lambda + D} \right\rangle \langle J \rangle \langle R \rangle_q, \tag{I3}$$

$$\begin{aligned} \langle R^2 \rangle &= \left\langle \frac{c}{(\lambda + D)^2} \right\rangle \langle J^2 \rangle \langle R^2 \rangle_q \\ &+ [\langle (K^{\text{out}})^2 \rangle - c] \left\langle \frac{1}{(\lambda + D)^2} \right\rangle \langle J \rangle^2 \langle R \rangle_q^2, \end{aligned} \tag{I4}$$

$$\begin{aligned} \langle |R|^2 \rangle &= \left\langle \frac{c}{|\lambda + D|^2} \right\rangle \langle |J|^2 \rangle \langle |R|^2 \rangle_q \\ &+ [\langle (K^{\text{out}})^2 \rangle - c] \left\langle \frac{1}{|\lambda + D|^2} \right\rangle \langle |J|^2 \rangle \langle |R \rangle_q|^2. \end{aligned} \tag{I5}$$

Note that Eqs. (I3)–(I4) generalize Eqs. (G6)–(G8) for the case of constant $D = d$.

2. Undirected graphs with random couplings

We derive the recursion Eqs. (117) and (116) for the random matrix model Eq. (110). Random matrices in this model are locally treelike, and therefore, we can use Eqs. (F19), (F24), (F31), and (F32) derived in Appendix F2. In order to obtain a set of recursive distribution equations, we define the joint distributions

$$p_{R,G}(r, g|\mathbf{A}) = \frac{1}{n} \sum_{j=1}^n \delta(r - R_j) \delta(g - G_j) \tag{I6}$$

and

$$q_{R,G}(r, g|\mathbf{A}) = \frac{1}{c n} \sum_{k=1}^n \sum_{j \in \partial_k} \delta(r - R_k^{(j)}) \delta(g - G_k^{(j)}), \quad (17)$$

where ∂_k is the neighborhood of node k , as defined in Eq. (9). Since \mathbf{A} is locally treelike, the random variables on the right-hand side of Eqs. (F19), (F24), (F31) and (F32) are independent, and we readily obtain the recursive distributional Eqs. (116) and (117).

-
- [1] A. Barrat, M. Barthelemy, and A. Vespignani, *Dynamical Processes on Complex Networks* (Cambridge University Press, Cambridge, 2008).
- [2] M. E. J. Newman, *Networks: an Introduction* (Oxford University Press, Oxford, 2010).
- [3] M. Barthélemy, *Phys. Rep.* **499**, 1 (2011).
- [4] S. N. Dorogovtsev and J. F. Mendes, *Evolution of Networks: From Biological Nets to the Internet and WWW* (Oxford University Press, Oxford, 2013).
- [5] A.-L. Barabási, *Network Science* (Cambridge University Press, Cambridge, 2016).
- [6] P. Gai and S. Kapadia, Contagion in financial networks, *Proc. R. Soc. A* **466**, 2401 (2010).
- [7] A. G. Haldane and R. M. May, Systemic risk in banking ecosystems, *Nature (Nature)* **469**, 351 (2011).
- [8] M. Bardoscia, S. Battiston, F. Caccioli, and G. Caldarelli, Pathways towards instability in financial networks, *Nat. Commun.* **8**, 14416 (2017).
- [9] K. S. McCann, The diversity–stability debate, *Nature (Nature)* **405**, 228 (2000).
- [10] J. A. Dunne, R. J. Williams, and N. D. Martinez, Food-web structure and network theory: The role of connectance and size, *Proc. Natl. Acad. Sci. USA* **99**, 12917 (2002).
- [11] J. Bascompte, Disentangling the web of life, *Science* **325**, 416 (2009).
- [12] U. Bastolla, M. A. Fortuna, A. Pascual-García, A. Ferrera, B. Luque, and J. Bascompte, The architecture of mutualistic networks minimizes competition and increases biodiversity, *Nature (London)* **458**, 1018 (2009).
- [13] S. Allesina and S. Tang, Stability criteria for complex ecosystems, *Nature (London)* **483**, 205 (2012).
- [14] K. Z. Coyte, J. Schluter, and K. R. Foster, The ecology of the microbiome: Networks, competition, and stability, *Science* **350**, 663 (2015).
- [15] Y. Moreno, M. Nekovee, and A. F. Pacheco, Dynamics of rumor spreading in complex networks, *Phys. Rev. E* **69**, 066130 (2004).
- [16] A. V. Goltsev, S. N. Dorogovtsev, J. G. Oliveira, and J. F. F. Mendes, Localization and Spreading of Diseases in Complex Networks, *Phys. Rev. Lett.* **109**, 128702 (2012).
- [17] L. Weng, F. Menczer, and Y.-Y. Ahn, Virality prediction and community structure in social networks, *Sci. Rep.* **3**, 2522 (2013).
- [18] D. M. Grobman, Homeomorphism of systems of differential equations, *Dokl. Akad. Nauk. USSR* **128**, 880 (1959).
- [19] P. Hartman, A lemma in the theory of structural stability of differential equations, *Proc. Am. Math. Soc.* **11**, 610 (1960).
- [20] R. M. May, Will a large complex system be stable?, *Nature (London)* **238**, 413 (1972).
- [21] H. Sompolinsky, A. Crisanti, and H.-J. Sommers, Chaos in Random Neural Networks, *Phys. Rev. Lett.* **61**, 259 (1988).
- [22] Y. Ahmadian, F. Fumarola, and K. D. Miller, Properties of networks with partially structured and partially random connectivity, *Phys. Rev. E* **91**, 012820 (2015).
- [23] J. Aljadeff, D. Renfrew, M. Vegué, and T. O. Sharpee, Low-dimensional dynamics of structured random networks, *Phys. Rev. E* **93**, 022302 (2016).
- [24] J. Kadmon and H. Sompolinsky, Transition to Chaos in Random Neuronal Networks, *Phys. Rev. X* **5**, 041030 (2015).
- [25] A. Amir, N. Hatano, and D. R. Nelson, Non-hermitian localization in biological networks, *Phys. Rev. E* **93**, 042310 (2016).
- [26] T. Gibbs, J. Grilli, T. Rogers, and S. Allesina, Effect of population abundances on the stability of large random ecosystems, *Phys. Rev. E* **98**, 022410 (2018).
- [27] P. A. Haas, N. M. Oliveira, and R. E. Goldstein, Subpopulations and stability in microbial communities, *Phys. Rev. Research* **2**, 022036 (2020).
- [28] A. Broder, R. Kumar, F. Maghoul, P. Raghavan, S. Rajagopalan, R. Stata, A. Tomkins, and J. Wiener, Graph structure in the web, *Comput. Networks* **33**, 309 (2000).
- [29] R. Pastor-Satorras and A. Vespignani, *Evolution and Structure of the Internet: A statistical Physics Approach* (Cambridge University Press, Cambridge, 2007).
- [30] N. Brunel, Dynamics of sparsely connected networks of excitatory and inhibitory spiking neurons, *J. Comput. Neurosci.* **8**, 183 (2000).
- [31] *The Handbook of Brain Theory and Neural Networks*, edited M. A. Arbib (MIT Press, Cambridge, Massachusetts, 2003).
- [32] O. Sporns, *Networks of the Brain* (MIT Press, Cambridge, Massachusetts, 2010).
- [33] A. Mislove, M. Marcon, K. P. Gummadi, P. Druschel, and B. Bhattacharjee, Measurement and analysis of online social networks, in *Proceedings of the 7th ACM SIGCOMM Conference on Internet Measurement* (ACM, New York, 2007), pp. 29–42.
- [34] S. A. Myers, A. Sharma, P. Gupta, and J. Lin, Information network or social network? the structure of the twitter follow graph, in *Proceedings of the 23rd International Conference on World Wide Web* (ACM, New York, 2014), pp. 493–498.
- [35] M. Molloy and B. Reed, A critical point for random graphs with a given degree sequence, *Random Struct. Alg.* **6**, 161 (1995).
- [36] M. Molloy and B. Reed, The size of the giant component of a random graph with a given degree sequence, *Comb. Probab. Comput.* **7**, 295 (1998).
- [37] B. Bollobás and B. Béla, *Random Graphs* (Cambridge university press, Cambridge, 2001), Vol. 73.
- [38] A. Dembo and A. Montanari, Gibbs measures and phase transitions on sparse random graphs, *Braz. J. Probab. Stat.* **24**, 137 (2010).

- [39] M. E. J. Newman, S. H. Strogatz, and D. J. Watts, Random graphs with arbitrary degree distributions and their applications, *Phys. Rev. E* **64**, 026118 (2001).
- [40] S. N. Dorogovtsev, J. F. F. Mendes, and A. N. Samukhin, Giant strongly connected component of directed networks, *Phys. Rev. E* **64**, 025101(R) (2001).
- [41] G. Timár, A. V. Goltsev, S. N. Dorogovtsev, and J. F. F. Mendes, Mapping the Structure of Directed Networks: Beyond the Bow-Tie Diagram, *Phys. Rev. Lett.* **118**, 078301 (2017).
- [42] T. Rogers and I. P. Castillo, Cavity approach to the spectral density of non-hermitian sparse matrices, *Phys. Rev. E* **79**, 012101 (2009).
- [43] S. Allesina, J. Grilli, G. Barabás, S. Tang, J. Aljaffeff, and A. Maritan, Predicting the stability of large structured food webs, *Nat. Commun.* **6**, 7842 (2015).
- [44] I. Neri and F. L. Metz, Eigenvalue Outliers of Non-Hermitian Random Matrices with A Local Tree Structure, *Phys. Rev. Lett.* **117**, 224101 (2016).
- [45] F. L. Metz, I. Neri, and T. Rogers, Spectral theory of sparse non-hermitian random matrices, *J. Phys. A: Math. Theor.* **52**, 434003 (2019).
- [46] W. Tarnowski, I. Neri, and P. Vivo, Universal transient behavior in large dynamical systems on networks, *Phys. Rev. Research* **2**, 023333 (2020).
- [47] M. Krivelevich and B. Sudakov, The largest eigenvalue of sparse random graphs, *Comb. Probab. Comput.* **12**, 61 (2003).
- [48] F. Chung, L. Lu, and V. Vu, The spectra of random graphs with given expected degrees, *Internet Math.* **1**, 257 (2004).
- [49] V. A. Susca, P. Vivo, and R. Kühn, Top eigenpair statistics for weighted sparse graphs, *J. Phys. A: Math. Theor.* **52**, 485002 (2019).
- [50] T. Rogers, I. P. Castillo, R. Kühn, and K. Takeda, Cavity approach to the spectral density of sparse symmetric random matrices, *Phys. Rev. E* **78**, 031116 (2008).
- [51] T. Rogers, C. P. Vicente, K. Takeda, and I. P. Castillo, Spectral density of random graphs with topological constraints, *J. Phys. A: Math. Theor.* **43**, 195002 (2010).
- [52] F. L. Metz, I. Neri, and D. Bollé, Spectra of sparse regular graphs with loops, *Phys. Rev. E* **84**, 055101(R) (2011).
- [53] D. Bollé, F. L. Metz, and I. Neri, On the spectra of large sparse graphs with cycles, *Spectral Analysis, Differential Equations and Mathematical Physics: A Festschrift in Honor of Fritz Gesztesy's 60th Birthday*, edited by H. Holden *et al.*, Proceedings of Symposia in Pure Mathematics, Vol. 87 (American Mathematical Society, 2013), pp. 35–58.
- [54] M. Mézard and G. Parisi, The bethe lattice spin glass revisited, *Eur. Phys. J. B* **20**, 217 (2001).
- [55] M. Mézard and G. Parisi, The cavity method at zero temperature, *J. Stat. Phys.* **111**, 1 (2003).
- [56] C. Bordenave and M. Lelarge, Resolvent of large random graphs, *Random Struct. Alg.* **37**, 332 (2010).
- [57] I. Kryven, Emergence of the giant weak component in directed random graphs with arbitrary degree distributions, *Phys. Rev. E* **94**, 012315 (2016).
- [58] D. Aldous and J. M. Steele, The objective method: Probabilistic combinatorial optimization and local weak convergence, in *Probability on Discrete Structures*, Encyclopaedia of Mathematical Sciences (Probability Theory), Vol. 110, edited by H. Kesten (Springer, New York City, New York, 2004), pp. 1–72.
- [59] N. C. Wormald, The asymptotic distribution of short cycles in random regular graphs, *J. Comb. Theory, Ser. B* **31**, 168 (1981).
- [60] R. A. Horn and C. R. Johnson, *Matrix Analysis* (Cambridge University Press, Cambridge, 1985).
- [61] J. G. Restrepo, E. Ott, and B. R. Hunt, Approximating the largest eigenvalue of network adjacency matrices, *Phys. Rev. E* **76**, 056119 (2007).
- [62] Y. Kabashima, H. Takahashi, and O. Watanabe, Cavity approach to the first eigenvalue problem in a family of symmetric random sparse matrices, *J. Phys.: Conference Series* **233**, 012001 (2010).
- [63] Y. Kabashima and H. Takahashi, First eigenvalue/eigenvector in sparse random symmetric matrices: Influences of degree fluctuation, *J. Phys. A: Math. Theor.* **45**, 325001 (2012).
- [64] H. Takahashi, Fat-tailed distribution derived from the first eigenvector of a symmetric random sparse matrix, *J. Phys. A: Math. Theor.* **47**, 065003 (2014).
- [65] J. Kosterlitz, D. Thouless, and R. C. Jones, Spherical Model of A Spin-Glass, *Phys. Rev. Lett.* **36**, 1217 (1976).
- [66] V. L. Girko, Circular law, *Theory Probab. Appl.* **29**, 694 (1985).
- [67] Z. D. Bai, Circular law, *Ann. Probab.* **25**, 494 (1997).
- [68] F. Götze and A. Tikhomirov, The circular law for random matrices, *Ann. Probab.* **38**, 1444 (2010).
- [69] T. Tao and V. Vu, Random matrices: Universality of ESDs and the circular law, *Ann. Probab.* **38**, 2023 (2010).
- [70] C. Bordenave and D. Chafaï, Around the circular law, *Probab. Surveys* **9**, 1 (2012).
- [71] T. Tao, Outliers in the spectrum of iid matrices with bounded rank perturbations, *Probab. Theory Relat. Fields* **155**, 231 (2013).
- [72] Y. V. Fyodorov and B. A. Khoruzhenko, Nonlinear analog of the May-Wigner instability transition, *Proc. Natl. Acad. Sci. USA* **113**, 6827 (2016).
- [73] S. Franz, M. Mézard, F. Ricci-Tersenghi, M. Weigt, and R. Zecchina, A ferromagnet with a glass transition, *Europhys. Lett.* **55**, 465 (2001).
- [74] L. A. N. Amaral, A. Scala, M. Barthelemy, and H. E. Stanley, Classes of small-world networks, *Proc. Natl. Acad. Sci. USA* **97**, 11149 (2000).
- [75] R. Albert and A.-L. Barabási, Statistical mechanics of complex networks, *Rev. Mod. Phys.* **74**, 47 (2002).
- [76] A. Clauset, C. R. Shalizi, and M. E. Newman, Power-law distributions in empirical data, *SIAM Rev.* **51**, 661 (2009).
- [77] R. Abou-Chacra, D. Thouless, and P. Anderson, A self-consistent theory of localization, *J. Phys. C: Solid State Phys.* **6**, 1734 (1973).
- [78] F. L. Metz, I. Neri, and D. Bollé, Localization transition in symmetric random matrices, *Phys. Rev. E* **82**, 031135 (2010).
- [79] R. P. Sear and J. A. Cuesta, Instabilities in Complex Mixtures with A Large Number of Components, *Phys. Rev. Lett.* **91**, 245701 (2003).
- [80] K. Rajan and L. F. Abbott, Eigenvalue Spectra of Random Matrices for Neural Networks, *Phys. Rev. Lett.* **97**, 188104 (2006).
- [81] J. Grilli, T. Rogers, and S. Allesina, Modularity and stability in ecological communities, *Nat. Commun.* **7**, 12031 (2016).

- [82] J. Aljadeff, M. Stern, and T. Sharpee, Transition to Chaos in Random Networks with Cell-Type-Specific Connectivity, *Phys. Rev. Lett.* **114**, 088101 (2015).
- [83] A. Kuczala and T. O. Sharpee, Eigenvalue spectra of large correlated random matrices, *Phys. Rev. E* **94**, 050101 (2016).
- [84] J. Moran and J.-P. Bouchaud, May's instability in large economies, *Phys. Rev. E* **100**, 032307 (2019).
- [85] N. Hatano and D. R. Nelson, Localization Transitions in Non-Hermitian Quantum Mechanics, *Phys. Rev. Lett.* **77**, 570 (1996).
- [86] G. H. Zhang and D. R. Nelson, Eigenvalue repulsion and eigenvector localization in sparse non-hermitian random matrices, *Phys. Rev. E* **100**, 052315 (2019).
- [87] M. R. Gardner and W. R. Ashby, Connectance of large dynamic (cybernetic) systems: Critical values for stability, *Nature (London)* **228**, 784 (1970).
- [88] H. M. Hastings, The may-wigner stability theorem, *J. Theor. Biol.* **97**, 155 (1982).
- [89] W. Pentney and M. Meila, Spectral clustering of biological sequence data, in *AAAI '05, Proceedings of the 20th national conference on Artificial Intelligence* (2005), Vol. 2, pp. 845–850.
- [90] F. Krzakala, C. Moore, E. Mossel, J. Neeman, A. Sly, L. Zdeborová, and P. Zhang, Spectral redemption in clustering sparse networks, *Proc. Natl. Acad. Sci. USA* **110**, 20935 (2013).
- [91] P. Bonacich and P. Lloyd, Eigenvectorlike measures of centrality for asymmetric relations, *Social Networks* **23**, 191 (2001).
- [92] A. N. Langville and C. D. Meyer, *Google's PageRank and Beyond: The Science of Search Engine Rankings* (Princeton University Press, Princeton, 2011).
- [93] L. Ermann, K. M. Frahm, and D. L. Shepelyansky, Google matrix analysis of directed networks, *Rev. Mod. Phys.* **87**, 1261 (2015).
- [94] T. Lesieur, F. Krzakala, and L. Zdeborová, Constrained low-rank matrix estimation: Phase transitions, approximate message passing and applications, *J. Stat. Mech.* (2017) 073403.
- [95] C. Bordenave, S. Coste, and R. R. Nadakuditi, Detection thresholds in very sparse matrix completion, [arXiv:2005.06062](https://arxiv.org/abs/2005.06062).
- [96] C. Bordenave, M. Lelarge, and L. Massoulié, Nonbacktracking spectrum of random graphs: Community detection and non-regular Ramanujan graphs, *Ann. Probab.* **46**, 1 (2018).
- [97] L. Zdeborová and F. Krzakala, Statistical physics of inference: Thresholds and algorithms, *Adv. Phys.* **65**, 453 (2016).
- [98] T. Kawamoto, Algorithmic detectability threshold of the stochastic block model, *Phys. Rev. E* **97**, 032301 (2018).
- [99] B. Mohar, Y. Alavi, G. Chartrand, and O. Oellermann, The laplacian spectrum of graphs, *Graph theory, combinatorics, and applications* **2**, 12 (1991).
- [100] J. Ståring, B. Mehlig, Y. V. Fyodorov, and J. M. Luck, Random symmetric matrices with a constraint: The spectral density of random impedance networks, *Phys. Rev. E* **67**, 047101 (2003).
- [101] R. Kühn, Spectra of random stochastic matrices and relaxation in complex systems, *Europhys. Lett.* **109**, 60003 (2015).
- [102] E. Agliari and F. Tavano, The exact laplacian spectrum for the dyson hierarchical network, *Sci. Rep.* **7**, 39962 (2017).
- [103] R. G. Margiotta, R. Kühn, and P. Sollich, Glassy dynamics on networks: Local spectra and return probabilities, *J. Stat. Mech.* (2019) 093304.
- [104] D. A. Levin and Y. Peres, *Markov Chains and Mixing Times* (American Mathematical Society, Providence, Rhode Island, 2009), Vol. 107.
- [105] C. Monthus and T. Garel, An eigenvalue method for computing the largest relaxation time of disordered systems, *J. Stat. Mech.* (2009) P12017.
- [106] E. Agliari, A. Annibale, A. Barra, A. Coolen, and D. Tantari, Immune networks: Multitasking capabilities near saturation, *J. Phys. A: Math. Theor.* **46**, 415003 (2013).
- [107] M. D. Donsker and S. S. Varadhan, Asymptotic evaluation of certain markov process expectations for large time, I, *Commun. Pure Appl. Math.* **28**, 1 (1975).
- [108] M. Donsker and S. Varadhan, Asymptotic evaluation of certain markov process expectations for large time, II, *Commun. Pure Appl. Math.* **28**, 279 (1975).
- [109] M. Donsker and S. Varadhan, Asymptotic evaluation of certain markov process expectations for large time-III, *Commun. Pure Appl. Math.* **29**, 389 (1976).
- [110] M. D. Donsker and S. S. Varadhan, Asymptotic evaluation of certain markov process expectations for large time. IV, *Commun. Pure Appl. Math.* **36**, 183 (1983).
- [111] C. De Bacco, A. Guggiola, R. Kühn, and P. Paga, Rare events statistics of random walks on networks: Localisation and other dynamical phase transitions, *J. Phys. A: Math. Theor.* **49**, 184003 (2016).
- [112] J. Feinberg and A. Zee, Non-hermitian localization and delocalization, *Phys. Rev. E* **59**, 6433 (1999).
- [113] A. Goetschy and S. E. Skipetrov, Non-hermitian euclidean random matrix theory, *Phys. Rev. E* **84**, 011150 (2011).
- [114] I. Neri and F. L. Metz, Spectra of Sparse Non-Hermitian Random Matrices: An Analytical Solution, *Phys. Rev. Lett.* **109**, 030602 (2012).
- [115] M. E. J. Newman, Spectra of networks containing short loops, *Phys. Rev. E* **100**, 012314 (2019).
- [116] P. V. Aceituno, T. Rogers, and H. Schomerus, Universal hypotrochoidal law for random matrices with cyclic correlations, *Phys. Rev. E* **100**, 010302(R) (2019).
- [117] A. Coolen, A. De Martino, and A. Annibale, Constrained markovian dynamics of random graphs, *J. Stat. Phys.* **136**, 1035 (2009).
- [118] A. Annibale, A. Coolen, L. Fernandes, F. Fraternali, and J. Kleinfjung, Tailored graph ensembles as proxies or null models for real networks I: Tools for quantifying structure, *J. Phys. A: Math. Theor.* **42**, 485001 (2009).
- [119] G. Bianconi and M. Marsili, Loops of any size and hamilton cycles in random scale-free networks, *J. Stat. Mech.* (2005) P06005.
- [120] D. Bickson, Gaussian belief propagation: Theory and application, Ph.d. Thesis, Hebrew University of Jerusalem, 2008, [arXiv:0811.2518](https://arxiv.org/abs/0811.2518).
- [121] Y. Weiss and W. T. Freeman, Correctness of belief propagation in gaussian graphical models of arbitrary topology, *Neural Comput.* **13**, 2173 (2001).

- [122] J. S. Yedidia, W. T. Freeman, and Y. Weiss, Understanding belief propagation and its generalizations, *Exploring artificial intelligence in the new millennium* **8**, 236 (2003).
- [123] B. Bollobás, *Modern Graph Theory* (Springer Science & Business Media, New York, 2013), Vol. 184.
- [124] T. Tao, *Topics in Random Matrix Theory* (American Mathematical Society, Providence, Rhode Island, 2012), Vol. 132.
- [125] Z. D. Bai, Methodologies in spectral analysis of large dimensional random matrices, a review, *Adv. Stat.* **174** (2008).